TERRACE FORMATION AND FLOODPLAIN SEDIMENTATION IN THE NORTHERN DELAWARE RIVER VALLEY, NEW JERSEY, USA: FLUVIAL RESPONSE TO POSTGLACIAL CLIMATIC, ENVIRONMENTAL, ISOSTATIC, AND ANTHROPOGENIC INFLUENCES

by

KELSEY S. BITTING

A dissertation submitted to the

Graduate School-New Brunswick

Rutgers, The State University of New Jersey

In partial fulfillment of the requirements

For the degree of

Doctor of Philosophy

Graduate Program in Geological Sciences

Written under the direction of

Gregory Mountain

And approved by

____

____

____

____

New Brunswick, New Jersey

May, 2013

ABSTRACT OF THE DISSERTATION

TERRACE FORMATION AND FLOODPLAIN SEDIMENTATION IN THE NORTHERN DELAWARE RIVER VALLEY, NEW JERSEY, USA: FLUVIAL RESPONSE TO POSTGLACIAL CLIMATIC, ENVIRONMENTAL, ISOSTATIC, AND ANTHROPOGENIC INFLUENCES

By KELSEY S. BITTING

Dissertation Director:

Gregory M. Mountain

Shifts in temperature, precipitation, and tectonic uplift have impacted the Northeastern USA since glacial retreat, resulting in changes in regional gradient, vegetation, water budget, sediment grain size and flux to river systems. Along the northern Delaware River in Pennsylvania and New Jersey, the T2 terrace, located 6-9 m above the modern river, records most of the last 21 ka. This study elucidates the depositional history and associated temporal framework of the T2 and adjacent landforms at a locality on the eastern (New Jersey) bank of the river at 41°10'3"N, 74°53'39"W.

Ground-penetrating radar (GPR) facies and bounding surfaces, descriptions of six Geoprobe© sediment cores, and basic geochemical analyses are used to characterize the alluvial architecture of the T2. The landform is comprised of five units of varying sedimentary composition, radar facies, and degree of soil formation, separated by four bounding surfaces identified by radar terminations, changes in grain size, or buried soils. A grid of GPR profiles shows unit thickness, distribution, and geometry, but channel versus overbank grain size is difficult to distinguish, and smaller-scale deposits cannot be resolved.

Seven cores from the primary study site, and one core each from the T2 landform at another site and from an eolian landform nearby, are interpreted in terms of radiocarbon ages and approximate optically-stimulated luminescence (OSL) ages and the published record of the paleoclimatic, paleoenvironmental, isostatic, and anthropogenic factors impacting the valley. Incision of Units 1 and 1a (deposited as proglacial braidplain sediments) began before 14.8 +/- 0.8 ka, and seasonally-stratified lakes formed on the surface of Unit 1. Later climatic amelioration allowed the accumulation of traction sands to floodplain fines in Units 2, 3, and 4, with the most widespread unconformity and buried soil associated with the solar insolation maximum around 9 ka. Warm events (Medieval Climate Anomaly, Holocene Hypsithermal) and significant anthropogenic disturbance are associated with channel destabilization, which foreshadow the effects of future anthropogenic climate change. Finally, this study contributes to a growing body of literature that shows climate change is the dominant driving force behind changes in fluvial deposition and terracing.

Acknowledgements

The research compiled in this dissertation was supported and funded by the following grants and fellowships: National Science Foundation Graduate Research Fellowship, Rutgers University Torrey Fellowship, Geological Society of America Graduate Student Research Award, Graduate School-New Brunswick Special Study Award, American Association of Petroleum Geologists Richard W. Beardsley Grant, and an SEPM Robert J. Weimer Grant. The New Jersey Geologic Survey provided invaluable resources and assistance without which this project would not have been possible.

The author would also like to thank the dissertation committee for their input and feedback: Gregory Mountain, Gail Ashley, Craig Feibel, and Frank Pazzaglia. Other collaborators responsible for the work and ideas presented herein include Ryan Earley, Ron Witte, Jeff Waldner, Joel Spencer, Regina DeWitt, Don Monteverde, Gregg Steidl, Scott Stanford, and Michael Stewart.

Finally, the author expresses her gratitude to her family, especially Jay Rimmer, Tracey & Harry Bitting, and Margaret & Joe Figueroa, as well as friends and mentors including Martha Withjack, Teresa Delcorso, Barbara Bender, Don Monteverde, Janna Ferguson, Lauren Neitzke-Adamo, Tayo Jolaosho, Dave Bord, Morgan Schaller, Ashley Harris, Alex Nikulin, and many others.

TABLE OF CONTENTS

LIST OF TABLES

List of Illustrations

INTRODUCTION

During the time since the retreat of the Laurentide ice sheet, the previously glaciated Northeastern USA has experienced abrupt and gradual shifts in temperature and precipitation as well as extended tectonic uplift due to isostatic rebound. These events have affected rivers by causing changes in gradient, vegetation, and water and sediment dynamics (Ellis et al., 2004; Li et al., 2006; Maenza-Gmelch, 1996; Stanford, 1993). The geomorphic response of river systems records these changing conditions as episodes of terrace aggradation and incision and changes in alluvial sedimentation rates and processes, all of which reflect the system's quest for equilibrium (Pazzaglia, in press). In addition to contributing to our understanding of the geologic record surrounding deglaciation, the sedimentary record of the early to middle Holocene is likely the best analog for future conditions that will result from anthropogenic climate change. While lake and marsh sediments (which provide temporally-continuous records) are most commonly studied to understand paleoclimate, the effects of environmental impacts on naturally-transient, economically-valuable, and often densely-populated landforms such as floodplains and river terraces have greater significance for our society.

Stream terraces preserved within the Delaware Water Gap National Recreation Area (a 70,000 acre area on both sides of the Delaware River stretching roughly from Milford, PA in the north to the Delaware Water Gap near East Stroudsburg, PA in the south) provide an ideal opportunity for in-depth study of natural fluvial landforms and their response to climatic, environmental, and isostatic influences since the last glacial maximum. At a site just south of the Shapanack Island (Shapanack Island Terrace Site, hereafter referred to as SIT), this study focuses on the T2 (middle) terrace that contains the bulk of the Holocene depositional record, as well as one additional T2 at another study site and the adjacent T1 landform at the SIT site. Through ground-penetrating radar, Geoprobe® coring, sediment analysis, and OSL dating, this study seeks to answer the following three research questions:

1) What is the depositional history of the T2 and T1 landforms at the SIT site? This question includes the following sub-questions: 1a. What stream morphologies and 1b. alluvial processes are responsible for the construction of this terrace?

2) What is the temporal framework associated with this depositional history? This question includes the following sub-questions: 2a. Over what time periods were individual sedimentary units deposited, and 2b. when did significant shifts in depositional character occur?

3) What is the impact of postglacial climate, environment, isostatic rebound, and humans on the development of these landforms? 3a. How have water budget (including meltwater, groundwater discharge, and the balance between precipitation and evaporation or transpiration), deposition rate, and sediment source changed through time? 3b. How does the documented sedimentary record correspond to the timing of climatic and environmental changes, isostatic uplift, and human landscape alterations documented to have affected the region in the scientific literature?

A detailed depositional history of this terrace will permit future comparison with other river valleys, improving the understanding of how postglacial fluvial processes vary with different drainage basin characteristics and influences. Documenting the timing of significant shifts in depositional character allows inferences regarding their causative factors, and a chronological framework roughly constrains the rates and timing of fluvial responses to changing conditions.

This study seeks to apply ground-penetrating radar (GPR) and optically stimulated luminescence (OSL) dating in a setting that has rarely benefitted from such an integrative analysis. Hence, in addition to the fundamental research questions stated above, there are three methodological objectives: 1) To utilize GPR stratigraphic analyses to guide coring and excavation, identify relevant subsurface horizons such as paleosols, and target horizons for OSL dating; 2) To identify obstacles to accurate OSL dating in terrestrial depositional settings characterized by unconformities and paleosols, and move toward developing procedures for optimizing results in these situations; and, 3) To seek methods that will provide an alternate, and less time- and labor-intensive, means for OSL studies to identify disequilibrium in radioactive decay series using established methods for analysis of chemical weathering and pedogenic (soil) development.

The first methodological objective will enhance understanding of the ways in which GPR can be used to quickly provide a baseline understanding of stratigraphy necessary for targeted OSL dating, which requires sensitive treatment to prevent exposure to light during the coring procedure. This method will also highlight the use of GPR for identification of paleosols based on known radar response to sediment composition. The second methodological objective will improve OSL dating accuracy in terrestrial environments that are often characterized by unconformities and paleosols or buried soil horizons. The third objective is to test the applicability of weathering and pedogenic analyses to the identification of disequilibria will significantly decrease the amount of time involved in calculating OSL dates where such alteration is suspected.

Study setting

Chapters 1, 2, and 3 focus primarily on the Shapanack Island Terrace (SIT) study site on the eastern (New Jersey) bank of the Delaware river, at 41°10'3.26"N, 74°53'38.62"W (Fig. 1). The nearest major confluence streams are approximately 14 km upstream and 11 km downstream from the SIT site. Data from two additional study sites, the Alonso Depue House (ADH, 41°14'51"N, 74°50'39"W) and Dingman's Ferry (DF, 41°13'29"N, 74°51'37.86"W) will be included in Chapter 3 to provide additional insights into events at the primary study site (Fig. 1).

The study site is located in the northern Delaware River Valley in the Delaware Water Gap National Recreation Area, Pennsylvania and New Jersey. The Tocks Island dam project (http://delawarewatergap.org/TOCKS_ISLAND_DAM_PROJECT.html), initiated formally by the congressional Flood Control Act of 1962, prompted the Army Corp of Engineers to evict inhabitants who would be affected by flooding upstream of the proposed dam. Subsequent work showed that the site of the Tocks Island Dam, approximately 21 km downstream from the SIT study site (Fig. 1), would be geologically unsuitable to support the massive dam structure. Therefore, the project was abandoned, leaving behind one of the longest stretches of undammed river in the Northeastern US. The land was then turned over to the National Park Service, which prevented widespread settlement and development and largely preserved the natural glacial and alluvial landforms.

Bedrock geology

In the study area, the Delaware River flows though a narrow, entrenched valley that follows the strike of northwest-dipping Silurian and Devonian shale and limestone units (Fig. 2) (Witte, 2001). Ridges in the area are comprised of harder sandstone and quartzite units of comparable age, stratigraphically situated both above and below the less-resistant units underlying the valley. The Delaware valley delineates the boundary between the Valley and Ridge province to the southeast (Kittatinny Mountain forms the southeastern valley wall) and the Appalachian Plateau province to the northwest (the Pocono plateau forms the steep northwestern valley wall). The width of the valley in the study area ranges from about 1.25 miles to less than 0.5 miles, restricting the path of the river to a low-sinuosity course (Witte, 2001).

Surficial geology

During the last glacial maximum, the Laurentide ice sheet extended down the Delaware Valley to Belvidere, New Jersey (Stanford, 2003), approximately 38 km south of the study site. During glacial retreat, the northern portion of the valley was inundated by an abundance of glacially-derived sediment. That sediment was deposited as 1) drumlins and aprons on north-facing hillslopes, 2) recessional and ground moraines, 3) glaciofluvial valley-train and outwash-fan deposits, and 4) kame terrace deposits (Fig. 3) (Witte, 2001). Fluvial activity incised into glacial and glaciofluvial deposits, creating gravel “meltwater” terraces, while eolian transport during the immediate postglacial left dune and windblown sand sheets mantling many older landforms on the eastern (New Jersey) side of the valley (Witte, 2001).

A recessional moraine at the northern tip of the Delaware drainage basin in New York State was radiocarbon dated to >18.2 ka (Ridge, 2003), suggesting that all glacial meltwater was diverted from the Delaware basin into the neighboring Hudson and Susquehanna drainage basins around this time. Later fluvial processes generated three alluvial terraces, shown in Figure 4 (Witte, 2001): an upper terrace (T3), ~40-50 ft (12-15 m) above the modern river; a middle terrace (T2), ~20-30 ft (6-9 m) above the modern river; and the modern floodplain or floodplain bench (T1), ~12 ft (4 m) above the modern river (Witte, 2001). Other, less well-defined terraces may also exist between the major breaks, but are not yet well documented (Witte, personal communication).

A radiocarbon date of 870 +/- 40 ^{14}C years BP (Witte, personal communication) from the upper layers of one T3 deposit indicates that the most extreme late Holocene floods still reach this high elevation in some areas. These Holocene sediments are likely to be a thin veneer atop older Pleistocene fluvial deposits, but since the terrace sediments are often devoid of organic remains for radiocarbon dating, no age dates are yet available for the bulk of the upper terrace (T3).

Carbon dates and archaeological excavations in the middle terrace (T2) during the past four decades have shown that this terrace dates to the latest Pleistocene to earliest Holocene, carbon-dated to a maximum age of about 11.5 ka (Witte, 2001). However, the basal overbank deposits in this terrace are notably poor in organic matter in cores and excavated sections, perhaps limiting the usefulness of radiocarbon dating for constraining the initiation of deposition of this terrace.

The lowest terrace (T1), or floodplain bench, is generally considered by archaeologists to be too young to contain Native American remains (Orr & Campana, 1991). This landform is frequently inundated by modern floods, as observed by the author on multiple occasions in 2006.

Archaeological context

The animals attracted to and supported by the river, and the rich floodplain soils for agriculture, drew Native American settlers to the Delaware River valley long before the arrival of Europeans (McNett et al., 1977), and proximity to water may have been a primary consideration in selection of Native American habitation sites (e.g. Schrabisch, 1915). Early excavations yielded over 150 archaeological sites in Warren and Hunterdon Counties, NJ, alone, including a wide variety of lithic tools, ceramics, beads, and human burials (Schrabisch, 1915). Excavation sites multiplied rapidly during the 1970's in a concentrated effort to preserve these cultural artifacts before the completion of the Tocks Island project. The Shawnee-Minisink site, considered one of the most important Native American localities in the northeast, yielded a stratified record of Native American habitation from approximately 11 ka (at a depth of 493 cm) up through immediate pre-European settlement times (McNett et al., 1977). Archaeological investigations in the Delaware terraces continue today, spearheaded by Dr. Michael Stewart of Temple University (Stewart, 1991).

Chapter topics

Chapter 1, titled "Alluvial architectural analysis using an integrated ground-penetrating radar and coring approach" presents an analysis of the alluvial architecture of

T2 at the study location, based on ground-penetrating radar (GPR) facies and bounding surfaces, Geoprobe© sediment core descriptions, and basic geochemical analyses. GPR profiling reveals five depositional units with different reflector characteristics, separated by four bounding surfaces marked by radar reflector terminations above and below, as well as changes in grain size and soil development. In addition to revealing the sediment character and unit geometries of the alluvial units, this chapter evaluates the capacity of 100 MHz GPR, alone and in concert with sediment description and geochemical analysis, to document channel versus overbank characteristics valuable to reservoir modeling.

Chapter 2, "Optically stimulated luminescence dating of the central (T2) alluvial terrace in the Delaware Valley, New Jersey, USA," discusses the author's attempts at OSL dating of the terrace units and boundaries described in Chapter 1. Depths estimated from GPR profiles are used to select coring sections to be preserved for OSL dating, which requires careful handling to prevent any possible exposure of the sediment to light. In addition to presenting approximate OSL ages for some depositional units, this chapter elucidates complications associated with OSL dating in the context of paleosols and unconformities. This method depends on the assumption that grains are bleached by exposure to light during transport, and accumulate ionizing radiation from the environment starting upon deposition and burial. However, the upper 10-20 cm of a soil profile commonly contains abundant optically-bleached grains due to extensive bioturbation, resulting in an age that reflects burial of the soil surface, rather than deposition. Further, OSL studies commonly measure only the main parent radioactive elements found in the sediment sample (K, Th, Rb, and U), and estimate expected quantities of intermediate radioactive daughter products. However, some products of U-series decay are particularly susceptible to leaching, a process that commonly occurs in soils exposed to groundwater infiltration and throughflow. Time-consuming, high-resolution gamma mass spectrometry analyses, as done in this study, are commonly employed to identify disequilibria in OSL studies. However, leaching is evaluated in chemical weathering and paleosol studies using major and minor element ratios, which can be calculated from mass spectrometry data collected in standard OSL procedures. Chapter 2 presents major and minor element ratio analyses to evaluate chemical weathering and compares these results to hi-resolution gamma mass spectrometry results.

Chapter 3, titled "Postglacial influences on fluvial processes and landscape formation history of the northern Delaware River valley, New Jersey," integrates the results from Chapters 1 and 2 and additional data from the T1 landform. This chapter presents a depositional history of the study site from deglaciation to present and interprets the forcing mechanisms responsible for initial terrace aggradation, subsequent incision, and later alluvial deposition and hiatuses within T2, as well as the late-Holocene formation of T1. The chapter brings together the published record of the paleoclimatic, paleoenvironmental, isostatic, and anthropogenic factors impacting the valley with the documented alluvial response to these factors in other basins worldwide. This chapter also includes preliminary data from one core from the T2 landform at the Dingman's Ferry (DF) site (approximately 7 km northeast of the SIT site), one core from an eolian landform at the Alonso Depue House (ADH) site (approximately 3 km northeast of the DF site), and isotope data from mussel shells recovered from archaeological sites that date to the Medieval Climate Anomaly to provide additional constraints on climate and river response.

The conclusion synthesizes the dissertation's contribution to geomorphology, geology, and archaeology and posits directions for future work.

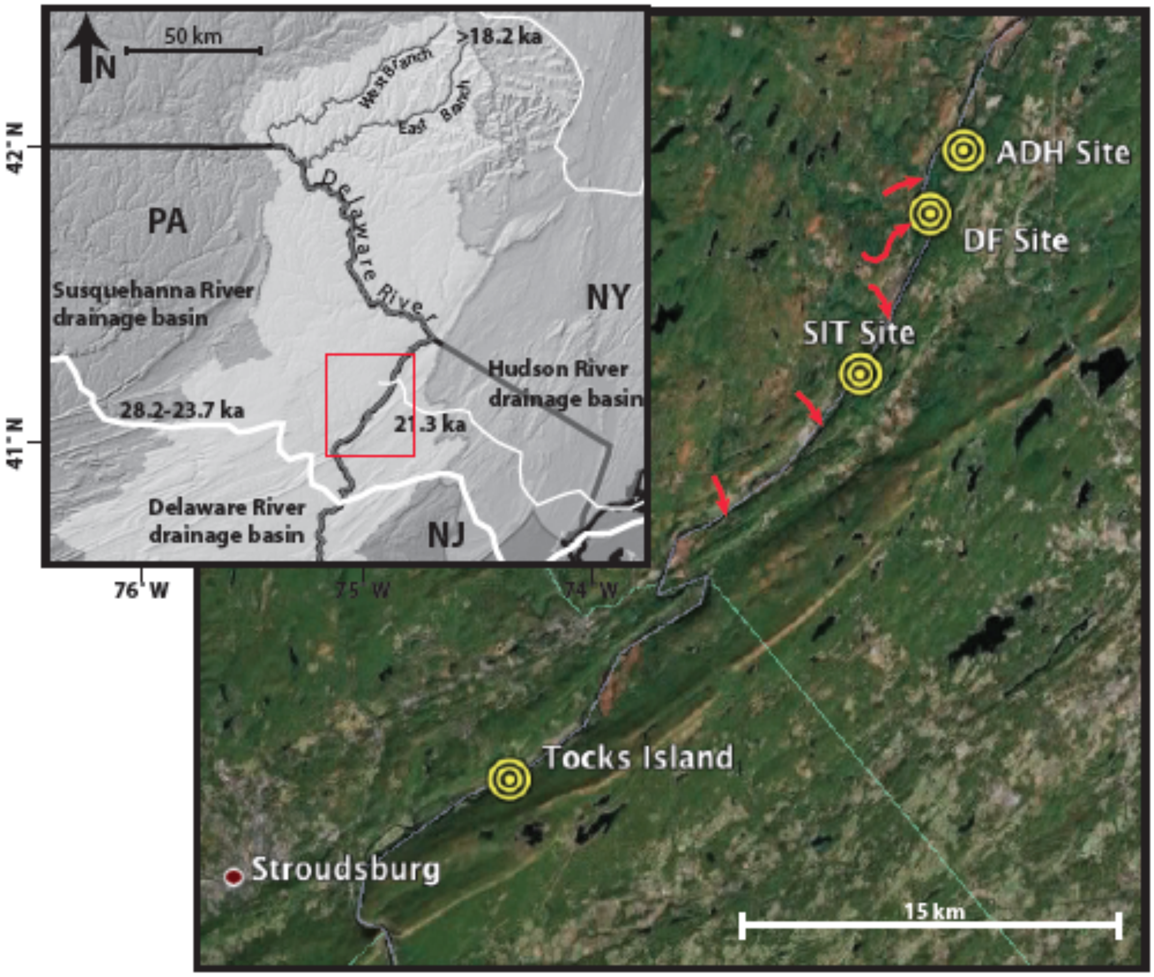

Figure 1 (inset, upper left): Study area in the main figure is shown by the red square. The last glacial maximum terminal moraine is shown by the bold white line; relevant recessional moraines are shown by the thin white lines (from Ridge, 2001). The Delaware River drainage basin is shaded in light gray, while the neighboring Hudson and Susquehanna watersheds are shown in a slightly darker shade.

Figure 1 (main figure, lower right): The study area is located in the Delaware Water Gap National Recreation Area, an area of natural alluvial terraces and landforms in Pennsylvania and New Jersey. Chapters 1, 2, and 3 focus primarily on the Shapanack Island Terrace (SIT) study site on the eastern (New Jersey) bank of the river at 41°10'3.26"N, 74°53'38.62"W. Data from the Alonso Depue House (ADH, 41°14'51"N, 74°50'39"W) and Dingman's Ferry (DF, 41°13'29"N, 74°51'37.86"W) sites, also on the eastern bank, are included in Chapter 3 to provide additional insights into events at the primary SIT study site. The alluvial landforms at the study sites landforms were preserved as a consequence of a 1962 congressional act mandating the construction of a dam at Tocks Island, NJ, and the later cancellation of that project and subsequent preservation of the land as a National Recreation Area. Minor, modern-day confluences with first- and second- order streams in the vicinity of the SIT study site are marked by the red arrows.

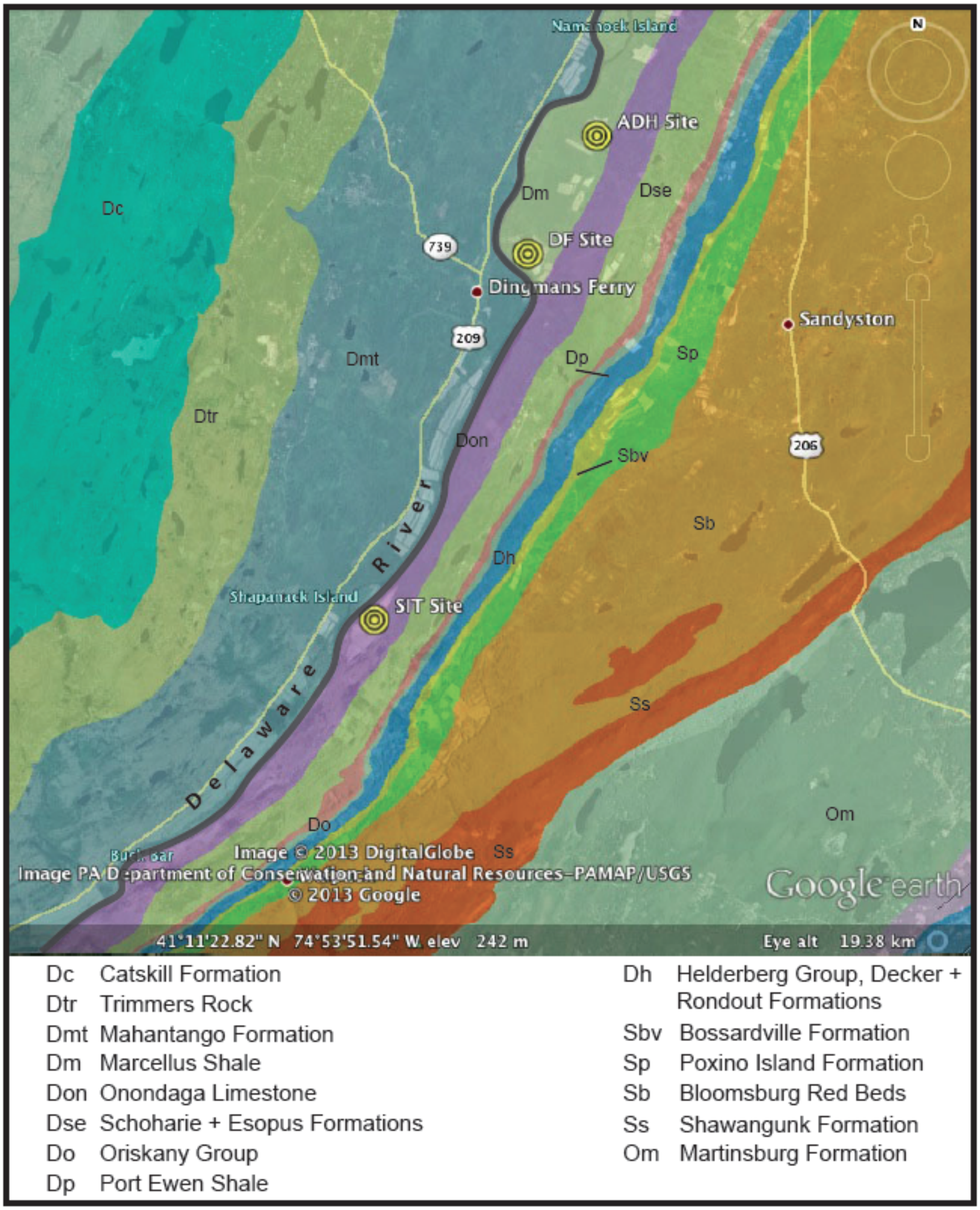

Figure 2: Bedrock geology in the study area. Onandaga Limestone underlies the SIT study site, and Marcellus Shale underlies the DF and ADH sites. The Delaware River follows the strike of the northwest-dipping limestone and shale units between ridges made of sandstone and conglomerate units of the Trimmers Rock and the Bloomsburg Red Beds. Figure by Don Monteverde.

Figure 3: Schematic representing the assemblage and relative vertical position of glacial and alluvial landforms in the northern Delaware River Valley. Qem = recessional moraine, Qov = valley train (lower number represents older deposit), Qkt = kame terrace, Qof = outwash fan, Qft = meltwater terrace, T3 = abandoned Pleistocene flood plain, T2 and T2a = abandoned Holocene flood plains, Tg = buried gravel cut terrace. Figure modified from Witte, 2001.

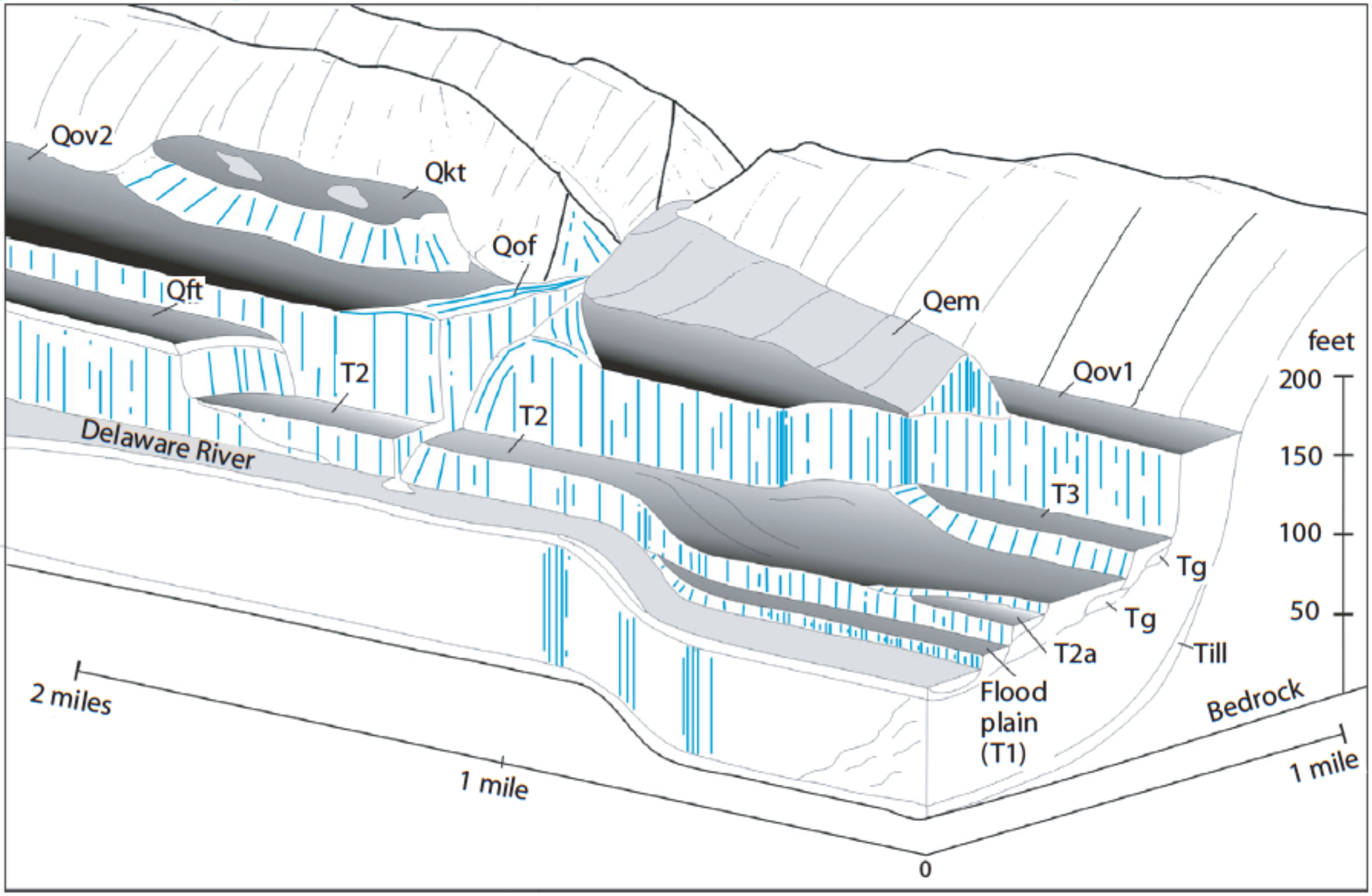

CHAPTER 1: ALLUVIAL ARCHITECTURAL ANALYSIS USING AN INTEGRATED GROUND-PENETRATING RADAR AND CORING APPROACH

Introduction

The study of alluvial architecture seeks to define the geometry, scale, and distribution of individual depositional units within a fluvial setting (Allen, 1978; Leeder, 1978). Architectural models improve outcomes in subsurface prospecting for economic resources and managing contaminant transport in alluvial deposits by predicting locations and interconnectedness of permeable channel (channel belt or channel fill) deposits and less-permeable overbank (floodplain, natural levee, or crevasse splay) deposits. Characterization of texture, structure, geometry, and arrangement of units also helps to elucidate the overall geomorphological evolution of the system (Houben, 2007) in response to autogenic (intra-basinal) and allogenic (extra-basinal) forcing mechanisms such as sea level change, tectonics, and climate change (Blum and Valastro, 1994; Aslan and Autin, 1999; Gouw and Erkens, 2007; Autin, 2008; Karssenberg and Bridge, 2008).

The majority of alluvial architectural studies characterize deposits based on core and outcrop description (Blum and Valastro, 1994; Heller and Paola, 1996; Aslan and Autin, 1999; Gouw and Erkens, 2007; Autin, 2008; Gouw and Autin, 2008). Cores allow a 1-dimensional characterization of lithologies, sedimentary structures, thicknesses of units, and stacking patterns at individual locations on an ancient landscape, which are then interpolated to create a three-dimensional model of the subsurface. Outcrops provide the same information for two-dimensional cross-sections, providing greater spatial coverage of data in some areas. Ultimately however, cores and outcrops cannot provide subsurface information with the spatial resolution needed to hone existing models of alluvial architecture (Mackey and Bridge, 1995; Paola, 2000; Gouw and Erkens, 2007; Gouw and Autin, 2008).

Subsurface profiling tools such as seismic reflection or ground-penetrating radar (GPR) have the potential to provide widespread and evenly-spaced data coverage, enhancing ties between cores and outcrops and illustrating subsurface architecture with greater detail and continuity (Asprion and Aigner, 1999; Corbeanu et al., 2001; Mumpy et al., 2007). GPR provides rapid data collection to depths as great as 10-20 m, and therefore lends itself to architectural characterization of modern alluvial deposits that often serve as analogues for ancient, much more deeply buried deposits.

The appearance of common fluvial architectural elements at varying scales in GPR profiles have not yet been documented in the existing literature. This study examines a late glacial-Holocene alluvial fill terrace in the upper Delaware River Valley, USA, and seeks to determine which alluvial architectural units, observed in sediment cores, can then be identified and characterized using a grid of two-dimensional 100 MHz GPR profiles and one 200 MHz GPR profile.

Setting

This study examines a latest-Pleistocene to Holocene alluvial fill terrace on the eastern bank of the Delaware River in Sussex County, New Jersey, USA (Fig. 1). The main stem of the Delaware River is the longest stretch of un-dammed river in the Northeastern US, and the establishment of the Delaware Water Gap National Recreation Area in 1965 has preserved alluvial deposits largely in their original condition. Removed from the influence of sea level, this upland location provides the opportunity to isolate and evaluate the effects of postglacial climatic events and isostatic rebound on alluvial architecture, providing added value to this case study. Finally, the site is located away from any confluence with tributary streams, and therefore should provide a spatially-averaged perspective of events along the main stream with minimal effects of flashy discharge of smaller streams and slackwater deposition.

In the study area, the river is entrenched within southwest-striking Silurian and Devonian shale and limestone (Witte, 2001) which limit the valley to 2 to 0.8 km wide and confine the channel to a low-sinuosity course. The Laurentide ice sheet advanced across the study area (Stanford et al., 2001; Stanford, 2003), effectively eliminating previous sedimentary landforms. A recessional moraine 10 km north of the study site dates to 21.3 ka, providing a maximum age for alluvium here. After glacial retreat, glacio-fluvial and fluvial deposition and later downcutting produced three discontinuous, paired terraces (Fig. 2).

T3, the uppermost and oldest terrace, is thought to represent braided stream deposition soon after glacial retreat (Witte, 2001). This landform sits 12-16 m above the modern river and is preserved only in isolated locations. T2, the middle terrace, sits 6-9 m above the river. Radiocarbon dates indicate that its deposition began at least 11,000 years ago (Witte, 2001) and the author has observed alluvium deposited on this terrace during extreme floods in the past 10 years. Thus, the T2 terrace represents the bulk of the Holocene depositional record in the valley and is therefore the focus of this study. T1 (sometimes called T0), or the modern floodplain “bench,” sits 4 m above the river (Witte, 2001). T1 is mainly confined to narrow (<500 m wide) landforms along T2, T3, or valley walls, or islands in the channel. At the study site only T2 and T1 are present (Fig. 2). The GPR survey covers the southern ~1/3 of the T2 landform, which is widest near the center and tapers out gradually against the valley wall to the north-northeast and south-southwest. At the study site, T2 is bounded by a thin (up to 115 m wide) strip of T1 to the west-northwest and the valley wall to the east-southeast, which will not be discussed in this paper.

Methods

Field Methods

GPR Profiling

Ground-penetrating radar (GPR) uses wavelets of high-frequency (MHz to GHz) electromagnetic energy transmitted into the ground (Fig. 3). Variations in subsurface electromagnetic properties such as dielectric permittivity reflect some of this energy back to the surface to be detected by the receiver. Radar profiles are first understood in terms of two-way travel time (in nanoseconds, ns). Two-way travel time of reflected energy is proportional to depth of the corresponding reflector, the distance of separation between the transmitting and receiving antennae, and the velocity of EM transmission through the subsurface. In soil such as encountered in this study, this latter value is typically less than half the speed of light in a vacuum (i.e., $< 1.5 \times 10^8$ m/sec) but is controlled by the dielectric permittivity of the soil and can vary about this value by as much as a factor of 2 (Table 1).

Resolution of features in the subsurface depends on the frequency of the GPR source wavelet, which, in turn, is determined by the length of the transmitting antenna. A 1-m-long antenna will produce an approximately 100 MHz pulse; one that is 0.5 m produces a pulse with twice this frequency (200 MHz). These frequencies correspond to wavelengths of roughly 3 m and 1.5 m, respectively. Theory indicates the best possible vertical resolution, or the ability to accurately locate and distinguish two closely spaced subsurface reflectors in terms of space or time, is about a quarter of the dominant wavelength of the GPR wavelet (Neal, 2004). In practice, to generate a sharp reflector, the vertical distance over which there is a change in dielectric permittivity (a measure of a material's capacity to store charge) must be slightly greater than this theoretical value, approximately 1/3 of the wavelength (Annan et al., 1991; Van Dam, 2001; Neal, 2004).

Horizontal resolution, or the width of the radar "footprint," is wider in the direction perpendicular to the long axis of the antennae (which run parallel to the ground surface), and thinner in the parallel direction (Engheta et al., 1982; Lehmann et al., 2000; Neal, 2004). This means that the horizontal positions of two objects in the subsurface can be resolved in the direction parallel to the antenna axis better than they could be resolved in the perpendicular direction; hence, most surveys are conducted with antennae oriented parallel to the survey line, as was done in this study. Horizontal resolution changes with depth and average dielectric permittivity, and generally allows only 15% the precision of vertical resolution at a depth of 1 m (Neal, 2004).

For this study, a series of 100 MHz GPR lines were collected in March 2006 with a Mala Geoscience RAMAC radar using 100 MHz antennae with a common offset of one meter between the transmitting and receiving antennae, perpendicular to the profile direction. One set of GPR lines runs perpendicular to the modern channel, to show variations in sedimentary packages from proximal (near-channel) to distal (near valley wall) areas of the terrace, while a second set runs parallel to the channel (Fig. 2). Vertical resolution for these lines is estimated at 33 cm (or 1/3 the wavelength) at best. At 1 m depth and using a dielectric permittivity of 7, the radar footprint is about 220 cm at its widest (perpendicular to the profile) (equation from Neal, 2004) indicating that features smaller than this cannot easily be resolved.

During collection of the 100 MHz dataset, gains were used incorrectly, making amplitude information unreliable. Therefore, a smaller dataset of 200 MHz lines was collected in April 2009 using a GSSI radar system for relative amplitude comparisons. A 5-point time-varying gain curve was applied during collection of the 200 MHz data to account for some signal loss with increasing depth. In this paper, one 200 MHz line is shown (Fig. 2). Vertical resolution of the 200 MHz data is estimated at 16.5 cm at best, and the horizontal radar footprint (at 1 m depth and using a dielectric permittivity of 7) is 146 cm at its widest.

Geoprobe Coring

Cores were recovered using a Geoprobe® Model 5410 direct-push coring system. The Geoprobe uses a 122 cm long, 5 cm diameter steel drill pipe with an internal plastic sleeve. Drive rods are added at 122 cm increments to extend penetration depth. When each section is recovered, the cutting shoe is removed, and 5 cm of sediment at the base of the core are lost. Sleeves 117 cm long are capped for later core description and analysis. Due to compaction and possible loss of loose sands at the bottom of sections, core recovery is typically around 80-90%, but can occasionally be as low as 65% per 122-cm section. No compaction corrections are made in the subsequent discussions, with core depth reflecting the thickness recovered in the field, plus the known 5 cm loss.

State regulations dictate that drill holes deeper than 730 cm must be capped and sealed using concrete; for convenience, cores for this study did not penetrate beyond that depth. In some cases, depth was first limited by lithology (i.e., gravel) or equipment difficulty due to water-saturated conditions. Coring depths in this study ranged from 470 to 730 cm.

Two cores at the study location were collected by the New Jersey Geologic Survey in spring 2005. Based on GPR data and preliminary analyses of the initial cores, four additional cores were collected in May 2007 (Fig. 2). These were collected along one GPR line to provide the most direct tie to the profile data. Core locations were recorded using a Garmin GPSmap76CS handheld unit, with an estimated horizontal precision of +/- 5 m.

Laboratory Methods

GPR Data Processing

This study has employed minimal data processing beyond that done automatically during data collection (primarily a time varying gain). Without data migration, dipping reflectors appear to have shallower dips than the actual surfaces; diffractions may obscure primary reflections; synclines are distorted to appear narrower, and anticlines broader, than their true widths; and out-of-plane reflectors may be present (Yilmaz, 1987;

Robinson and Çoruh, 1988; Kearey and Brooks, 1991; Yilmaz, 2001; Neal, 2004). In addition, multiples, high-frequency ringing, signal saturation, and reflections from objects above the ground surface (e.g. trees, fence posts, etc.) may obscure subsurface features (Neal, 2004). However, apparent reflector terminations and reasonable ties to cores indicate that the GPR data maintains fidelity with the subsurface conditions. No interpretations of dip angle or width of subsurface features are made here.

In order to convert two-way travel time to depth, a velocity estimate is required (distance = velocity x time). Typical radar velocities in common substrates are shown in Table 1 and can be used for a general approximation. In the field, a common-midpoint survey (in which spacing between transmitting and receiving antennae is progressively increased from a common center point) can be conducted for velocity determinations by way of a normal moveout correction. For this study, a common midpoint survey yielded variable velocities (approximately 4 to 14 cm/ns) with an average of 9 cm/ns. Using this velocity, the depths of the upper two units and upper two surfaces described below coincide within 10 cm of stratal features in the cores discussed below. However, this same velocity leads to an apparent overestimate of the thickness of the middle unit and to depths to surfaces below it by as much as 1 m, indicating the radar velocity in this middle unit is less than 9 cm/ns. The deepest unit completely resolved by the GPR data again matches to within 10 cm of the thickness of its assumed equivalent in the core.

Because relative reflector amplitude is inaccurate due to the incorrect use of collection gains, 100 MHz lines are displayed as the cosine of the phase, which eliminates accurate reflector amplitudes. However, this display clearly shows reflector continuity, which can be difficult to interpret where amplitudes are low.

A time-zero drift correction was used on both datasets to remove time before the first arrival. The air wave, or the energy traveling directly from transmit to receive antennae is typically the first reflector in a GPR dataset. In the data shown here, the air wave has been removed, placing the ground surface at the top of the record. Background noise removal was applied to the 200 MHz data by averaging multiple traces and subtracting the result from each to remove a low-frequency ringing of unknown origin (Earley, personal communication, 2007). No topography correction was applied, so reflectors are shown with depth relative to the ground surface. Actual topography across the study area varies by up to 2 m. Both datasets were viewed using SeismicUn*x using the suximage command.

GPR Data Interpretation

After data collection, individual radar traces measured in travel time are placed side-by-side to create a GPR profile of radar reflectors. Water content is considered the most important factor in generating radar reflections, due to the large dielectric permittivity contrast between water and sediment or air (Table 1) (Davis and Annan, 1989; Van Dam, 2001). The water table or its capillary fringe produce a strong radar response under certain conditions (Huisman et al., 2003). Changes in grain-size, organic matter content, and iron-oxide content influence water retention, and are typical causes of reflectors (Van Dam, 2001). Since soils are often characterized by enhanced water retention (due to increased organic carbon, clays, or iron-oxides) (Retallack, 1990;

Birkeland, 1999), high-amplitude reflectors may represent buried soils, particularly where they coincide with a bounding surface (van Dam et al., 2002; Bennett et al., 2006).

Many beds observed in the cores in this study are thinner than the 33-cm vertical resolution of GPR at the 100 MHz frequency. Thus, the true geometries of features smaller than this are suspect.

Packages of radar reflectors are then separated into "radar facies" based on characteristics such as shape of reflectors (e.g. planar, concave, wavy, etc.), dip of reflectors (dip angle and direction), relationships between reflectors (e.g. parallel, oblique, divergent), and continuity of reflectors (Huggenberger, 1993). Radar facies have been shown to correlate strongly with the stratigraphy of sedimentary deposits (Van Dam, 2001), and once verified using cores, can be used to extrapolate depositional units over a wide area and understand their subsurface geometry.

Based upon methodologies developed to interpret seismic profiles, radar facies are separated by bounding surfaces that are identified by reflectors that terminate against them (Nystuen, 1998). Onlap, in which flat reflectors of the upper unit terminate at progressively shallower elevations against the lower Unit (Fig. 4 a), indicates gradual, horizontal deposition infilling of paleotopographic lows. Downlap, in which reflectors of the upper unit curve downward onto the lower unit (Fig. 4 b), indicates lateral accretion of sediments building across the surface of the older deposit. Erosional truncation, in which multiple reflectors of the lower unit terminate abruptly at the upper boundary (Fig. 4 c), indicates the removal of some of the older deposit prior to its burial by the younger strata.

Core Description and Analysis

Cores were split lengthwise and the exposed sediment was planed off before description to enhance examination of sedimentary structures. Samples were collected at 5 cm intervals. Preliminary descriptions included color (using Munsell color charts for Cores 5-7), sedimentary or soil structures, nature of stratal contacts, and visual estimation of grain size. Contacts between beds were often slightly distorted by coring, creating a concave-down bow shape of up to 2 cm at the edges of the cores, prohibiting accurate assessment of paleotopography.

Percent organic carbon and carbonate were determined using standard loss-on-ignition procedures by weight loss at 550°C and 950°C, respectively, for two hours each (according to procedures outlined in Heiri et al., 2001). Magnetic susceptibility measurements collected for the three initial cores were so low as to be within error of background values, and are not presented here. Visual evaluation of grain size of select samples was corroborated using a Horiba laser particle size analyzer (0.4 mm to 2 mm diameter). Four samples from Core 7 were subjected to fusion ICP-MS and ICP-OES measurements for major and minor element composition (Joel Spencer, personal communication), which are then converted to chemical weathering ratios using established formulas (Chittleborough, 1991; Fedo et al., 1995; Harnois, 1988; Jenny, 1941; Nesbitt & Young, 1989; Parker, 1970; Price & Velbel, 2003; Ruxton, 1968).

Results

Based on the two datasets, the alluvial terrace is divided into five main unconformity-bounded units (Table 2). Units 1 and 1a (the deepest of the five) are composed of nested channel elements including braidplain pebbles and channel sands. Unit 2 is made up of both channel and overbank elements, including traction sheet sands, varved lake clays, overbank suspended-load fine sands-clays, and crevasse splay sands. Unit 3 is comprised of overbank elements, including overbank suspended-load fine sands-clays, and crevasse splay sands. Unit 4 also includes channel and overbank elements, ranging from traction sands to overbank suspended-load fine sands-clays. Table 2 describes all architectural elements contained within the five units, including radar geometry and facies, sediment texture, structure, and geometry. Figure 5 shows the GPR data grid with bounding surfaces interpreted. Figure 6 shows the logs of three cores in association with the GPR data and interpretations. Figure 7 shows the overall radar facies, architectural elements, and channel/floodplain classifications of the five main, unconformity-bounded units, as well as a composite stratigraphic column for the deposit.

Bounding surfaces in the 100 MHz GPR data define the five units' geometry, which shows little correspondence to channel vs. overbank deposition at the study location. Similarly, radar facies, bounding surfaces, and amplitudes do not provide a distinction between traction sands and overbank fines in Units 2 and 4. Crevasse splays and lake clays are below the resolution of the primary 100 MHz GPR used in this survey.

Unit 1

Description

Defined by its upper bounding surfaces B1a and B1, Unit 1 is present across the entire study area and is >4 m thick in some areas (its total thickness is not resolved by

GPR or cores; Fig. 5). This unit is laterally-extensive, and characterized by an undulating surface topography that is mirrored to some degree in all depositional units above. The unit's overall geometry cannot be described, since this study did not resolve its lower boundary.

The radar facies of this unit is highly variable, depending on the orientation of the line relative to the modern channel or valley axis. At one end member of the spectrum of radar facies, perpendicular to the modern channel, GPR profiles show abundant discontinuous reflectors that lack consistent orientation (Fig. 5). In channel-parallel GPR profiles such as profile 9 (Fig. 5), the radar facies is considerably more organized: Broad, concave, continuous reflectors bound smaller packages of shorter, discontinuous reflectors with internally-consistent orientations that vary in direction and angle.

Cores 5 and 1 penetrate Unit 1 (Fig. 2 and 6). Sediments are typically clast-supported, poorly-sorted, subrounded to subangular pebbles of locally-derived lithologies (limestone, chert, shale, and rare red sandstone). These pebbles have variable matrix sediments ranging from very poorly sorted clay and sand to sand. Occasional medium to coarse, moderately well-sorted sand beds are interspersed with the pebbles. No evidence of soil development was observed at the top of this unit, and the boundary between Units 1 and 2 is distinguished in cores based on the change from pebbles below the boundary to sands and silts above. Cores did not penetrate the contact between Units 1 and 1a.

Interpretation

The wide, concave-down reflectors visible in channel-parallel lines resemble cross-sectional profiles of point bar deposits (Leclerc and Hickin, 1997; Ritter et al., 2002). However, disorganized reflectors in channel-perpendicular lines are inconsistent with cross-valley meander migration. Rather, the more orderly appearance of reflectors in channel-parallel lines indicates that the deposit was constructed by building downstream. Multiple orientations of packages of discontinuous reflectors in channel-parallel lines indicate lateral aggradation in multiple directions, such as might be expected from many small, transient channels. Overall, the radar facies is consistent with an aggradational braidplain such as a proglacial outwash plain (Fig.7, Table 1).

Subrounded to subangular clast-supported pebbles, interrupted in some places by medium and coarse well-sorted sands, make up the unit in cores (Table 1). The relatively immature pebble units were likely deposited soon after glacial retreat, before fluvial activity had thoroughly reworked the glacial deposits (similar to those documented in Boothroyd and Ashley, 1975). Poor sorting and variable matrix present within these units also support a proglacial origin. Sand units likely represent small, transient channels transporting concentrations of meltwater (Table 1).

Based on the 100 MHz GPR dataset and the core descriptions together, Unit 1 is characterized as a channel deposit (Fig. 7). However, the different matrices within pebble units would result in variable internal permeability, with relevance for the predictive potential for alluvial architecture (discussed in the conclusion).

Unit 1A

Description

Defined by bounding surface B1 below and B1a above, Unit 1a is a wedge-shaped unit, <1 m thick at its maximum observed width near the modern Delaware river (Fig. 5). The unit pinches out onto the B1 boundary below, and is truncated by B1a boundary above. Radar reflectors within this unit are short and slightly more continuous than reflectors in Unit 1. In the 200 MHz data, the B1a surface at the top of unit 1a coincides with one of two sets of high-amplitude reflectors (Fig. 5).

Core 7 sampled this unit (Fig. 2 and 6). Sediments are clast-supported pebbles that show slightly more rounding and sorting than the pebbles in Unit 1, but are composed of the same locally-derived lithologies. Matrix ranges from silt to very coarse sand. No evidence of soil formation is observed at the top of the unit at B1a.

Interpretation

Radar reflectors of Unit 1a are more continuous than in Unit 1, and appear to indicate lateral aggradation away from the modern channel. However, since only a small area of Unit 1a is preserved, no interpretations of directionality can reliably be made. Deposition near the modern channel more likely suggests greater accommodation space near the axis of the valley for preservation of the unit, rather than a relationship to the modern stream.

Sediments in the cores are slightly more mature (rounded and sorted) than those in Unit 1, as would be expected slightly later in time. This unit may represent sedimentation in a braided or low-sinuosity stream channel that was responsible for reworking glacial outwash in the valley (Boothroyd and Ashley, 1975). Since no soil character is observed at the upper B1a boundary, the high-amplitude reflector is interpreted as a change in porosity associated with the transition from pebbles and matrix to sands above. As with Unit 1, the unit is characterized as a channel deposit with internally-variable permeability.

Unit 2

Description

Defined by bounding surfaces B1 and B1a below and B2 above, Unit 2 is ~2-m thick except where it thins out in the far distal portion of the terrace (Fig. 5). Reflectors within this unit are continuous and follow the topography of the lower (B1-B1a) boundary. Atop a paleo-topographic high, one reflector suggests minor erosional truncation by the B2 boundary above (figure 6a, approximately 20 m from the distal end of the profile). In the 200 MHz data the upper B2 surface coincides with the second set of high amplitude reflectors (Fig. 5).

Sediments of Unit 2 are present in all cores (Fig. 2 and 6) and range from loamy clays to sands, with sands being dominant and thickest near the modern channel. Individual beds within the unit are commonly well or moderately sorted, though some localized deposits are poorly sorted. Some sandy beds fine or coarsen upward. Overall, the average grain size in Unit 2 fines-upward in all cores except Core 3 (Fig. 2), which is closest to the modern channel. The B2 boundary coincides with peaks in organic carbon and carbonate contents of up to 1.5% (Fig. 6). Visual examination of cores at this depth showed gradational boundaries between beds.

Major and minor element concentrations from three sediment samples from this unit in Core 7 were used to calculate intensity of alteration via chemical weathering ratios (Jenny, 1941; Ruxton, 1968; Parker, 1970; Harnois, 1988; Retallack, 1990; Birkeland, 1999; Price and Velbel, 2003). These ratios indicate relatively minimal alteration of sample S4 at the base of the unit, some alteration of sample S3 (only 10 cm above S4), and significant alteration of sample S2 from just beneath the B2 boundary (Table 3).

Interpretation

The relatively flat and widely continuous reflectors of the 100 MHz radar data parallel the upper B2 and lower B1/B1a boundaries, suggesting a draping style of deposition and vertical accretion (Leclerc and Hickin, 1997). These reflectors do not suggest the diversity of sediment character within the unit that is revealed by coring: well-sorted and ungraded medium and coarse sands interpreted as traction sands, finer sands and silts interpreted as suspended load settling, and graded beds indicating probable crevasse splay sedimentation (Bristow et al., 1999). Traction sands may not represent sedimentation within a channel, since no evidence of channelization was observed in either dataset; rather, these sands may have been carried in traction across the low-elevation floodplain. Fining-upward through the unit is consistent with floodplain sedimentation, with higher energy toward the base of the unit and decreasing energy as the surface builds to higher elevations (Nanson and Croke, 1992).

Chemical weathering analyses of sample S2 (Table 2) and organic carbon and carbonate peaks, finer grain sizes, and darker colors at the top of Unit 2 (at boundary B2) all indicate soil formation that would have accompanied a significant hiatus (Retallack, 1990; Birkeland, 1999). The high-amplitude 200 MHz reflector at the B2 surface provides additional evidence of soil development. The widespread unconformity at B2 atop Unit 2 would have provided the time necessary to form this soil (Retallack, 1990; Birkeland, 1999).

Grain size distributions of the traction sands near the base of the unit suggest permeability consistent with channel deposits for alluvial architectural purposes; all other sediments in this unit (crevasse splay, suspended load) are sufficiently localized or inferred to have low enough permeability to be described as overbank. Therefore, Unit 2 is a combination of the two basic alluvial sedimentation types that cannot be disentangled by the 100 MHz radar survey or the amplitude information from the 200 MHz dataset. However, the 200 MHz dataset is too limited in scope to determine whether radar facies at this resolution would provide evidence of the different lithofacies encompassed by the unit.

Unit 3

Description

Defined by bounding surface B2 below and B2a above, Unit 3 is a thin (max ~1 m), wedge-shaped unit present only on the proximal edge of the T2 terrace (Fig. 5). GPR reflectors of this unit build up and terminate onto a preexisting topographic high at its distal edge. Reflectors are semicontinuous to discontinuous, and generally approximate the topography of the underlying B2 boundary, although they do onlap and downlap onto this surface (see figure 6a, distal portion of Unit 3 beneath the topographic high). One reflector appears erosionally-truncated by the B2a boundary above.

Cores 3 (Fig. 2) and 7 (Fig. 2 and 6) sampled this unit. Sediments range from loamy clays to medium sands, with finer grain sizes dominating (Fig. 6). Sand units are sometimes uniform, and sometimes graded. Poorly-sorted units are also locally present. Organic carbon and carbonate values show multiple peaks (Fig. 6) and boundaries are generally gradational. Chemical weathering ratios of sample S1 in this unit from Core 7 show the sample has experienced moderate subaerial chemical weathering and alteration, though not to the same degree as S2 (Table 2).

Interpretation

The relatively smooth reflectors of the middle unit in the 100 MHz GPR profiles suggest laminar overbank (floodplain) deposition (Leclerc and Hickin, 1997), and increasing topographic relief toward the distal edge of the unit suggests construction of a natural levee (Nanson and Croke, 1992). The typically fine-grained sediments in this unit also indicate deposition in a relatively low-energy setting, while interspersed medium sand units are interpreted as occasional high-magnitude floods or crevasse splays, where graded (Bristow et al., 1999; Nobes et al., 2001). Multiple carbon and carbonate peaks and gradational boundaries suggest increased soil development throughout Unit 3 relative to most of Unit 2, which would correspond to lower deposition rates or more episodic deposition. Overall, localized deposition near the modern channel suggests lower-magnitude flooding at this time. Based on these observations, this unit is composed entirely of overbank deposits.

Unit 4

Description

Defined by bounding surface B2a and B2 below and the modern land surface above, Unit 4 displays a consistent thickness of roughly 2 m, and deepens to infill topographic lows on the antecedent topography (Fig. 5). GPR reflectors are continuous and parallel to the land surface (flat in GPR data without topography correction). The uppermost reflector is the ground wave, or the reflection of electromagnetic energy directly off the ground surface. Deeper reflectors infill paleo-topographic lows and onlap onto highs of the lower (B2a/B2) boundary.

All cores intersect this unit near the apex of each paleotopographic high (Fig. 2 and 6). At the base of each core, a few 10s of cm of massive to graded traction sands suggest that the paleotopographic lows are infilled with coarse material. Above, the unit is comprised of suspended load sediments ranging from loamy clays to fine sands, with finer grain sizes dominating. Most cores exhibit a fining-upward trend except Core 7, which is significantly coarser-grained in its upper meter. Organic carbon and carbonate values generally increase throughout this unit with multiple peaks, and roots and rootlets are abundant in the upper ~1.5 m of sediment.

Interpretation

The relatively flat and continuous reflectors of the unit suggest laminar deposition and vertical accretion for Unit 4 (Leclerc and Hickin, 1997). Basal traction sands are interpreted as one or more extremely high-magnitude floods, perhaps deposited in channelized flow through paleotopographic lows, though no evidence of channel structure is observed (Leclerc and Hickin, 1997). Overbank fine sands, silts, and clays above are deposited in a relatively low-energy floodplain setting (Nanson and Croke, 1992), though the radar facies does not distinguish traction sands from overbank sediments. Soil development (evidenced by dark-colored clay-rich horizons, gradational boundaries, and higher organic carbon and carbonate) suggests slow or episodic deposition for the upper (overbank) portion of the unit. Overall, Unit 4 (like Unit 2) is comprised of both channel and overbank deposits.

Discussion

Based on the 100 MHz GPR survey used at the study site, the unit geometries and map-view distributions were characterized with greater precision than would have been possible using the cores alone. However, several smaller-scale architectural elements (crevasse splays and floodplain ponds) were below the resolution and would have gone undetected without the use of cores. Therefore, alluvial architecture of a given site may be best characterized using multiple resolutions of GPR surveys to maximize both depth and resolution. It is unclear whether the improved survey resolution of a 200 MHz or 400 MHz survey would have been sufficient to identify the combined traction sands and overbank deposits identified in Units 2 and 4, but the amplitude information from the 200 MHz line does not provide any additional evidence of this distinction. Ultimately, while GPR is an excellent supplement to architectural studies, GPR surveying must be conducted in conjunction with coring or outcrop description.

Glacial deposits often serve as important aquifers in the New Jersey area. Groundwater flow is commonly modeled, but the complexities of glacial aquifers necessitate mapping of the types of deposits for meaningful analysis (Stanford and Ashley, 1998.) This study shows that GPR provides the opportunity to quickly identify larger-scale units such as glaciofluvial outwash in the subsurface without time- and labor-intensive coring or trenching (which might also expose an aquifer to potential contamination). Nonetheless, GPR does not reveal the full complexity of grain size and permeability of the units in this study.

The alluvial record observed through GPR surveying and coring is complex and reveals several shifts in the sedimentologic and hydrologic conditions in the valley. These changes document the Delaware River's response to postglacial climatic and environmental shifts and isostatic rebound, which could otherwise be obscured in downstream reaches of the river by the influence of sea-level rise.

The B1 boundary beneath Unit 1a likely represents a shift in depocenter away from this area as the glaciofluvial valley train migrated back and forth across the valley. The B1 and B1a surfaces merge in the distal area of the terrace, and together represent the change from glaciofluvial braided stream deposition to overbank deposition by the later single-channel stream.

Although no soil formation is observed at the B1 or B1a surfaces, clay laminae atop the B1a surface are interpreted as evidence of a small lake, with occasional floods contributing sands to the alternatingly oxic and anoxic reservoir. Therefore, the B1-B1a boundary likely represents an extended period of time of unknown duration (dating of the units and bounding surfaces is discussed in Chapter 2). The initial cessation of braided stream deposition and apparently minimal fluvial activity may coincide with glacial retreat from the drainage basin, resulting in a hydrologic lull prior to the reestablishment of a temperate precipitation regime (an idea that is explored further in Chapter 3).

Relatively rapid deposition of the bulk of Unit 2 is evidenced by minimal soil formation. The initial deposition of this unit may correspond to the cessation of dry, catibatic winds and increased precipitation. However, the apparent shift from braided to straight/meandering stream may be due to isostatic rebound which reversed drainage directions on small streams south of the study site by 10,430 +/- 30 BP (Stanford, 1993), as the river downcut and sought to reestablish an equilibrium profile (Blum and Tornqvist, 2000; Maddy and Bridgland, 2000).

Unit 2 fines upward in a pattern typical for overbank sedimentation, and is topped by the most well-developed buried soil in the deposit. This soil coincides with the B2 unconformity and together they represent a relatively stable paleolandscape, an ideal target for future cultural excavations. This soil may also coincide with one of the many climatic events to occur in New England and the Mid-Atlantic regions during the latest Pleistocene and Holocene, such as the Older or Younger Dryas, Bolling-Allerod, 9.2 Ka event, 8.2 Ka event, or Holocene thermal maximum or Hypsithermal (Peteet et al., 1990; Kneller and Peteet, 1993; Peteet et al., 1993; Peteet et al., 1994; Maenza-Gmelch, 1996; Mullins, 1998; Shemesh and Peteet, 1998; Kneller and Peteet, 1999; Peteet, 2000; Mullins and Halfman, 2001; Meyers, 2002; Ellis et al., 2004; Kaplan and Wolfe, 2006; Li et al., 2006; Newby et al., 2011).

Sedimentation of Unit 3 was relatively slow, since markers of soil formation such as organic carbon and carbonate content are relatively high throughout. This is consistent with localized deposition near the channel in the levee landform seen in the GPR data. Therefore, this unit represents a period of renewed sedimentation relative to the B1 surface, but slow deposition relative to units below. Soil formation atop the B1 surface is no more significant than the soil formation within, suggesting that the unconformity visible in the GPR data does not represent extended stability.

Finally, sedimentation of Unit 4 is bimodal: first coarser grained sediments infill lows, followed by slow and episodic overbank sedimentation as evidenced by high organic carbon and carbonate marking soil formation comparable to that in Unit 3. Deposition throughout this time is widespread and more volumetrically-abundant than during Unit 3's time. The basal, sandy beds may coincide with increased sedimentation during the period from 400-900 years ago that are found at the Manna archaeological site, a few km north of this locality (Stinchcomb et al., 2011). Future dating results may further constrain the timing of the two modes of sedimentation and their connection to events at other localities.

Conclusions

GPR surveying can supplement data provided by cores or two-dimensional outcrop studies. This study examines an alluvial fill terrace along the Delaware River, USA, and demonstrate the utility and limitations of GPR surveying as an alluvial architectural tool. Further, (as will be shown in Chapter 3) alluvial architectural information can be brought together with climate and isostasy or tectonism to understand extrinsic forcing mechanisms.

1) GPR shows unit thickness, distribution, and geometry to supplement information gleaned from cores and outcrops.
2) GPR at different frequencies (i.e. resolutions) is necessary to characterize smaller-scale elements of alluvial architecture such as crevasse splays and lake clays.
3) Differences between channel and overbank sediments and the full range of associated permeability characteristics may not be fully resolved with GPR.
4) GPR survey and core analysis at the study site reveals five allostratigraphic units bounded by four unconformable surfaces. High-amplitude radar reflectors are associated with two of these bounding surfaces, one associated with a dramatic change in grain size from gravel below to sand above, and one associated with increased organic matter and clay content coincident with a buried soil.

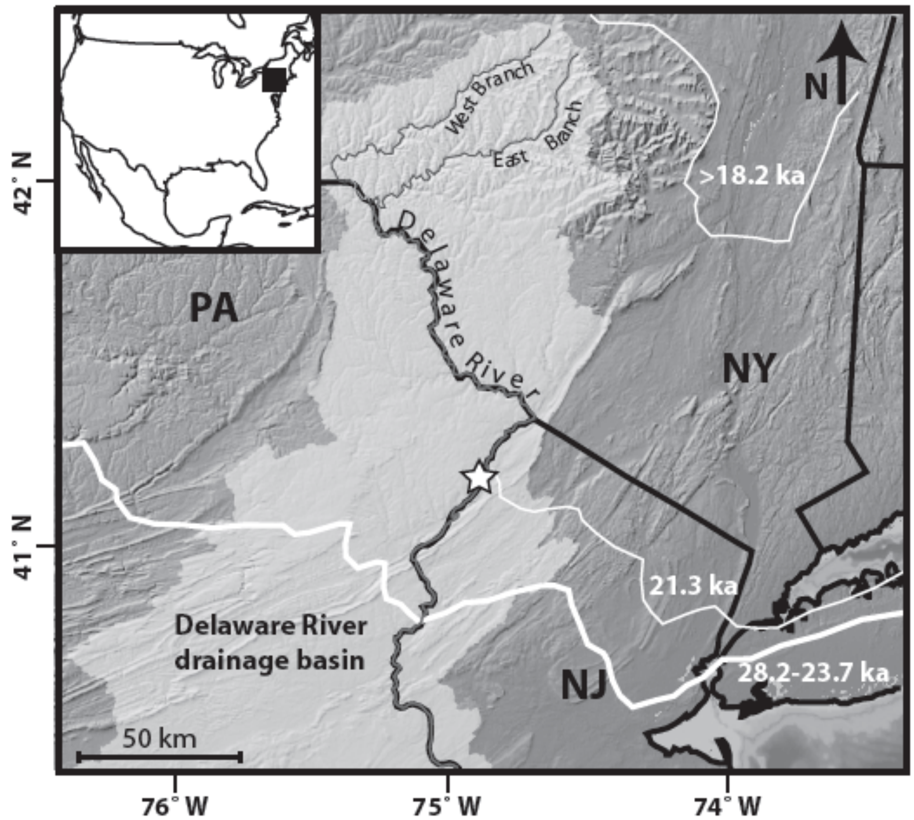

Figure 1: SIT study location, shown by the star, is located on the New Jersey bank of the Delaware River at 41°10'3"N, 74°53'39"W (detail of study area is shown in Figure 2). The last glacial maximum terminal moraine is shown by the bold white line; relevant recessional moraines are shown by the thin white lines (from Ridge, 2001). The Delaware River drainage basin is shaded in light gray. Inset map shows the location of the larger map by the square.

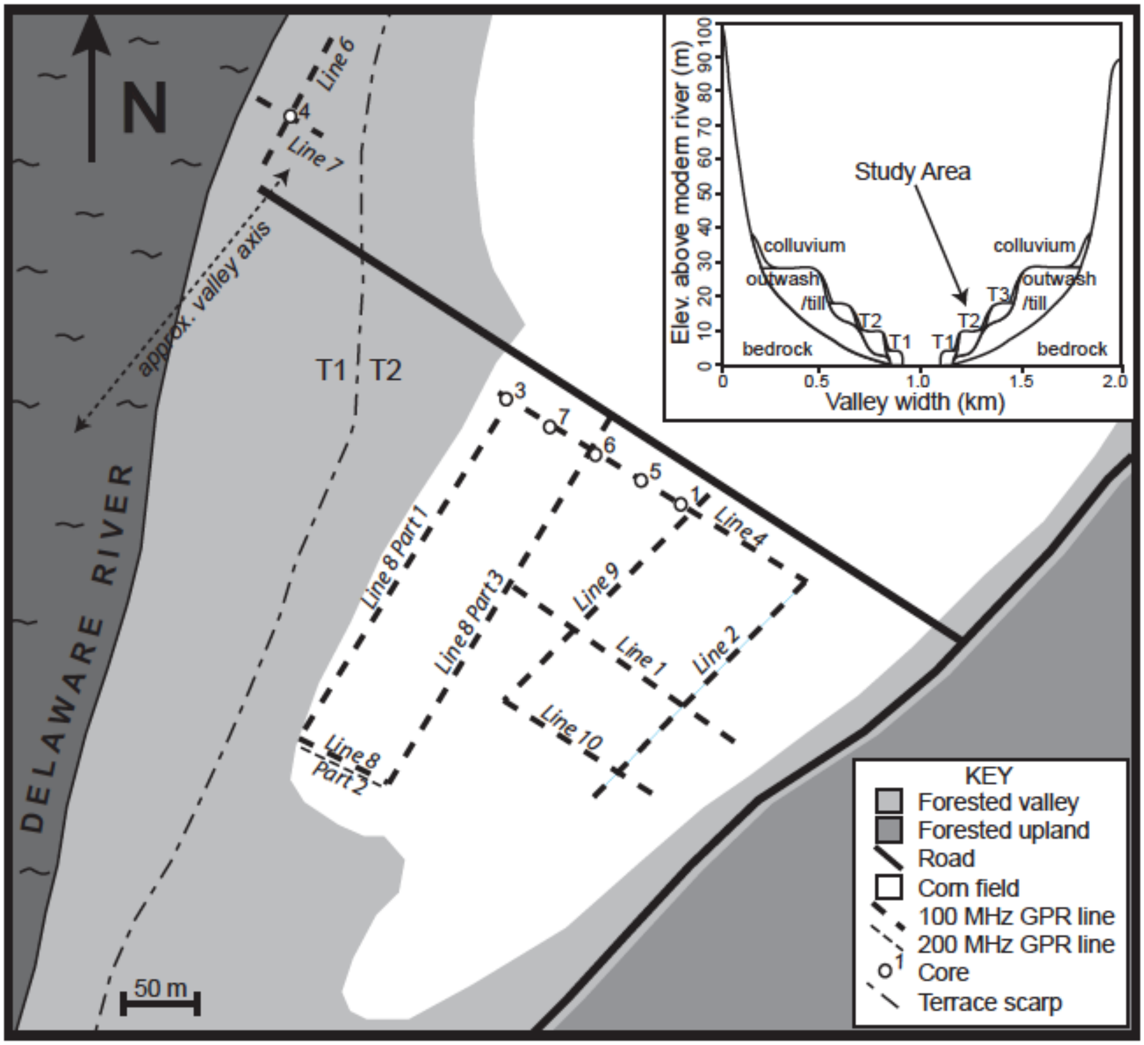

Figure 2: Locations of GPR lines and cores at the the SIT study site. All cores and GPR data shown here are located on the T1 and T2 terraces; T1 is examined in Chapter 3, and T3 is not present at the study site. Cores 1,3, 5, 6, and 7 were collected along one GPR line for direct comparison to radar facies and bounding surfaces. Glacial and alluvial landforms in the northern Delaware Valley are shown in the inset with generalized relative heights above the modern river.

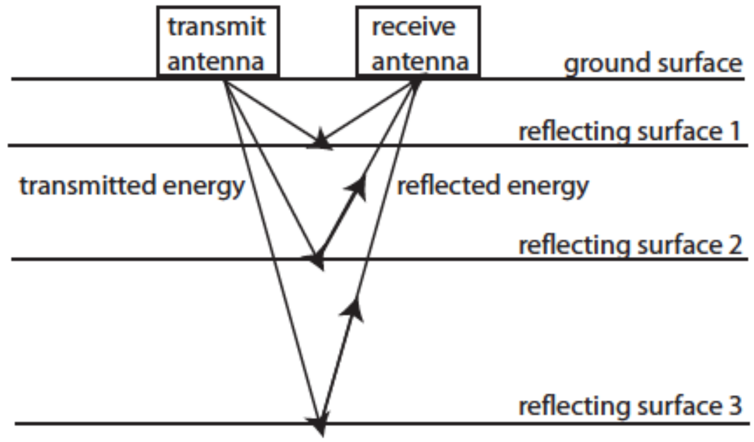

Figure 3: Diagram showing setup of radar antenna and transmitted and reflected energy with respect to subsurface contrasts in electromagnetic properties. Figure modified from Neal (2004).

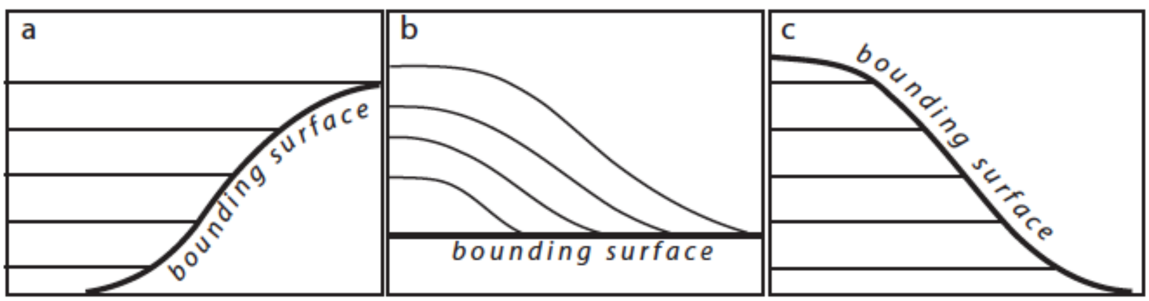

Figure 4: Sequence stratigraphic reflector terminations of onlap (a), downlap (b), and erosional truncation (c) define bounding surfaces between units within GPR data.

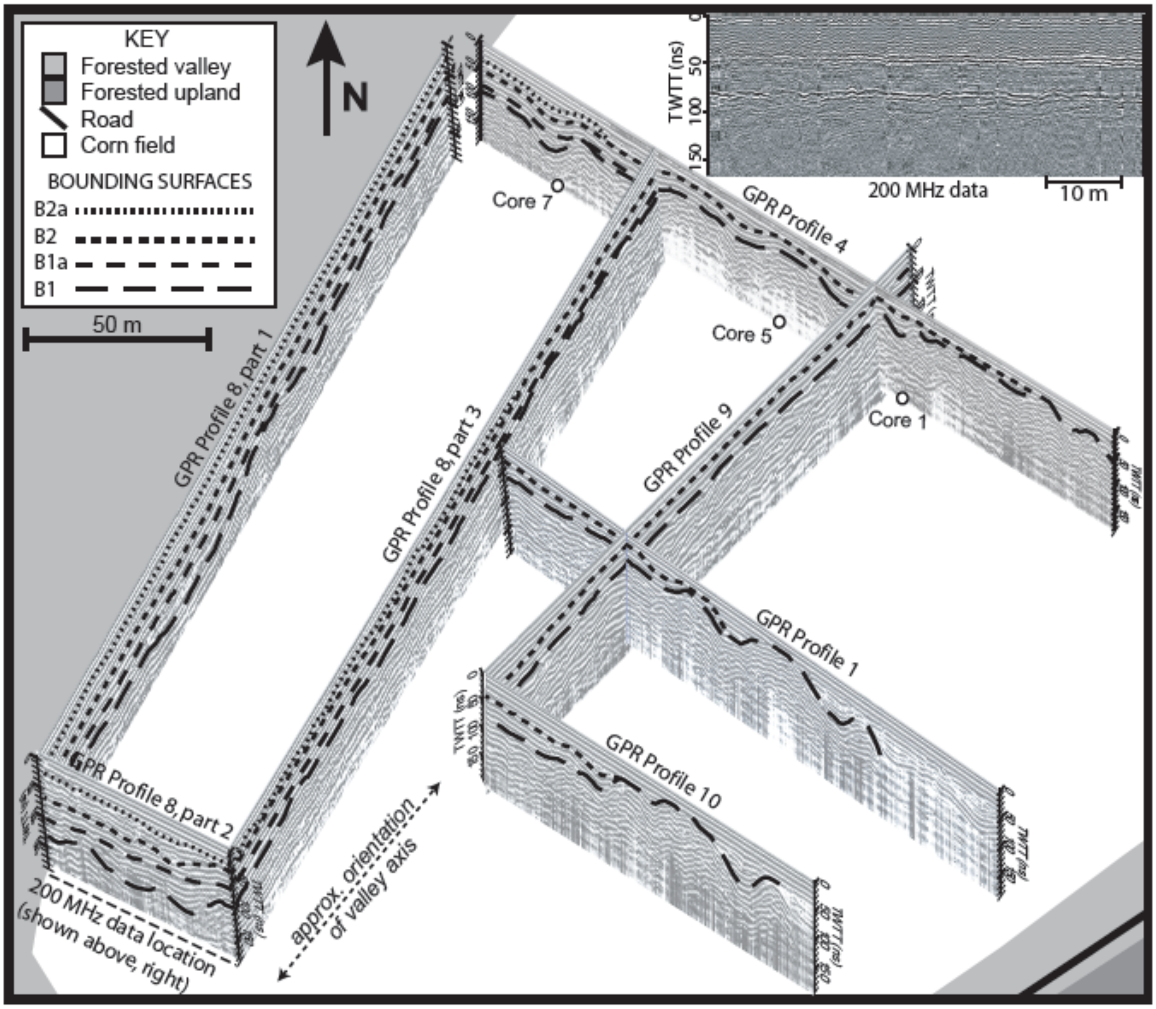

Figure 5: Fence diagram depiction GPR data from the study site, with bounding surfaces in 100 MHz data marked by dotted and dashed lines (see legend). Four bounding surfaces divide the strata into five depositional units. Two of the bounding surfaces (B1a and B2a) and two of the units (Unit 1a and Unit 3a) are present only in areas of the terrace proximal to the modern river (off the upper left corner of the figure). Three cores (1, 5, and 7) shown in the next figure are marked here; all core locations are shown in Figure 2. Orientation of the valley axis, shown by the dashed line, is shown for relative comparison to GPR profiles, since radar facies appearance of Unit 1 (below B1) varies relative to this axis. 200 MHz radar data shown at top right is located at bottom left (where marked)- radar amplitudes of this line show a dramatic increase in radar reflector strength coincident with the B1a and B2 bounding surfaces.

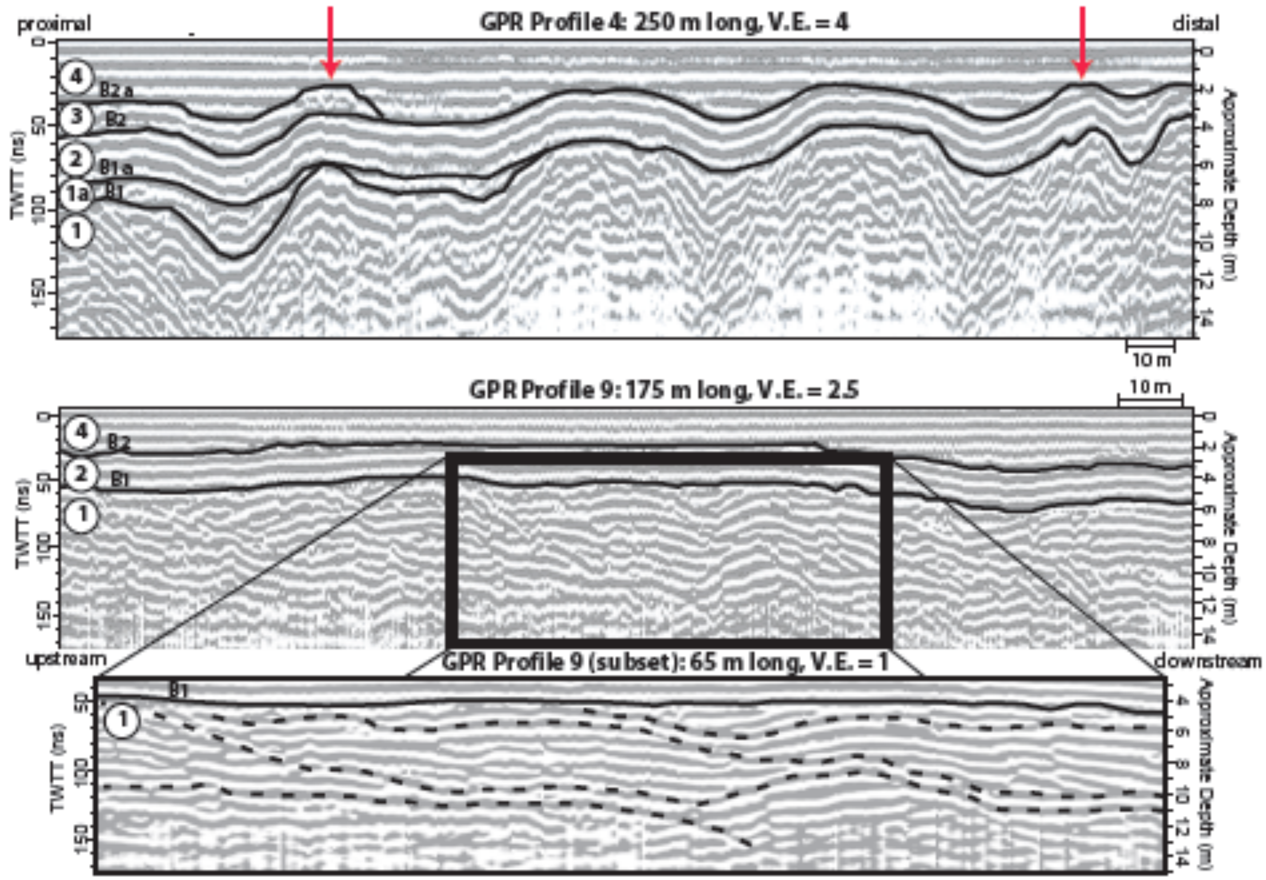

Figure 6a (top): GPR Profile 4, which runs perpendicular to the valley axis (and perpendicular to the modern river channel). Left arrow points to area of onlapping/downlapping reflectors in Unit 3; right arrow points to possible reflector termination of Unit 2. Figure 6b (bottom): GPR profile 9, which runs parallel to the valley axis (and parallel to the modern river channel).

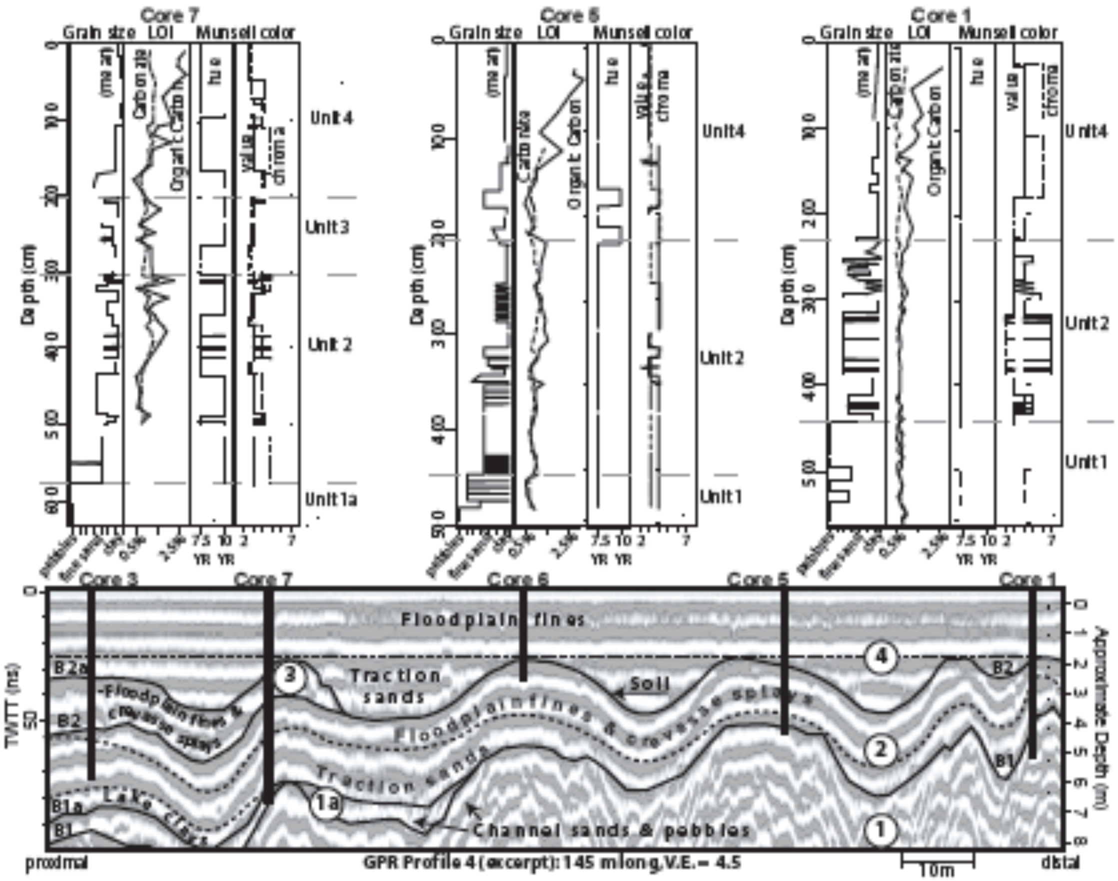

Figure 7: Part of GPR Line 4 (location shown on Figure 2), with bounding surfaces and units where it crosses Cores 7, 5, 1. Logs for Cores 7, 5, and 1 show mean grain size, Munsell color values, organic carbon and carbonate. Units distinguished based on GPR data are clearly visible in core logs as well, and thicknesses are within +/-10 cm for Units 3, 3a, and 1a, but GPR significantly overestimates the thickness of Unit 2.

Unit	Description of Radar Facies and Geometry	Architectural Elements	Classification
4	Moderate thickness, variable due to infilling of lows. Present across entire study area. Continuous, horizontal reflectors onlap onto boundary.	Buried soils Traction sands Overbank fines Backchannel	Channel and Floodplain
3	Wedge, thins rapidly away from channel. Semicontinuous, subhorizontal reflectors, onlap and downlap onto lower boundary. One erosional-trancation by upper boundary.	Buried soils Crevasse splays Levee sediments	Floodplain
2	Drape geometry thins at distal edge. Continuous, parallel, subhorizontal reflectors mirror lower bounding surface. Possible erosional truncation atop one high, onlaps onto lower boundary at thinning edge.	Buried soil Crevasse splays Overbank fines Traction sands Lake clays	Channel and Floodplain
1a	Drape or infilling near modern channel. Discontinuous reflectors onlap and downlap onto lower boundary and are truncated by upper boundary.	Outwash plain and braidplain channels	Channel
1	Total thickness unknown, but greater than 4 m, and present across entire study area. Undulating surface topography. Discontinuous reflectors onlap and downlap onto and are truncated by convex-upward, continuous reflectors dipping downstream. Short, discontinuous, and erratic reflectors.	Outwash plain and braidplain channels	Channel

Figure 8: Units distinguished at the study site are shown with radar facies depictions and descriptions, general descriptions, architectural elements, and classification of depositional environment. The composite stratigraphic section to the left shows a general trend of fining upward and increased soil development, as expected in terrace sediments. However, the bounding surfaces and variability of the units across the study area indicates several separate depositional regimes.

Material	**Relative dielectric permittivity (ε_r)**	**Electromagnetic wave velocity (m/nsec)**
Air	1	0.3
Freshwater	80	0.03
Unsaturated sand	2.55 - 7.5	0.1 - 0.2
Saturated sand	20 - 31.6	0.05 - 0.08
Unsaturated sand and gravel	3.5 - 6.5	0.09 - 0.13
Saturated sand and gravel	15.5 - 17.5	0.06
Unsaturated silt	2.5 - 5	0.09 - 0.12
Saturated silt	22 - 30	0.05 - 0.07
Unsaturated clay	2.5 - 5	0.09 - 0.12
Saturated clay	15 - 40	0.05 - 0.07

Table 1: Typical dielectric permittivities and radar velocities for different Earth materials. From Neal, 2004.

Lithofacies and Geometry	Radar Facies and Geometry	Architectural Element	Depositional Environment	Units
Predominantly clay layers with relatively high organic carbon; overall thickness less than other areas.	Basin-filling in incised channel, localized against valley wall. Reflectors planar with rapid attenuation of radar energy.	Back-channel	Floodplain	3
Fine sand, silt, and clay beds with high organic carbon and carbonate and gradational boundaries. Thins rapidly away from channel, max thickness 1 m.	Wedge, tapers away from channel and builds upon existing topography. Semi-continuous reflectors onlap and downlap onto surface below.	Levee	Floodplain	3a
Loamy silt and clay beds with ped structure, occasional root traces, and gradational lower and internal contacts.	Not resolved	Buried soil	Floodplain	2, 3a, 3
Gradational coarsening upward or fining-upward, moderately- to well-sorted, fine to coarse sands with a sharp lower boundary. Localized, 10s of cm thick.	Not resolved	Crevasse splay	Floodplain	2, 3a, 3
Loamy silt and clay beds with sharp basal contacts.	Laterally-extensive drape. Continuous reflectors planar or parallel to underlying surface.	Overbank	Floodplain	2, 3
Massive to graded, moderate- to well-sorted, medium to very coarse sand beds with occasional pebbles.	Laterally-extensive drape. Continuous reflectors planar or parallel to underlying surface.	Traction sands	Channel/ Floodplain	2, 3
Alternating oxidized/reduced clay laminae with occasional medium-coarse sand layers within. Basin-filling; max. thickness not cored.	Not resolved	Seasonally-stratified lake	Floodplain	2
Pebbles and gravels with variable sand/silt/clay matrix, thicknesss unresolved; medium-coarse sand units 10s of cm thick.	Laterally-extensive with relief on upper surface; and localized, basin-filling. Downstream-building clinoforms with internal packages of small reflectors, or discontinous.	Outwash plain and braidplain channels	Channel	1, 1a

Table 2: Description of architectural components of unconformity-bounded units at the study location. Lithofacies and geometry of each element is based on core descriptions; radar facies and geometry is derived exclusively from 100 MHz radar data.

Parameter	Chemical Weathering Ratio Formula	S1	S2	S3	S4	Change with Chemical Weathering/ Pedogenesis
LOI (%) *[1,3,9]	Δ mass after ignition	2.51	4.99	1.38	1.43	increase
Ba : Sr *[9]	Ba : Sr	7.46	8.71	7.21	6.75	increase
Silica : Sesquioxides *[1,9,10]	SiO_2 : (Al_2O_3+Fe_2O_3)	9.02	5.52	12.98	12.81	decrease
Bases : Alumina *[1,9,10]	(K_2O+Na_2O+CaO+ MgO): Al_2O_3	0.37	0.36	0.40	0.40	decrease
Parker's weathering index (WIP) *[7,8]	100 (K_2O/0.25 + Na_2O/0.35 + CaO/0.7 + MgO/0.9)	661	974	469	491	increase
Vogt's residual index (V) *[8]	(Al_2O_3+ K_2O)/(MgO +CaO+Na_2O)	7.02	7.61	6.36	6.38	increase
Chemical Index of Alteration (CIA) *[2,3,6,8]	100(Al_2O_3/(Al_2O_3+Na_2O+CaO+K_2O))	77.94	78.88	77.78	77.04	increase
Chemical Index of Weathering (CIW) *[2,4,8]	100(Al_2O_3/(Al_2O_3+Na_2O+CaO))	92.48	93.46	92.69	92.04	increase
Plagioclase Index of Alteration (PIA) *[8]	(100)((Al_2O_3- K_2O)/(Al_2O_3+CaO+ Na_2O- K_2O))	90.75	91.98	90.96	90.11	increase

Table 3: Chemical weathering ratios from four samples from Core 7, showing variations in degree of subaerial weathering consistent with soil formation ([1]Birkeland, 1999; [2]Chittleborough, 1991; [3]Fedo, Nesbitt, & Young, 1995; *[4]Harnois, 1988; *[5]Jenny, 1941; [6]Nesbitt & Young, 1989; [7]Parker, 1970; [8]Price & Velbel, 2003; [9]Retallack, 1990; [10]Ruxton, 1968).

Chapter 2: Optically stimulated luminescence dating of the central (T2) alluvial terrace in the Delaware Valley, New Jersey, USA

Introduction

The alluvial architecture of the T2 terrace records the influence of postglacial environmental changes, climatic events, and isostatic rebound on Delaware River sedimentation, but which factors influenced sedimentation and how is unclear from the alluvial record alone. Commonly used proxies for climate and environment such as isotopic signatures, pollen, and microfossils are often derived from lakes, which provide a better environment for their preservation than the high-energy, discontinuous sedimentation on a floodplain. Isostatic rebound is inferred primarily from shifting lake shorelines and reversals of drainage patterns at key points on the regional landscape in response to changing gradients. Therefore, firm correlations between alluvial deposition and the influence of climate, environment, or isostasy, or between local and regional-to-global events, depend on absolute age dates derived independently from all relevant records. Furthermore, knowledge of the timing of deposition allows rate calculations of processes such as aggradation, incision, or lateral migration.

Radiocarbon dating is one of the first radiometric dating techniques developed, and is the method most often used to determine the age of latest Pleistocene and Holocene alluvial deposits. However, at the study location, the only material suitable for radiocarbon dating was recovered from a charcoal-bearing interval in the T1 landform. Therefore, this method was not able to provide temporal constraints on the complex depositional record of the T2 terrace, believed to represent most of the Holocene sedimentary record in the valley, and other methods were necessary to provide age constraints on the deposition of the terrace through time.

Radiation dosimetry methods such as optically stimulated luminescence (OSL), thermoluminescence (TL), and electron spin resonance (ESR) directly date the time at which a sediment grain (usually quartz or feldspar) was last exposed to heat or daylight, providing an alternative age-dating option for environments without preserved organic carbon. These methods depend on the displacement of electrons within the structure of a mineral grain at a specific rate through time due to ambient radioactivity, which can be back-calculated to determine the time of burial. This chapter describes the OSL dating of four samples from the study site to constrain the timing of deposition of the alluvial architectural elements of the T2 landform.

Overview of OSL Dating

Introduction to Radiation Dosimetry

Radiation dosimetry dating methods (OSL, TL, and ESR) all depend on a similar process of mineral response to radiation in the environment. Mineral grains in the natural subsurface are exposed to three primary sources of radioactivity. The first source is alpha, beta, and gamma decay products from radioactive elements (especially U, K, Th, and Rb) incorporated into the dated grains themselves and the surrounding sediments. The second source of radioactivity is decay products produced by radioactive elements (particularly U) transported in groundwater. Finally, the third source is ionizing radiation from the atmosphere (Prescott & Hutton, 1994). Radioactive decay particles bombard the mineral grain, shifting electrons to higher-energy states in defects in the mineral's crystal lattice where they become trapped (Wintle, 1997). When exposed to light or heat, these electrons are excited and are able to migrate back to their appropriate sites (recombine), effectively re-zeroing the dating clock (Wintle, 1997). When these electrons move back into place, some energy is emitted in the form of light, which can be measured in a laboratory setting using sensitive photomultiplier tube detectors.

The amount of light emitted, called "natural luminescence intensity," is proportional to the radiation dose, or quantity of radiation the grain has been exposed to since its OSL 'clock' was last 'zeroed' by sunlight. However, each source material may respond differently to a given radiation dose due to the distinctive mineralogic properties created by that sediment's unique composition and history of crystallization, weathering, and diagenesis (Shulkov et al., 1997; Wintle, 1997; Zhou & Wintle, 1994). Therefore, radiation dose for each sample must be measured by calibrating natural luminescence intensity against artificial signals induced using a laboratory radiation source whose emission characteristics are well quantified (Wintle, 1997). In Single-Aliquot Regenerative (SAR) protocols which monitor for sensitivity changes that may result from laboratory treatments (Murray & Roberts, 1998; Wintle & Murray, 1999; Wintle & Murray, 2000), a series of induced signals are used to generate a dose response curve, from which the radiation dose that would produce the natural luminescence signal is interpolated (Wintle, 1997).

Radiation dose is acquired over time at a given dose rate. The dose rate from the surrounding sediment, which contributes the greatest portion of the signal, can be inferred from elemental data or measured directly (Adamiec & Aitken, 1998). Cosmic dose is calculated using two factors: the latitude of the study site and the depth of the sample due to attenuation (Prescott & Hutton, 1994). Finally, water table position information introduces additional uncertainty into the dose rate calculations due to the flux of water-soluble radiometric elements. Luminescence age, or the time since last exposure to sunlight, is calculated by comparing radiation dose with dose-rate.

Of these dating methods, OSL bleaching in quartz occurs most rapidly with exposure to daylight, making it most applicable for sediment dating purposes (Godfrey-Smith et al., 1988). Depending on the number of available electron traps in the mineral lattice and the dose-rate, which together determine the timing of signal saturation, quartz OSL may be applicable for sediments as young as one year up to nearly a million years of time since deposition (Huntley et al., 1985).

Common complications of OSL dating in alluvial settings

Achieving an accurate age with OSL is not without problems, particularly in alluvial settings. Grains only 'partially bleached' prior to their most recent burial retain the record of previous radiation dosage and yield an erroneously old age. Furthermore, unconformities, soils, and paleosols may have a wide range of affects on dose rate through time and dose distribution for individual grains within an aliquot. These concerns are discussed in the two sections below.

Partial Bleaching in an Alluvial Environment

Partial bleaching of the OSL signal, variability in the dose rate through time, radiometric disquilibrium between parent and daughter products in the decay chain, and non-uniform dose distribution are common complications which must be evaluated during the dating process (Krbetschek et al., 1994; Prescott & Hutton, 1995; Rodnight et al., 2006; Rosholt et al., 1966; Singarayer et al., 2005).

Partial bleaching of grains occurs when previously-dosed mineral grains are not exposed to full daylight during erosion and transport in the natural environment. In alluvial transport within the water column, individual mineral grains are commonly exposed to variable attenuation and scattering of daylight intensity and spectrum (Berger & Luternauer, 1987; Berger, 1990). Incomplete bleaching of grains may result in erroneously old ages, since the natural luminescence intensity measured will include movement of displaced electrons from radiation that occurred prior to the most recent depositional event (Wintle, 1997). Partial bleaching can be identified through careful examination of OSL age distributions for multiple aliquots (Rodnight et al., 2006; Singarayer et al., 2005). Where multiple statistical populations can be distinguished from various aliquots of a single sample, a minimum age model (MAM) can be used to separate out the youngest age population and eliminated inherited signal (Galbraith et al., 1999); where only one statistical population of ages is observed, as in this study, the effects of partial bleaching are assumed to be negligible and a central age model (CAM) is used.

The relative risk of partial bleaching may also be assessed to some degree by evaluation of the individual components of the luminescence signal. Different types of electron traps within the mineral’s crystal lattice may result in a gradation of response times in the re-zeroing process, translating to multiple emissions peaks that make up the continuous wave OSL decay (Bailey et al., 1997; Murray & Wintle, 2003; Singarayer & Bailey, 2003). Electrons that respond to the light or heat rapidly are termed the "fast" luminescence component, and make up the majority of the signal typically measured in the laboratory for most samples (A. S. Murray & Wintle, 2003). Using a technique called linearly-modulated OSL, additional peaks of light emission occur in succession over longer time periods of measurement, often called the medium and slow components, each broader than the last (Singarayer & Bailey, 2003). Significant contribution from a medium or slow luminescence component may contribute to partial bleaching, since these traps require longer exposure to light in order to be re-zeroed (Spencer, personal comm.).

Dose Rate Variation Due to Unconformities, Soils, and Paleosols

Dose rates for the conversion of radiation dose to age are, as described above, calculated based on the elemental composition or observed radioactivity of the sediment, the latitude and burial depth of the sample, and the influence of the water table. However, deposition in floodplain and alluvial terrace settings is inherently discontinuous, and periods of non-deposition (unconformities) often represent the vast majority of time within these deposits (Birkeland, 1999; Nanson & Croke, 1992; Retallack, 1990; Ritter et al., 2002). This complex environment continuously changes the sample's depth of burial with time, and with it the proportion of cosmic component of ionizing radiation time exposure vs. radiation from surrounding sediments. Cosmic radiation contributes only a small fraction (less than 10%) of an OSL dose; therefore, this only need be corrected for when dealing with unconformities on the order of tens of thousands of years (Spencer, personal comm.). Sediments within 30 cm of the surface also receive significantly less beta and gamma radiation from the surrounding sediment, potentially lowering the dose until further burial (Spencer, personal communication). Finally, sediment near this interface will receive radiation from sediments overlying and underlying the unconformable surface. If the two units have significantly different compositions, with different amounts of radioactive materials, dose rate must be calculated using components of the overlying and underlying sedimentary units (Spencer, personal comm.).

Dose rate is commonly estimated based on U, Th, K, and Rb in the sediment (where it cannot be measured in the field), with the assumption that parent elements have been present in the sediment since deposition, and daughter products were produced by in-situ radioactive decay and retained within the sediment (Adamiec & Aitken, 1998). However, uranium is soluble in oxidizing conditions (Ivanovich & Harmon, 1992); daughter ^{234}U is subject to preferential leaching over its parent ^{238}U (Krbetschek et al., 1994; Prescott & Hutton, 1995; Rosholt et al., 1966), and is thus subject to redistribution or removal from the profile. Radium is soluble as well, and radon is subject to removal from the sediments by gaseous diffusion (Krbetschek et al., 1994; Prescott & Hutton, 1995). Changes in the abundance of these isotopes with time will result in variability in dose rate. Therefore, dose rate must be re-evaluated where disequilibrium is suspected (Guibert et al., 2009; Krbetschek et al., 1994; Olley et al., 1996).

Unconformities in floodplain sediments are often marked by variable degrees of soil development (Birkeland, 1999; Retallack, 1990). The process of soil formation, or pedogenesis, is the alteration of the original characteristics of bedrock or a sedimentary deposit by the processes of additions, losses, transformations, and translocations (Jenny, 1941). Additions of biological materials such as plant debris and eolian sediment contribute new substances to the profile, while throughflow of water removes others. Original minerals are transformed in-situ to produce secondary minerals, such as the transformation of feldspars to clays. Translocation of fine-grained particles and soluble salts from the zone of eluviation (the A horizon) downward to the zone of illuviation (the B horizon), which gradually decreases with depth to unaltered material (the C horizon). The rates and proportions of these four processes in a given soil are influenced by a series of five specific soil-forming factors: climate, organisms, relief, parent material, and time (Jenny, 1941). Together, these processes impart soil profiles with their characteristic horizons and gradational internal boundaries. Depending on flood frequency and the thickness of sediment deposited in a given flood event, soils may be isolated within the sedimentary sequence, stacked one atop another, or even overprint the characteristics of a buried soil beneath (Kraus, 1999).

The process of soil formation can promote radiometric disequilibrium, relevant to OSL dating, in multiple ways (Rosholt et al., 1966). Leaching occurs in soils through groundwater infiltration and throughflow, removing soluble elements and elements that are sequestered in less stable minerals as those minerals break down in the near-surface environment. Alternatively, clay-rich soil horizons may present barriers to groundwater infiltration (Birkeland, 1999; Retallack, 1990), causing soluble elements to build up at this interface.

Finally, turbation within a soil can result in significant reworking of sediments, as mechanisms such as burrowing, root action, and even frost heave may redistribute grains vertically and laterally through the profile (Birkeland, 1999; Retallack, 1990). Non-uniform dose distribution from single aliquot measurements may suggest turbation of sediments, and single-grain measurements with D_e approaching zero within a profile can confirm downward motion of recently bleached grains (Bateman et al., 2007a; Bateman et al., 2007b; Forrest et al., 2003). Detailed down-profile studies demonstrate that zero-dose grains are most abundant in the top 5 to 50 cm of a soil (Bush & Feathers, 2003; Forrest et al., 2003). In fact, Bush and Feathers (2003) suggest that the abundance of zero-age grains in the top 5 cm is sufficient to allow a calculation of paleosol age, rather than depositional age. The depth to which grains are re-worked is likely to depend on the rate of biological activity in a soil profile and the duration of soil development, though tests of these ideas have not been reported in the scientific literature.

The presence of unconformities and associated paleosols can be detected with GPR profiles (see Chapter 1) tied to a coring program that provides sediment description and chemical weathering analyses (Birkeland, 1999; Retallack, 1990).

Study Methods

Core Recovery

OSL samples must be carefully protected from daylight during the coring and sampling process. Therefore, not all cores, nor all sections of a given core could be preserved for dating. Core sections for OSL dating were collected using specially prepared opaque plastic liners. These liners were left inside the metal core barrel in the field, and were removed from the core barrel at night with no additional light source.

Two four-foot (122-cm) sections of core SIT7 (Fig. 1), collected near the northwestern end of GPR Profile 4 (Chapter 1, Figures 2 and 5), were selected for preservation based on depths to the two major surfaces in the GPR data (Fig. 1). The third core section (8-12 feet or 244-366 cm) was preserved with the rationale that it would intersect the B2 bounding surface and provide dates for above and below this unconformity. The sixth and deepest core section (20-24 feet, or 610-732 cm) was preserved to constrain the initiation of deposition atop B1, the deepest bounding surface observed (Fig. 1). During Geoprobe coring, these two sections were collected using black opaque plastic core liners. The liners were left in the metal drill pipes in the field, to prevent any possible exposure to daylight. Plastic core liners were later transferred under darkness to thick, opaque PVC pipes with caps for storage until sampling. After OSL sampling (described below), the remainder of the core was split, sampled, and analyzed according to procedures outlined in the previous chapter.

OSL Sampling and Treatment

Core 7 was split and sampled for OSL dating under low-intensity red safe-lighting at Rutgers University in May of 2009. 10-cm samples were obtained at 277-287 cm (sample S1), 332-342 cm (S2), 630-640 cm (S3), and 650-660 cm (S4), with depth calculated by adding depth within the individual core section to the known depth of the top of each core section; two additional samples at a depth of 243-253 cm and 697-707 cm were collected but not processed or dated. Weight was recorded immediately upon sample collection from the cores to estimate water content in the field. Cores including the three lower samples (S2, S3, and S4) were completely water-saturated when collected, indicating that they were located below the water table at that time.

Further preparation was conducted at the Kansas State University luminescence laboratories under low-intensity red safe-lighting. Samples were dried at 50°C until mass stabilized (approximately four hours), then weighed and compared to wet mass to calculate original water content. Dried samples were sieved to isolate the 175-212 µm and 125-175 µm fine sand (coarse luminescence) grain size fractions to be used for dating; selection of the size fraction ultimately used for dating was based only on the volume of sample remaining after processing was complete. Samples were treated with 10% HCl for one hour to remove carbonates and 30% H_2O_2 for several days to remove organic matter. Heavy liquid separation using 2.70 gcm^{-3} lithium metatungstate (LMT) was used to isolate the silicate minerals, which were then subjected to one hour of 40% HF etching to remove feldspar grains and etch the surface of the quartz grains. This was followed by a final 10% HCl etch to remove any re-precipitates.

OSL measurements were performed on aliquots of ~5 mm diameter circles of quartz grains for each sample. Measurements were made using a Risø TL/OSL controller model TL/OSL-DA-20 (Bøtter-Jensen et al., 2003) using a modified single-aliquot regenerative-dose (SAR) protocol (Wintle & Murray, 2006) with post-IR blue light stimulation (Spencer & Robinson, 2008). Appropriate preheat treatments to isolate the thermally-stable OSL signal were determined by performing plateau tests using multiple aliquots of each sample (Spencer & Robinson, 2008), and cutheat was held at 125°C to prevent accumulation of charge in the 110°C TL trap (Murray & Wintle, 1998).

The first measurement of the OSL dating protocol for each aliquot measured the natural luminescence signal. Subsequently, the SAR dose-response curve was constructed by dosing the sediment with increasingly higher amounts of radiation that ultimately exceed the natural dose, followed by a measurement with no given dose, and a repetition of the first (lowest laboratory-induced) dose to evaluate any change in sensitivity from the first to last doses. The recycling ratio, or the ratio of the coordinates of the first and last data points (both given the same dose), was considered acceptable if it fell within 1.10 to 0.9 (Murray & Wintle, 2000). The zero-dose data point gives an indication of charge transferred from deeper electron traps, which will cause a small signal to appear even in the absence of a dose. This recuperation signal is described as a percentage of the equivalent dose (D_e), and aliquots with a recuperation signal >5% were discarded (Murray & Wintle, 2000). Dose recovery tests in response to given laboratory doses were performed on each aliquot to determine variations in sensitivity and precision of the measurement (Murray & Wintle, 2000). A ratio outside 10% of unity was considered unacceptable, meaning that if less than 90% or greater than 110% of the induced dose could be recovered, the measurement was considered unreliable and the measurement from that aliquot was not included in the calculation of dose for the sample.

Equivalent dose (D_e) values were estimated by interpolation of the natural OSL with saturating exponential best-fit curves for regenerative OSL measurements. Dose-distribution from replicated D_e measurements was assessed using radial plots (Galbraith,

1990) and estimates of over-dispersion, σ_b (Galbraith et al., 2005), together with geomorphological and sedimentological observations from the core samples. On the basis of this assessment an appropriate age model (Galbraith et al., 1999) was used to calculate D_e for each sample.

Dose Rate and Disequilibrium

20-g sub-samples of each of the four sediment samples collected for OSL dating were milled to a fine powder using a tungsten carbide mill in a shatter box, and approximately 3 g of powder was sent away to a commercial laboratory for ICP-MS and ICP-OES using Li-metaborate fusion. Results provided data on major and minor element abundance, from which a preliminary dose rate was derived based on U, Th, Rb (from ICP-MS) and K_2O (from ICP-OES). These values converted to annual dose using conversion factors from Adamiec and Aitken (1998), estimates of field moisture (Adamiec & Aitken, 1998), and latitude and depth of burial to assess the ionizing cosmogenic radiation component (Prescott & Hutton, 1994).

Quantities of all four samples were sent to Dr. Regina DeWitt and quantities of samples S2 and S4 were sent to Dr. Art Lukas, both at the Oklahoma Center for Radiation Physics at Oklahoma State University, for high-resolution gamma spectrometry to evaluate the possibility of radiometric disequilibrium. These measurements evaluated the emission lines of ^{234}Th (63 and 92 keV), ^{226}Ra (186 keV), ^{214}Bi and ^{214}Pb (295 keV, 351 keV, 609 keV, 1120 keV, and 1764 keV) and ^{210}Pb (46 keV). Of particular relevance are ^{234}Th and ^{226}Ra: ^{234}Th is used as an indicator of ^{238}U, the parent isotope for the U decay series (Fig. 2). ^{226}Ra is measured for itself, but is also an indicator of ^{234}U, the soluble daughter isotope of ^{238}U which cannot be directly measured. The average of the ^{226}Ra, ^{214}Bi, and ^{214}Pb emissions was used as a baseline, and radioactive disequilibrium was assumed if the difference between ^{234}Th and the baseline exceeded twice the standard error of the difference.

Results

Relevant Sedimentary and GPR Observations

Careful description of the sedimentary sections from which OSL samples are taken provides critical context for the data and ages obtained, as noted above. Sample S1 is located within unit 3a, which is characterized by fine grain sizes, gradational boundaries between beds, relatively dark colors, and relatively high organic carbon and carbonate contents, indicative of some soil formation (Fig. 3 this chapter and Ch. 1 Table 2). However, the absence of a pervasive unconformable surface at this depth in the GPR data suggests that the buried soils are not likely to be well-developed.

GPR ties to Core 7 suggested that sample S2 at 332 cm was likely above the B2 boundary (Fig. 1). However, GPR depths are first measured in two-way travel time to a buried feature and converted to depth using an average radar velocity. Small-scale velocity variations are common, and core-to-GPR ties can be off by up to 15% of calculated depth in this study (lithologic features suspected of generating radar reflector were found within +/- 20 cm of depths calculated from radar travel times converted to depth.). Examination of the core surrounding sample S2 under normal lighting conditions revealed darker colors and increased clay content, suggesting that the sample was likely from less than 10 cm below the unconformity (Fig. 3), within the lower A horizon (zone of eluviation) or upper B horizon (zone of illuviation) of the paleosol coincident with this unconformity. High organic carbon and carbonate values at the depth of the B2 surface in other cores provide further evidence of a paleosol, which would be expected to form on a surface that had been exposed for a significant period of time (Birkeland, 1999; Retallack, 1990).

Samples S3 and S4 are securely placed just above bounding surface B1 and within unit 2, and core descriptions of sediments at this depth are not indicative of any significant soil development (Fig. 3). Visual examination of the core under normal lighting conditions (after OSL samples were removed) suggests that the two samples are from the same depositional event, since they are within an individual bed with no variations in grain size or sedimentary structure.

Chemical Weathering Indices

ICP-MS and ICP-OES values derived for dose rate calculations also enabled the calculation of elemental ratios and weathering indices to estimate the degree of chemical weathering, including leaching, that a material has undergone (Birkeland, 1999; Chittleborough, 1991; Fedo et al., 1995; Harnois, 1988; Jenny, 1941; Nesbitt & Young, 1989; Parker, 1970; Price & Velbel, 2003; Retallack, 1990; Ruxton, 1968). Typically, these ratios are calculated based on chemical compositions of a given grain size (e.g. silt) only. However, since OSL procedures require bulk chemical data, ratios here are calculated using that bulk data in hopes that OSL researchers may be able to employ them with the data they already obtain. As a result, chemical weathering ratios using Ti have been eliminated, since it is more abundant in finer grain sizes (Chapman & Horn, 1968). Chemical weathering ratios for the four samples in this study are shown in Table 1.

Ba/Sr ratios in particular indicate degree of free drainage, leaching, and/or time of development of a soil horizon (Retallack, 1990). Commonly, Ba/Sr ratios are around 2 in most soils and rocks; however, in thoroughly-leached, acidic, sandy soils, Ba/Sr may approach 10 as Sr is preferentially dissolved and removed. Relatively high ratios in all four samples cannot indicate a lengthy time of formation, since the entire deposit likely accumulated within the past 14 ka. Therefore, the ratios must be taken to indicate some leaching throughout the profile, which is consistent with the commonly coarse-grained sediment. Despite its relatively fine grain size, which would impede free drainage, S2 again shows maximal alteration. This high value is most likely related to leaching during the formation of the paleosol, and suggests that U series disequilibrium will have the greatest impact on the OSL age for this sample.

Interpretations based on the weathering indices presented herein are most meaningful if the four samples are derived from the same, or similar, parent materials (same initial composition). Chemical indices to evaluate parent material uniformity have been developed (Anda et al., 2009; Chapman and Horn, 1968; Evans and Adams, 1975; Marsan et al., 1988; Reheis, 1990), but are not applied here due to the statistically-insignificant population of four samples. Therefore, relative parent material uniformity is assumed and chemical weathering ratios are interpreted (in the context of visual observations described above) to indicate some alteration of sample S1, significant alteration of sample S2, possible minimal alteration of sample S3, and little or no alteration of sample S4. These indicators are consistent with observations of pedogenic alteration (increased clay content, gradational boundaries) observed in the cores and LOI values discussed above.

Dose Rates and Disequilibria

Individual components of the dose rate, including the cosmic dose based on depth below surface, beta and gamma calculated by ICP-MS/ICP-OES, and beta and gamma measured during the two sets of high-resolution gamma spectrometry are shown in table 2. All three provided different results for the amount of parent radioactive isotopes present in the sediment, particularly K, resulting in a range of possible dose rates.

High-resolution gamma results from Dr. DeWitt conclusively demonstrated that samples S1 and S4 were in equilibrium, while samples S2 and S3 showed disequilibrium for ^{234}Th (an indicator of disequilibrium in ^{238}U).

OSL Dating Results

Measurement details for each sample are shown in table 2. A standard cutheat of 160ºC was used for all samples. Samples S1, S2, and S4 showed consistent plateau tests only at higher temperature preheats (240-280ºC out of a tested range of 180-280ºC). Sample S3 had inconsistent plateau tests at all preheat conditions, therefore its equivalent dose (D_e) could not be determined. Qualitative observations of linearly-modulated OSL showed that the luminescence signals are dominated by the fast component (Spencer, personal communication).

An example of a typical SAR growth curve for samples S1, S2, and S4 is shown in figure 4, with a single saturating exponential curve serving as the best fit for all data.

The D_e distributions for the samples are broadly symmetrical, suggesting one age population (Galbraith et al., 1999), and over-dispersion values (table 2) between 10-20% are consistent with typical natural doses. A central age model (Galbraith et al., 1999) was used to calculate D_e for each sample (Table 2).

Ages calculated using each set of dose rates from beta and gamma radiation and the resulting ages are shown in table 3. In addition to the three dose-rate results shown in table 2, a composite dose rate is calculated using the beta radiation detected by ICP and the gamma radiation measured by Dr. DeWitt (HRGS-1), which is considered the most reliable of the dose rates available (Spencer, DeWitt, personal communication).

Sample S1

Measurement of 36 aliquots of the 175-212 μm fraction of Sample S1 show that this sample has an equivalent dose D_e of 20.675 +/-0.323 Grays (Gy) (Fig. 5a). ICP method beta and gamma plus cosmic dose yield a total dose rate of 2.046 +/- 0.108 milliGrays per year (mGy/a), which is divided into D_e to translate to an age of 10.1 +/- 0.5 ka. HRGS-1 by Dr. DeWitt, plus cosmic dose, yields a much lower total dose rate of 1.437 +/- 0.061 mGy/a, or an age of 14.4 +/- 0.6 ka. Dr. Lukas did not measure sample S1, so HRGS-1 is the only set of high-resolution gamma spectrometry numbers available. The combination dose rate, using cosmic dose, gamma from HRGS-1, and beta from ICP, yields a dose rate of 1.783 +/- 0.092 mGy/a and an age of 11.6 +/- 0.6 ka, considered the best approximation of this sample's luminescence age. Overdispersion, a measure of variability within the set of 36 D_e measurements of sample S1 is 15%, suggesting one age population with possible minor turbation or partial bleaching.

Sample S2

Twenty-five individual aliquots of sample S2 were measured from the 125-175 μm fraction, resulting in a D_e of 22.122 +/-0.507 Gy (Fig. 5b). ICP-derived beta and gamma plus cosmic dose yield a total dose rate of 2.853 +/- 0.154 mGy/a, which translates to an age of 7.8 +/- 0.5 ka. HRGS-1 plus cosmic yields a dose rate of 1.816 +/- 0.070 mGy/a and an age of 12.2 +/- 0.5 ka, while HRGS-2 plus cosmic gives an intermediate dose rate of 2.612 +/- 0.094 mGy/a and an age of 8.5 +/- 0.4 ka. The composite ICP beta, HRGS-1 gamma, and cosmic dose rate for sample S2 is 2.704 +/- 0.133, giving an age of 8.2 +/- 0.4 ka. Overdispersion of S2 measurements is 20%, the highest for the three samples measured, suggesting one age population with some possible turbation or partial bleaching.

Sample S3

No D_e was determined due to the inconsistent behavior of aliquots of sample S3 under all preheat conditions, and no age can be estimated.

Sample S4

Twenty-two individual aliquots of the 175-212 μm fraction of sample S4 were measured, resulting in a D_e of 22.340 +/- 0.360 Gy (Fig. 5c). ICP plus cosmic doses give S4 a dose rate of 1.510 +/- 0.081 mGy/a and an age of 14.8 +/- 0.8 ka; HRGS-1 plus cosmic gives a dose rate of 1.186 +/- 0.055 mGy/a and an age of 18.8 +/- 0.9 ka; HRGS-2 plus cosmic gives a dose rate of 1.307 +/- 0.055 mGy/a and an age of 17.1 +/- 0.8 ka; finally, the combined ICP beta, HRGS-1 gamma, and cosmic dose rate is 1.377 +/- 0.073 mGy/a, translating to an age of 16.2 +/- 0.9 ka. Overdispersion for sample S4 is 11%, the lowest of the three samples, suggesting one age population with minimal turbation or partial bleaching.

Discussion

Dose-rate variability

Variations in dose rate between ICP-MS/OES and the two sets of high-resolution gamma spectrometry represent the greatest barrier to an age determination for samples S1, S2, and S4. The discrepancy in ages between ICP and HRGS-1 is greater than four thousand years for all three samples, an error of between 50-33% for the youngest sample, S2. The discrepancy between ages derived from HRGS-1 and HRGS-2 (available for samples S2 and S4) is more variable, at approximately 3,700 years (still perhaps 44% of the possible age) for S2 and 1,700 years (10% of the age) for S4.

Sample inhomogeneity is the primary hypothesis to explain the wide range of dose rates calculated using these three procedures. In order to obtain the 250 g of sediment necessary for the OSL dating procedure, each sample amalgamated approximately 10 cm of the approximately 5-cm diameter core sleeve. Individual beds observed in the cores at other intervals are commonly less than 1 cm thick, raising the possibility that each of the samples may include sediment from several sedimentologically and geochemically distinct layers. Furthermore, in soils or other sediments affected by subaerial weathering and leaching, such as sample S2, chemical weathering ratios may vary significantly centimeter-by-centimeter through the vertical section (Birkeland, 1999). Without thorough mixing, the sub-samples of the four samples that were measured by ICP, HRGS-1, and HRGS-2 may each have been geochemically distinct, resulting in the variable dose rates that plagued the study. While no clear conclusion can be reached, a careful homogenization process for samples recovered over such a 10-cm thickness of sediment might be recommended prior to dose rate measurements in the future. Alternately, cores larger than the 5-cm diameter Geoprobe cores used in this study, or multiple closely-spaced cores, should be used to increase sample volume.

S1-S2 Age Reversal

Sample S2 yields a slightly younger age than sample S1 for any single given set of dose rate results (i.e., comparing ICP to ICP, HRGS-1 to HRGS-1, and HRGS-2 to HRGS-2). The magnitude of this reversal within each set of dose rate results ranges from approximately 1,000-2,500 years, but the error bars for these measurements overlap, statistically indicating that these two samples have the same OSL age. The stratigraphic relationship between the two samples demonstrates that S2 was deposited, and buried, before sample S1 was deposited.

While dose rates are unclear already for reasons described above, the paleosol and its associated modifications in dose rate for samples S1 or S2 may cause S2 to appear younger than its burial age, or cause S1 to appear older. First, sample S2's location in the upper ~10 cm of a paleosol suggests that bioturbation, cryoturbation, or other soil circulation processes most likely mixed in zero-dose grains at the surface, delaying its acquiring a significant dose until that land surface became buried. Additionally, sample S1 is located less than 50 cm above the relatively clay-rich paleosol, which may serve as an impediment to infiltration of groundwater seeping downward through the strata during wet periods of the year. If this ponded groundwater carries significant dissolved ^{234}U, it may impart more radiation to sample S1 only for the period of time that the sediment remains saturated. This would mean that sample S1 received its given dose in less time, and the time over which the dose was acquired would be shorter (i.e., the sample would be younger) than the dose rates based only on the sediment geochemistry would suggest.

Correspondence Between Chemical Weathering Ratios and Disequilibrium

Given that radiometric disequilibrium occurs as a result of geochemical disruption, and that geochemical disruption is measured by chemical weathering ratios, it might be expected that there would be a relationship between samples' chemical weathering ratios and disequilibrium. All ratios indicate significant alteration of sample S2, the sample known to be in greatest U-series disequilibrium as demonstrated by high-resolution gamma mass spectrometry. However, most ratios show more alteration of sample S1 (known to be in equilibrium) than sample S3 (in disequilibrium). Since sample S1 is the only sample above the unconformity within the section, a difference in parent material could account for its relatively high ratios, and more data would be necessary to evaluate this possibility.

Nonetheless, the Chemical Index of Weathering (CIW), and the Plagioclase Index of Alteration (PIA) show sample S2 to be the most altered, and sample S3 to be the second-most altered, in correspondence with high-resolution spectrometry. More data and analysis from many locations may provide clear criteria by which these two ratios can be used to diagnose disequilibrium and the need for high-resolution spectrometry.

Inconsistent behavior of sample S3

All four samples dated in this study behaved inconsistently at the low preheat temperatures commonly used on young sediments. However, the likely provenance for this sediment is Paleozoic quartzite and sandstone from the New Jersey Highlands. Therefore, the sediment is likely to be geochemically altered and more similar to older sediments for the purpose of OSL dating, thus necessitating higher preheat temperatures.

Sample S3 showed inconsistent behavior even at 280°C, the highest recommended preheat temperature for OSL dating. No insights into this complication are available without further work and access to an OSL laboratory.

Conclusions

OSL dating of these samples did not result in firm geochronological constraint on the age of deposition, but the age ranges will be used in Chapter 3 to estimate timing of changes in deposition and boundaries between alluvial units. Several other important conclusions can be derived as a result of the work described herein:

1. OSL studies in terrestrial settings should take care to avoid unconformities and buried soils or paleosols due to associated complications with dose rate and mixing processes that complicate age determinations.
2. Samples from the Delaware River Valley show consistent plateau tests at higher preheat values than is common for young glacial and alluvial sediments, perhaps as a result of their provenance from the Paleozoic sedimentary bedrock of the Delaware Valley.

3. Radiometric disequilibrium affects some of the sediments of the Delaware River Valley alluvial terraces, and future attempts at OSL dating must take procedural steps to account for this disequilibrium.
4. Radiometric disequilibrium in sediments may be detected in some cases using the Chemical Index of Weathering (CIW), and the Plagioclase Index of Alteration (PIA). More work is needed to fully elucidate these relationships.
5. Coring for OSL dating should be conducted using core barrels larger than the standard 5-cm Geoprobe diameter, or with multiple closely-spaced cores to provide additional sample volume. Where such small core barrels are necessary and 10-cm thick core samples must be used, homogenization prior to treatment and measurement is recommended.

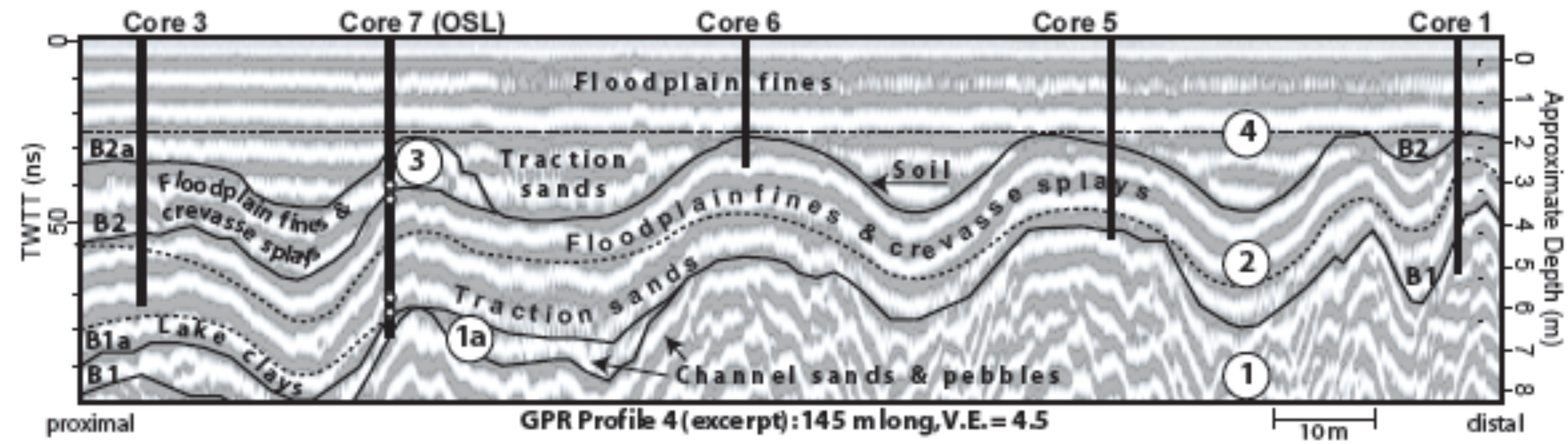

Figure 1: Part of GPR Line 4 (location shown on Chapter 1, Figure 2). Allostratigraphic units are marked with round numbered labels 1-4 (see Chapter 1). Bounding surfaces B1, B1a, B2, and B2a, are marked by solid black lines. Dashed lines separate traction and suspended load sediments not distinguished by radar facies. White circles on Core 7, the core sampled for OSL dating, show the depths of the OSL samples S1-S4. For detailed core logs of Core 7 with OSL age ranges, see Figure 3 (this chapter).

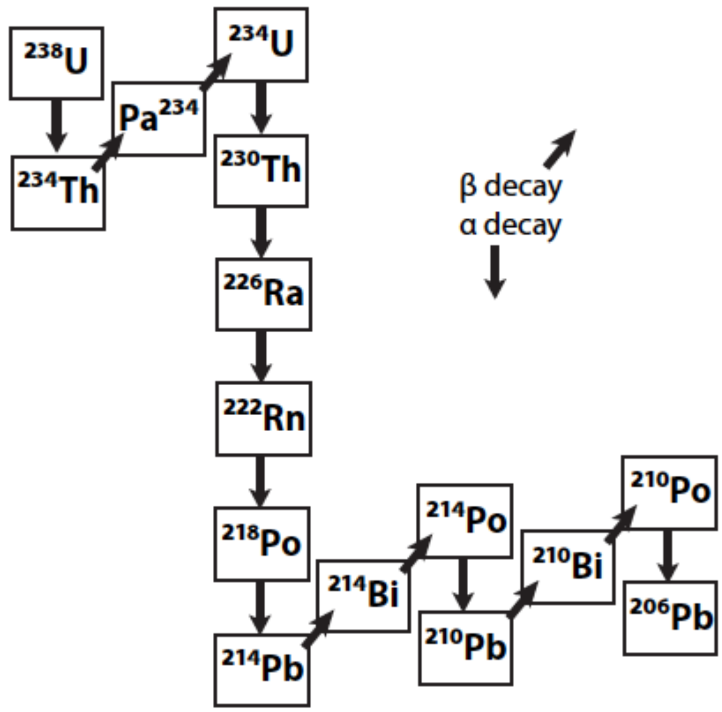

Figure 2: Primary Uranium decay series, reproduced from Hensaw and Camplin (http://www.camplin.talktalk.net/Tastrak/TNotes/Chap6.htm). High-resolution gamma mass spectrometry measurements evaluated the emission lines of Thorium-234, Radium-226, Bismuth-214, Lead-214 and Lead-210. Thorium-234 is used as an indicator of Uranium-238, while Radium-226 is measured for itself and as an indicator of Uranium-234. The average of the Radium-226, Bismuth-214, and Lead-214 emissions was used as a baseline, and if the difference between Thorium-234 and the baseline exceeded twice the standard error of the difference, radioactive disequilibrium was assumed.

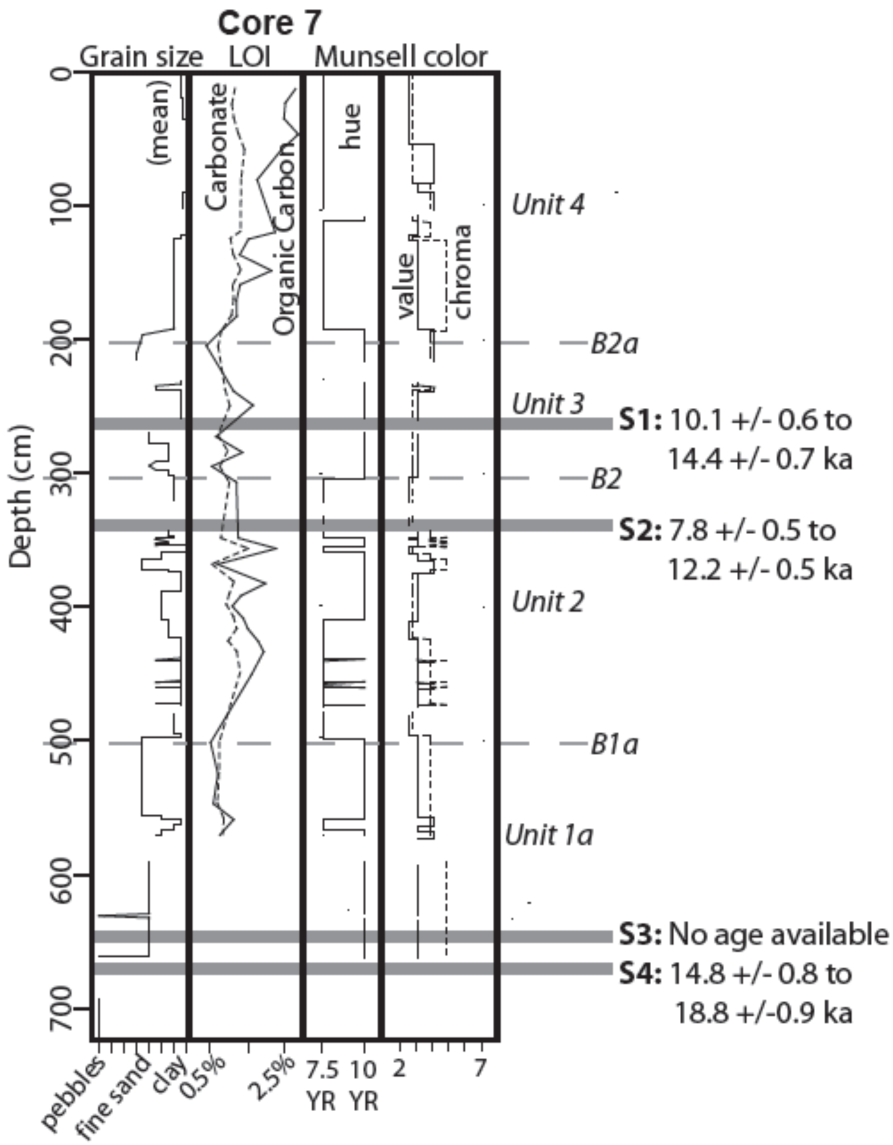

Figure 3: Depths and derived ages of OSL samples S1-S4 within Core 7 (location on Chapter 1, Figure 2), shown in context of the geochemical and physical properties of the core, as well as units and the bounding surfaces separating them. Ages for OSL samples S1, S2, and S4 are presented as ranges that include all four sets of calculations presented in Table 3.

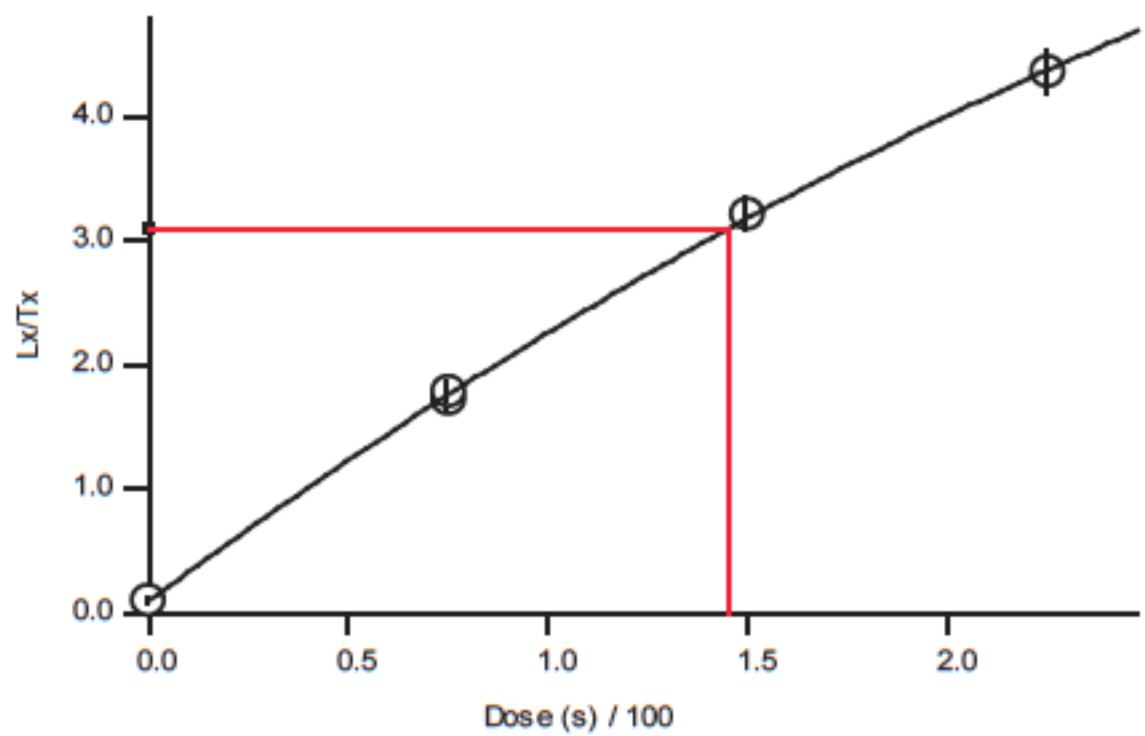

Figure 4: Representative single-aliquot regenerative dose curve for sample S4 as an demonstration of the OSL procedure'. First, natural luminescence response is measured (value shown by intersection of red box with luminescence response-Lx/Tx- axis). Then, known doses (in seconds, with a known dose rate of 0.1609 Gy/s) are administered to the same grain, and the luminescence response (Lx/Tx) to those doses is measured (data points shown) to reconstruct a quadratic curve to fit the data. Using this curve, the dose that corresponded to the natural response can be interpolated (value shown by intersection of red box with dose/100 axis). In this aliquot, the equivalent dose for the natural response was interpolated to be 145.28 +/- 6.81 seconds A single saturating exponential curve, as shown, was the best statistical fit for all data in this study.

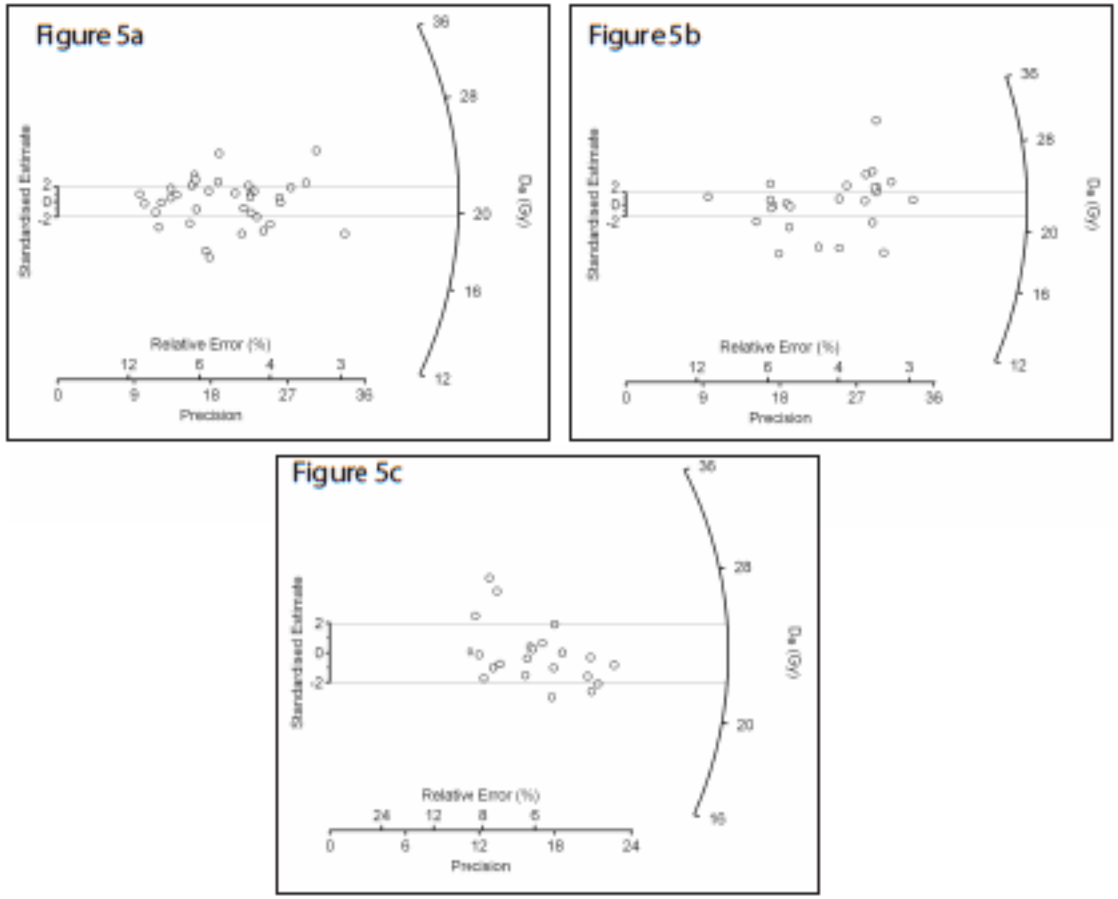

Figure 5a:Radial plot of equivalent dose for sample S1 (n = 36).
Figure 5b: Radial plot of equivalent dose for sample S2 (n = 25).
Figure 5c: Radial plot of equivalent dose for sample S4 (n = 22).

OSL dating summary data for samples from core #7

	S1		S2		S3		S4	
Sample details								
Grain size (μm)	175-212		125-175		175-212		175-212	
Sample depth (cm)	277		332		630		650	
Equivalent dose data								
No. aliquots	36		25		----		22	
σ_b (%)	15		20		----		11	
D_e (Gy)	20.7 ±	0.32	22.1 ±	0.51	----	----	23.3 ±	0.36
Heat treatments								
Preheat °C	280		240		----		280	
Cutheat °C	160		160		----		160	
Dose-rate data								
ICPMS/ICPOES								
U (ppm)	3.1 ±	0.47	5.2 ±	0.78	1.5 ±	0.23	1.6 ±	0.24
Th (ppm)	8.6 ±	0.86	11.9 ±	1.19	4.9 ±	0.49	5.2 ±	0.52
K_2O (%)	1.19 ±	0.06	1.81 ±	0.09	0.84 ±	0.04	0.88 ±	0.04
Rb (ppm)	50 ±	7.5	80 ±	12	33 ±	4.95	34 ±	5.1
HRGS-1 ($Bq.kg^{-1}$)								
U (ppm)	1.653 ±	0.12	2.13 ±	0.15	0.96 ±	0.07	1.01 ±	0.07
Th (ppm)	6.681 ±	0.41	8.86 ±	0.53	4.38 ±	0.27	4.37 ±	0.27
K (%)	0.869 ±	0.05	1.29 ±	0.05	0.67 ±	0.03	0.71 ±	0.04
HRGS-2 ($Bq.kg^{-1}$)								
^{226}Ra & daughters	----	----	2.8 ±	0.2	----	----	1.33 ±	0.09
^{228}Ra & ^{228}Th	----	----	12.1 ±	0.73	----	----	6.03 ±	0.36
^{40}K	----	----	2.05 ±	0.05	----	----	0.66 ±	0.02
$W_{in\ situ}$ (%)	23.13		30.97		5.78		8.34	

Table 1: OSL dating summary for samples S1-S4 from Core 7. De is equivalent dose, and σb is overdispersion.

Sample S1- D_e= 20.675 Gy, error=0.323 Gy, Cosmic dose rate= 0.144 +/- 0.014 $mGya^{-1}$

	ICP-MS and ICP-OES	*HRGS-1	**HRGS-2	ICP beta, HRGS-1 gamma
Beta ($mGya^{-1}$)	1.072 +/- 0.084	0.726 +/- 0.050	----------	1.072 +/- 0.084
Gamma ($mGya^{-1}$)	0.830 +/- 0.066	0.567 +/- 0.033	----------	0.567 +/- 0.033
Total dose rate ($mGya^{-1}$)	2.046 +/- 0.108	1.437 +/- 0.061	----------	1.783 +/- 0.092
Age (ka)	**10.1 +/- 0.6**	**14.4 +/- 0.7**	----------	**11.6 +/- 0.6**

Sample S2- D_e=22.122 Gy, error=0.507 Gy, Cosmic dose rate= 0.134 +/- 0.013 $mGya^{-1}$

	ICP-MS and ICP-OES	*HRGS-1	**HRGS-2	ICP beta, HRGS-2 gamma
Beta ($mGya^{-1}$)	1.541 +/- 0.121	0.961 +/- 0.056	1.449 +/- 0.076	1.541 +/- 0.121
Gamma ($mGya^{-1}$)	1.178 +/- 0.093	0.722 +/- 0.039	1.029 +/- 0.054	1.029 +/- 0.054
Total dose rate ($mGya^{-1}$)	2.853 +/- 0.154	1.816 +/- 0.070	2.612 +/- 0.094	2.704 +/- 0.133
Age (ka)	**7.8 +/- 0.5**	**12.2 +/- 0.5**	**8.5 +/- 0.4**	**8.2 +/- 0.4**

Sample S3- D_e undetermined, Cosmic dose rate= 0.094 +/- 0.009 $mGya^{-1}$

	ICP-MS and ICP-OES	*HRGS-1	**HRGS-2	ICP beta, HRGS-1 gamma
Beta ($mGya^{-1}$)	0.814 +/- 0.065	0.623 +/- 0.044	----------	0.814 +/- 0.065
Gamma ($mGya^{-1}$)	0.569 +/- 0.045	0.450 +/- 0.029	----------	0.450 +/- 0.029
Total dose rate ($mGya^{-1}$)	1.5 +/- 0.1	1.2 +/- 0.1	----------	1.4 +/- 0.1

Sample S4- D_e= 22.340 Gy, error=0.360 Gy, Cosmic dose rate= 0.091 +/- 0.009 $mGya^{-1}$

	ICP-MS and ICP-OES	*HRGS-1	**HRGS-2	ICP beta, HRGS-1 gamma
Beta ($mGya^{-1}$)	0.832 +/- 0.066	0.641 +/- 0.046	0.670 +/- 0.043	0.832 +/- 0.066
Gamma ($mGya^{-1}$)	0.586 +/- 0.046	0.453 +/- 0.028	0.546 +/- 0.034	0.453 +/- 0.028
Total dose rate ($mGya^{-1}$)	1.510 +/- 0.081	1.186 +/- 0.055	1.307 +/- 0.055	1.377 +/- 0.073
Age (ka)	**14.8 +/- 0.8**	**18.8 +/- 0.9**	**17.1 +/- 0.8**	**16.2 +/- 0.9**

**Analyses performed by Dr. Regina DeWitt*

***Analyses performed by Dr. Art Lukas*

Table 2: OSL dose rates via ICP, HRGS-1 (performed by Dr. DeWitt), and HRGS-2 (performed by Dr. Art Lukas), and their resulting ages. The combination of beta dose rate from ICP and gamma dose rate from HRGS-1 is considered most reliable.

CHAPTER 3: POSTGLACIAL INFLUENCES ON FLUVIAL PROCESSES AND LANDSCAPE FORMATION HISTORY OF THE NORTHERN DELAWARE RIVER VALLEY, NEW JERSEY

Introduction

Terraces and alluvial deposits worldwide have been studied as archives of climatic and environmental fluctuations, particularly in the context of the glacial-interglacial dynamic of the Quaternary (Blum & Tornqvist, 2000; Bridgland & Westaway, 2008; Bull, 1991; Starkel, 2003; Vandenberghe, 2003). These studies have provided general guidelines for how terraces and other alluvial deposits are formed and modified in areas of active uplift (Lewin & Gibbard, 2010; Maddy, 1997; Maddy et al., 2001; Olszak, 2011; Westaway et al., 2009) during glacial conditions, interglacial conditions, and transitions from glacial to interglacial (Brown et al., 2010; Church & Ryder, 1972; Dutta et al., 2012; Lewin & Gibbard, 2010; Olszak, 2011; Pazzaglia, in press; van den Berg, 2006; Vandenberghe, 2008), with variations in response according to features of a given basin or valley reach such as bedrock, latitude, altitude, prevailing moisture regime, and other factors (Blum & Valastro, 1994; Bull, 1991; Pazzaglia, in press; Vandenberghe, 2003). Documenting the late-Pleistocene to early-Holocene terrace formation and alluvial depositional changes along the Delaware places this valley within regional and global models of this response.

Beyond the basic response of the Delaware River to interglacial vs. glacial conditions, alluviation and terrace formation may have experienced the impact of some or all of the numerous late-Pleistocene and Holocene temperature and precipitation events that have been documented through mid-Atlantic and northeastern lake (Dwyer et al., 1996; Ellis et al., 2004; Kneller & Peteet, 1993; Li et al., 2006; Maenza-Gmelch, 1996; Meyers, 1996; Mullins, 1998; Mullins & Halfman, 2001; Peteet et al., 1993; Peteet et al., 1994; Yu, 2000; Yu, 2007; Zhao et al., 2010), bog (Russell & Stanford, 2000), marsh (Pederson et al., 2005;), and swamp (Peteet et al., 1990; Peteet et al., 1994) sediment records, including global or northern hemisphere-wide climatic fluctuations such as the Younger Dryas (Andres et al., 2003; Peteet, 1995), 9 ka insolation maximum and the subsequent Mid-Holocene Hypsithermal (Harrison et al., 2003), and the 8.2 ka cold event (Alley & Agustsdottir, 2005; Morrill & Jacobsen, 2005). These changes can have dramatic impacts on drainage basins and flood characteristics (Coulthard et al., 2005; Knox, 2000), even when the magnitude of climate change is modest (Knox, 1993; Macklin & Lewin, 2003). Deciphering the specific influence of past events on Delaware terrace (created primarily by past sedimentation) and floodplain (defined by active sedimentation) sedimentation will both provide a more nuanced understanding of the geologic record and perspective on the likely impact of future climate change (Goudie, 2006).

Finally, the human impact on sedimentation cannot be overlooked in the Delaware Valley. Current modeling and observational results demonstrate that Anthropocene (Crutzen & Stoermer, 2000) alteration of drainage basins has increased the magnitude and frequency of flood events by intensifying runoff, as well as promoting soil erosion and sediment mobilization (Burns et al., 2005; Chin, 2006; Inman & Jenkins, 1999; Jennings & Jarnagin, 2002; Knox, 2006; Milly et al., 2002; Rose & Peters, 2001).

However, Native Americans first entered the valley around 12,000 years ago (Stewart, 2005), and Europeans began to settle and utilize the valley for its natural resources soon after their arrival on the North American continent. Archaeological records and modeling results elsewhere have shown drainage system disruptions during the historical period (Casana, 2008; Dotterweich, 2008; Notebaert et al., 2011), and recent evidence has begun to point to a human influence on sedimentation in the Delaware Valley prior to European colonization (Stinchcomb et al., 2011; Stinchcomb et al., 2012). Further deciphering the record of sedimentation in the Delaware valley will help to clarify the timing and nature of the human impact on this alluvial system, the related landscapes upon which people reside, and the resources they require.

Background

Terrace Formation

The formation of terraces requires vertical channel incision to create accommodation space for the modern river and preservation of progressively older terraces at higher positions along a valley wall. According to fluvial theory and observation, rivers develop a longitudinally concave-up equilibrium profile that allows the prevailing discharge to efficiently transport sediment of the prevailing grain size in that river reach: Gradient is high upstream where discharge is low and mean grain size is large, gradient is low downstream where discharge increases and grain size is small (Baker & Ritter, 1975; Bull, 1979; Knox, 1975; Pazzaglia, in press; Sinha & Parker, 1996). During extended periods of equilibrium when the channel is at-capacity in terms of sediment load, it is best equipped for abrasion: Wide straths are carved through lateral incision, at a rate controlled by the ratio of discharge to sediment load (Hancock & Anderson, 2002; Montgomery, 2004; Pazzaglia, in press; Sklar & Dietrich, 1998).

Vertical incision occurs periodically as streams seek to reach a new equilibrium profile in response to a wide range of events that include 1) climate change (Vandenberghe, 2003), 2) base level fall through eustasy (Schumm, 1993a; Stanford, Ashley, & Brenner, 2001) and consequent knickpoint migration (Loget & Van Den Driessche, 2009), 3) post-glacial and denudational isostatic rebound and flexural deformation (Maddy & Bridgland, 2000; Pazzaglia & Gardner, 1993), 4) active tectonic deformation (Bridgland et al., 2003; Dutta et al., 2012; Litchfield & Berryman, 2006; Pazzaglia & Brandon, 2001; Turowski et al., 2006), or a combination thereof. Variations in the rate of channel downcutting allow the formation of the discrete terrace steps observed in many alluvial valleys around the world.

Quaternary glacial-interglacial climate change is widely regarded as driving changes in the rate of vertical incision (Bridgland & Westaway, 2008; Pazzaglia, in press; Vandenberghe, 2003), even in rapidly uplifting settings such as the sub-Himalaya fold and thrust belt (Dutta et al., 2012). In this context, alterations to basin hydrology increase or decrease overall discharge and its seasonality and intensity, affecting stream capacity (the total amount of sediment a stream can transport). Corresponding changes alter sediment grain size and sediment flux with the influence (or cessation of influence) of glacial erosion, rapid physical weathering due to freeze-thaw and frost wedging in the periglacial environment, and permafrost soil circulation processes, and the stabilizing influence of vegetation on hillslopes (Birkeland, 1999).

Climatically-controlled changes in discharge and sediment flux can cause transient episodes of vertical incision or aggradation as the channel moves back into equilibrium. When discharge is low or flashy, sediment flux is high, prevailing grain size large, aggradation occurs and the channel reach steepens locally to compensate (Pazzaglia, in press). When sediment input and grain size are relatively low and discharge relatively high, the channel incises vertically into bedrock to create a strath terrace, or into its previous alluvial deposit to create a fill terrace. Further vertical incision and profile adjustment may result from an increase in precipitation intensity and peak annual discharge (Deither, 2001; Pazzaglia, in press; Roe et al., 2002; Zaprowski et al., 2005).

Terrace formation in a given river system commonly occurs as a short-term response to a change in climate, rather than a steady-state process associated with a given regime. Vertical incision is estimated to account for perhaps 10-25% of the time of a given glacial-interglacial cycle (Pazzaglia, in press). The timing of different phases of terrace genesis is not uniformly in-phase with glacial and interglacial stages worldwide, but depends on factors such as altitude, latitude, presence of absence of glaciers, prevailing moisture regime, and substrate (Blum, 1993; Pazzaglia, in press; Wegmann & Pazzaglia, 2009). In colder, wetter, high-latitude, or glaciated valleys, strath-cutting (at capacity) or aggradation (at times of over-capacity) occurs during glacial conditions, when precipitation is decreased and sediment delivery is maximized by paraglacial, periglacial, and glacial erosion in the absence of stabilizing vegetative cover; interglacial periods are characterized by decreased sediment yield and incision of the previous alluvial fill, creating a fill terrace (Bull & Kneupfer, 1987; Church & Ryder, 1972;

Formento-Trigilio et al., 2002; Pazzaglia, in press; Ridge et al., 1992; Ritter et al., 1993; van den Berg & van Hoof, 2001). The Pleistocene upper Delaware valley was such a system. Conversely, semi-arid or Mediterranean climates in unglaciated areas typically receive increased moisture during the glacial period, allowing vegetation to colonize slopes and stabilize soils; later, as climate begins to warm the vegetation dies off in response to increasing aridity, and sediment delivery and channel aggradation therefore peak at the glacial-interglacial transition (Blum & Valastro, 1994; Bull, 1991; Pazzaglia, in press; Ritter et al., 2000). In temperate, lowland settings, both the transition to glacial and the transition to interglacial may be marked by periods of vertical incision, with preferential preservation of the former (Vandenberghe, 2008).

Vertical incision of a valley floor widened by strath cutting or buried by alluvial fill can be promoted by a change in gradient (Patton & Schumm, 1975; Pazzaglia, in press). In recently-glaciated areas, an increase in gradient during the interglacial can be achieved through isostatic rebound of the crust in response to glacial retreat (Maddy & Bridgland, 2000). Alternately, river reaches in coastal and lowland areas may incise due to a eustatic drop during the glacial period, depending on accommodation space, discharge, sediment flux, and slope of the exposed coast relative to that of the channel (Blum & Tornqvist, 2000; Bull & Kneupfer, 1987; Nesci & Savelli, 2003; Pazzaglia & Brandon, 2001; Pazzaglia, in press; Schumm, 1993b). While the upper Delaware is beyond the reach of eustatic influence, isostatic rebound and climatically-driven changes in moisture and temperature must be taken into consideration to understand terrace deposition and incision timing and influences at the study site.

Floodplain Sedimentation and Soil Formation

Alluvial sedimentation upon a floodplain or terrace records contemporary hydrologic conditions (Nanson & Croke, 1992). Details such as mean and maximum grain size correspond to stream capacity during flood events. Localized coarse-grained sedimentation and fining- or coarsening-upward within crevasse splays indicate smaller-scale or flood events and short-term conditions, and must be interpreted quite differently from long-term patterns of sorting or widespread sheet-floods of relatively coarse material blanketing the floodplain surface.

Flood frequency has a major impact on soil development across the floodplain (Birkeland, 1999; Kraus, 1999; Retallack, 1990). Where sedimentation is rapid and unsteady, weakly-developed soils are separated by thicknesses of unaltered sediment, called compound soils (Kraus, 1999). Where sedimentation occurs at a rate that is slower than soil formation, composite soils form in which a soil profile begins to affect underlying soils (Kraus, 1999). Where sedimentation is continuous and slow, thick cumulative soils form in which individual profiles are indistinguishable (Kraus, 1999). Since sedimentation rates vary across a floodplain due to the decrease in sedimentation away from the channel, up-section comparisons of different soil profiles are particularly useful for understanding changing sedimentary or hydrologic conditions if the channel location has remained fixed. Finally, given a uniform parent material, chemical analyses of weathering can further clarify relative soil alteration (Chittleborough, 1991; Harnois, 1988; Nesbitt & Young, 1989; Parker, 1970; Price & Velbel, 2003; Retallack, 1990; Ruxton, 1968).

In both sedimentation and pedogenesis, care must be taken to untangle the influence of natural, cyclic geomorphic events from external (allogenic) factors. For example, a variety of different forcing factors (avulsion relocating the channel, the building of floodplain height to an elevation above flood stage, or a decrease in flood frequency) may cause a similar decrease in grain size and increase in pedogenesis.

Postglacial Environmental Influences on the Study Site

Natural Climate Change

Superimposed on a general trend of end-Pleistocene warming, the Bølling event was an abrupt step toward increased temperatures at around 15 ka, represented in many regional lake and pollen records (Ellis et al., 2004; Y. Li et al., 2006; Peteet, 2000; Yu, 2007) as an increase in carbonate and organic carbon, warmer temperature proxies, and a shift toward temperate forest taxa. Multiple regional cold temperature reversals appear to be superimposed on the Bølling warm, including the Intra-Allerød cooling event around 13.5-13.2 ka (Donnelly et al., 2005; Ellis et al., 2004; Yu, 2007). The Bølling warming is represented in pollen record by an increase in temperate forest taxa (Peteet, 2000), which may be a forcing factor behind the first significant decrease in dust flux at 14.7 ka (Taylor et al., 1993). A further abrupt global increase in ocean and atmospheric temperature is documented at 14 ka (Broecker & Denton, 1989).

The Younger Dryas was an abrupt (i.e. change that occurs in less than a century-see Peteet, 2000) cold reversal at approximately 13-11.6 ka (Peteet, 2000), during which vegetation returned to boreal (taiga) coniferous forest taxa in the northeast (Maenza-Gmelch, 1996). Shifts in authigenic lake calcite $\delta^{18}O$ values indicates cooling during this interval (Ellis et al., 2004; Yu, 2007; Zhao et al., 2010). Drying during the Younger Dryas is apparent from soil moisture approximately 30% below modern values, as determined by comparing modern versus fossil pollen species in a given moisture regime (Webb et al., 1993), as well as low lake levels at some locations (Newby et al., 2011; Shuman & Donnelly, 2006; Shuman et al., 2006). Where arid conditions prevailed, they may have been associated with low summer precipitation (Shuman et al., 2001; Shuman et al., 2006), perhaps due to winds travelling off the ice sheet causing atmospheric subsidence (Webb et al., 1993).

Around 9000 BP at the Holocene peak in Northern Hemisphere summer solar insolation (Berger & Loutre, 1991), soil moisture values continued to be low relative to modern (Webb et al., 1993), and lake low stands are recorded (Dwyer et al., 1996; Newby et al., 2011). While most records suggest warmth at this time (Ellis et al., 2004), cool conditions are recorded at Lake Cayuga in upstate New York (Mullins, 1998), suggesting a non-linear temperature response to solar forcing. At the time of the 8.2 ka abrupt cooling event, cool and dry conditions are again recorded regionally (Morrill & Jacobsen, 2005; Newby et al., 2011; Shuman et al., 2006). The collapse of the ice sheet and its associated cold, dry air mass around this time may have promoted an increase in summer precipitation values soon thereafter (Shuman et al., 2006).

The Holocene Hypsithermal influence peaked between 7 and 6 ka, and while regional soil moisture is reconstructed as similar to modern (Webb et al. 1993), local differences between high lake levels (Dwyer et al. 1996) and low (Li et al., 2006) conditions occur, possibly due to a shift toward high-precipitation events during summer, when evaporation is relatively high. This interpretation is supported by sedimentological evidence of bank erosion and lateral migration of the Delaware channel around 6-5 ka (Stinchcomb et al., 2012), similar to high-magnitude summer precipitation channel erosion events and frequent overbank flooding observed in the American Southeast during the Hypsithermal (Goman & Leigh, 2004; Leigh & Feeney, 1995). Most proxies suggest warmth at this time (Carbotte et al., 2004; Mullins, 1998), punctuated by possible century-scale cooling events (Ellis et al., 2004).

Climatic cooling following the Hypsithermal, recorded by shifts in authigenic lake calcite $\delta^{18}O$, began at different locations between 5.8-5.2 ka (Ellis et al., 2004; Kirby et al., 2002; Zhao et al., 2010), with the latest onset of cooling in lake Cayuga around 3.4 ka (Mullins, 1998). A shift toward summer in the seasonality of precipitation (Kirby et al., 2002; Shuman et al., 2006), when evaporation levels are higher, also begins to drive lake levels lower again between 5.3-3 ka (Li et al., 2006; Mullins, 1998), though soil moisture values are calculated to stay near modern at 3 ka (Webb et al., 1993).

Later climatic events such as the Medieval Climate Anomaly and Little Ice Age are recorded from Chesapeake Bay north to the Great Lakes, but especially the Medieval Climate Anomaly between 1.4 and 0.7 ka (Cronin et al., 2010; Cronin et al., 2005) is marked by variable moisture regimes. For example, a lake highstand at Cayuga (upstate New York) at around 1 ka during the Medieval Climate Anomaly (Mullins, 1998) contrasts with a documented lowstand at White Lake, NJ at 1.3 ka (Li et al., 2006) and dry conditions and an influx of forest fire charcoal in the Hudson Estuary tidal marshes (Pederson et al., 2005). Little Ice Age conditions resulted in an increase in winter precipitation, shifting the balance between evaporation and precipitation and resulting in wet conditions around 0.35-0.2 ka (Cronin et al., 2010; Pederson et al., 2005).

Isostatic Rebound

The last advance of the Laurentide ice sheet reached 40 km SSW of the study area (Stanford and Harper, 1991). Leveling studies across southern New England (Oakely and Boothroyd, 2012) show this terminal moraine has since undergone 35 m of isostatic uplift. Constraints on the timing of isostatic rebound in the vicinity of the northern Delaware are based on reversed gradients of two terraces in the northern Lake Hackensack basin (Stanford et al., 2001) and a peat deposit indicating ponding of water due to rebound at the Delaware-Millstone divide (Stanford, 1993). Both sites are south of the study area, and indicate reversal of the drainage direction around 13 ka, consistent with observations that post LGM rebound began at roughly 14-13 ka in central New England (Koteff et al., 1993).

Anthropogenic Environmental Disturbance

Finally, human activities and landscape modification in the valley, particularly agriculture and timber harvesting, may have had a significant impact on sediment flux and related geomorphologic response. Stinchcomb et al. (2011) documented increased sedimentation around 0.9-0.4 ka (1100-1600 C.E.) on a T2 terrace (see Introduction) approximately 15 km north of the study site. While the interval of increased sedimentation coincides with the Medieval Climate Anomaly-Little Ice Age transition, the deposit is also marked by phytolith, macrofossil, and bulk soil $\delta^{13}C$ evidence of intensification of land use and disturbance of natural vegetation. Sediment flux can only have increased with the arrival of Europeans in the upper portion of the valley around 0.4-0.3 ka (1600-1700 C.E.) when the demand for timber to maintain the British naval fleet was at a peak, and later to support house construction and U.S. needs, led to the practice of timber rafting starting in the 1760s. Logs of all types would be harvested, lashed together, and ridden downstream by crews of men to Philadelphia and other minor commercial centers (Dale, 1996). For example, approximately fifty million feet of lumber was harvested from the Delaware Valley in 1828 C.E., and quantities steadily increased until the 1870s, leaving the valley completely deforested by the end of that century (Dale, 1996). This dramatic disturbance in vegetation would lead to a corresponding increase in sediment flux to the channel, as is directly documented in the Hudson Valley (Pederson et al., 2005; Russell et al., 1993).

Site Settings, Data, and Interpretations

General interpretations of depositional styles and events based on data from the T2 landform at the Shapanack Island Terrace (SIT) site, provided in Chapters 1 and 2, will be summarized and integrated here for clarity. Data from the SIT T1 landform will also be presented to provide a full description of alluvial and terrace deposits at this location, and preliminary analyses of SIT T2 parent materials are added to shed further light on the scope of depositional changes. While the primary focus of this dissertation is an analysis of the T2 landform at the SIT study site, additional constraints on postglacial conditions have been inferred from preliminary OSL dating of an eolian landform at the Alonso Depue House (ADH) site 10 km upstream of SIT (41°14'52"N, 74°50'39"W), and radiocarbon dates on a core of the T2 landform from the Dingman's Ferry (DF) site 7 km upstream of SIT (41°13'29"N, 74°51'37"W) (see Introduction, Fig. 1).

While the SIT site provides abundant insights into the river's behavior during the post-glacial time period, multiple study sites are necessary to determine the spatial and temporal variability in T2 depositional processes and landform history throughout the valley. At SIT, the New Jersey Geologic Survey collected 11 cores that were split, described, and analyzed in this study according to procedures in Chapter 1. One of these cores from the T2 landform (defined by elevation alone- see Introduction) contained organic material for four radiocarbon ages which provide sedimentation rates of the landform through time.

Sand dunes, sheets, and other eolian landforms such as those at the ADH site have been documented across the U.S. due to strong winds from the ice sheet mobilizing sediment across the sparsely-vegetated land surface during the latest Pleistocene (Connally et al., 1972; Donahue, 1977; Markewich et al., 2009; Rawling et al., 2008; Schaetzl & Loope, 2008; Stanford, 2003; Thorson & Schile, 1995; Witte, 2001). Most studies suggest these landforms were active for a brief period of time during the latest Pleistocene in previously-glaciated areas (Connally et al., 1972), and longer periods of time (perhaps the entire life span of the ice sheet) in areas south of the terminal ice margin (Markewich et al., 2009). However, reactivation of eolian landforms as late as the mid-Holocene has been recorded in some locations in the U.S. (Rawling et al., 2008) and Europe (Costantini et al., 2009), suggesting mid-Holocene Hypsithermal conditions may have resulted in widespread decreases in vegetative cover. To determine whether such reactivation occurred in the Delaware Valley, four geoprobe cores from dune-shaped landforms at the ADH site were collected by the New Jersey Geologic Survey in May, 2007; core 1 was twinned (i.e., a second core 1.a was obtained ~3 m away), and preserved from light for OSL dating.

Data from the ADH and DF sites are connected to the SIT site via a framework of terrace formation and alluvial sedimentation within climatic fluctuations in the discussion section that follows.

SIT Site Terraces

The SIT site, as described in prior chapters, is located in the upper Delaware River Valley on the eastern (New Jersey) bank, away from confluences with major tributary streams (approximately 14 km upstream and 11 km downstream). The nearest minor confluence is a first-order stream approximately 2.5 km north of the study site. Two distinct terraces, T1 and T2, are present at SIT. T2 sits approximately 6-9 m above the modern channel (see Introduction Figure 4) and covers most of the area at the site. It is skirted by a thin (<150 m wide) T1 (sometimes called T0 or the floodplain bench) at an elevation 4 m above the channel (see Introduction, Fig. 4 and Chapter 1, Fig. 2). T2 tread elevation varies by less than 2 m, 1 m of which is accounted for by the drop in elevation at the backchannel landform near the valley wall.

Summary of T2 units

The T2 alluvial terrace is divided into five allostratigraphic (unconformity-bounded) sedimentary units, based on radar geometry and facies, sediment texture and structure, soil development, and unit geometry (see discussion in Chapter 1).

Approximate age constraints on the evolution of this deposit are provided by OSL dates (Chapter 2 Table 3), as are chemical weathering ratios derived from the geochemical analysis of the four OSL samples (Chapter 1, Table 3). Figure 1 (this Chapter) shows the logs of Core 1 and Core 7 (as examples of core logs), OSL ages from three Core 7 samples, and a representative subsample of chemical weathering ratios of those Core 7 samples in association with the GPR data and interpretations.

T2- Unit 1 Description, Interpretation, and Age

Unit 1 underlies the entire T2 landform and is >4 m thick in some areas (its base is not resolved). The undulating topography of the upper boundary, B1, is diminished but maintained by all units above, ultimately determining the surface topography of the site. The radar facies of Unit 1 in channel-perpendicular orientations is comprised of short, discontinuous reflectors without consistent orientation, but in channel-parallel orientations is made up of broad, concave-downward reflectors bounding packages of shorter reflectors with internally-consistent orientations that vary in direction and angle. Sediments of Unit 1 are dominated by clast-supported, poorly-sorted, subrounded to subangular pebbles of local lithologies (limestone, chert, shale, and sandstone; Witte, 2001) with matrix ranging from very poorly sorted clay and sand to sand. Medium to coarse, moderately well-sorted sand beds are occasionally interlayered with pebble units. Soil development was not observed within Unit 1 or at the B1 upper bounding surface.

Based on the similarity of radar facies and sedimentology to features reported by Kostic and Aigner (2007), Unit 1 is interpreted as the product of downstream braidplain aggradation The relatively immature pebble units, with their poor sorting and variable matrices, were likely deposited soon after glacial retreat, before fluvial activity had thoroughly reworked the glacial deposits (characteristics similar to the immature glacial sediments documented by Boothroyd and Ashley, 1975). Sand units are interpreted as small, transient channels transporting concentrations of meltwater. Minimal or absent radar truncations at the B1 surface are indicative of minimal erosion or incision of Unit 1 prior to burial.

No age constraints were obtained for this unit through OSL dating. However, a recessional moraine 10 km north of the study site dates to 21.3 ka (Ridge, 2003), providing a maximum age for all post-Last Glacial Maximum sedimentary landforms at the site.

T2- Unit 1a Description, Interpretation, and Age

Unit 1a is a localized, wedge-shaped unit bounded by surface B1a above, with its relatively high-amplitude radar reflector, and B1 below. The unit is <1 m thick at its maximum near the valley axis, and it pinches out onto the B1 boundary below, and is truncated by B1a above. Radar reflectors within this unit are short and slightly more continuous than reflectors in Unit 1. Sediments of Unit 1a are slightly more rounded and sorted clast-supported pebbles of locally-derived lithologies (Witte, 2001), with matrix sediments of silt to very coarse sand. No soil formation is observed within the unit or at the B1a boundary.

Unit 1a sediments are similar to those below, but are slightly more mature. Due to the small area of Unit 1a preserved, no interpretations of directionality of the alluvial system can be reliably inferred from the radar facies. This unit may represent sedimentation in a braided channel that reworked glacial outwash (Boothroyd and Ashley, 1975). In the absence of soil development at the upper B1a boundary, the high-amplitude GPR reflector likely indicates the change in porosity associated with the transition from pebbles and matrix to sands above. Truncation of Unit 1a reflectors at the B1a boundary indicate that B1a is coincident with localized erosion (see Chapter 1, Figure 6).

As with Unit 1, Unit 1a was not dated directly. However, OSL dates at the base of the overlying Unit 2 (described below) determine it is older than the range of 14.8 +/- 0.8 to 18.8 +/- 0.9 ka.

T2- Unit 2 Description, Interpretation, and Age

Unit 2 is bounded by surfaces B1/B1a below and the high-amplitude reflector B2, above. The unit is ~2-m thick until it pinches out to the SE, and its continuous radar reflectors conform to the topography of the lower (B1-B1a) boundary. Sediments range primarily from clays to sands, with alternating layers of oxidized and reduced clays deposited at the base of the section in two paleo-topographic lows. Sands dominate the section overall and are thickest near the modern channel. Grains are typically well or moderately sorted, except in a few localized, poorly-sorted deposits. An overall fining-upward trend is observed in all cores except Core 3, closest to the modern channel. The B2 boundary coincides with peaks in organic carbon and carbonate contents, gradational boundaries between beds, and increased clay content. Major and minor element concentrations from three OSL samples from Unit 2 were used to calculate chemical weathering ratios (Jenny, 1941; Ruxton, 1968; Parker, 1970; Harnois, 1988; Retallack, 1990; Birkeland, 1999; Price and Velbel, 2003), which indicate relatively minimal alteration of sample S4 at the base of the unit, some alteration of sample S3 (only 10 cm above S4), and significant alteration of sample S2 from just beneath the B2 boundary.

The gently undulating, continuous radar facies suggests a drape style of deposition and vertical accretion (Leclerc and Hickin, 1997), but the uniformity of radar facies (at least at the 100 MHz resolution) masks a diversity of depositional styles. Alternating oxidized and reduced clays in topographic lows on the B1 surface are interpreted as clays deposited in a small pond or depression over several seasons during incision of Unit 1 and 1a. Well-sorted medium and coarse sands common near the base of the unit are interpreted as traction sands deposited across the entire low-elevation floodplain without channelization. Fine sands and silts are interpreted as drapes of suspended load, interspersed with localized graded beds understood as crevasse splays (Bristow et al., 1999). Overall fining-upward is consistent with floodplain sedimentation, with decreasing energy as the surface builds to higher elevations (Nanson and Croke, 1992). Chemical weathering analyses of sample S2, organic carbon and carbonate peaks, finer grain sizes, darker colors, and the high-amplitude B2 reflector at the top of Unit 2 (at boundary B2) all indicate soil formation that would have accompanied a significant hiatus (Retallack, 1990; Birkeland, 1999). Thicker dark and fine-grained deposits near the channel at the B2 boundary suggest possible formation of a cumulative soil profile. Minimal erosion may be associated with the B2 boundary and unconformity indicated by reflector truncation atop one paleo-topographic high (see Chapter 1 Figure 6).

OSL ages on sample S4, recovered from the traction sand deposits at the base of the unit, range from 14.8 +/- 0.8 to 18.8 +/- 0.9 ka. OSL ages on sample S2, located just beneath the B2 unconformity and within the associated buried soil, range from 7.8 +/- 0.5 to 12.18 +/- 0.5 ka. However, as noted in Chapter 2, the significant pedogenesis affecting sample S2 require that this age be interpreted as the time at which B2 was buried, and not the time at which deposition of the top of Unit 2 occurred.

T2- Unit 3 Description, Interpretation, and Age

Defined by bounding surface B2 below and B2a above, Unit 3 is a wedge-shaped unit up to 1 m thick that is present only on the proximal edge of the T2 landform (near the modern channel). Semicontinuous to discontinuous radar reflectors onlap and downlap onto the B2 surface below, build up and terminate onto a preexisting topographic high at the unit's distal edge, and one reflector is erosionally-truncated by the upper B2a boundary. Sediments are predominantly fine-grained, and range from clays to massive or graded fine to medium sands, with localized poorly-sorted beds. Multiple peaks of organic carbon and carbonate occur within the unit, and beds commonly exhibit gradational contacts. Chemical weathering ratios of sample S1 from this unit suggest moderate alteration.

Smooth reflectors again evoke laminar overbank (floodplain) deposition (Leclerc and Hickin, 1997), while wedge-shaped geometry and increasing topographic relief are characteristic of a natural levee (Nanson and Croke, 1992). Common fine-grained sedimentation indicates low-energy deposition, while interspersed sand units record higher-magnitude floods or crevassing (Bristow et al., 1999; Nobes et al., 2001).

Gradational boundaries, multiple carbon and carbonate peaks, and moderate chemical weathering suggest increased pedogenesis in Unit 3 relative to most of Unit 2, forming compound and composite soils corresponding to slower or more episodic deposition. The absence of any apparent continuation of the unit away from the channel onto the bulk of the landform suggests lower-magnitude flood events during this period compared to times represented by overlying and underlying units.

OSL ages on sample S1 from the lower part of Unit 3 range from 10.1 +/- 0.6 to 14.4 +/- 0.7 ka. As discussed in Chapter 2, complications with dose rate associated with ponding of U-enriched groundwater atop the B2 boundary below suggests that this age may post-date the actual time of deposition.

T2- Unit 4 Description, Interpretation, and Age

Bounded by B2a and B2 below and the modern land surface above, Unit 4 is 2 m thick or greater where it fills in antecedent lows. The radar facies is comprised of continuous reflectors that parallel the land surface (giving a flat appearance in GPR data) and onlap onto highs of the lower (B2a/B2) boundary where they fill subsurface swales. Since all cores intersect this unit near the apex of a B2a/B2 subsurface high, a few 10s of cm of massive to graded traction sands are taken to indicate that the lows are infilled with this type of coarse sediment. Above, sediments are dominated by suspended load and range from clays to fine sands. All cores fine upward except Core 7, which is coarser-grained in its upper meter. Organic carbon and carbonate values trend upward overall with multiple peaks, and roots are abundant in the upper ~1.5 m of the unit.

Laminar deposition and vertical accretion are again interpreted from relatively flat and continuous reflectors of Unit 4 (Leclerc and Hickin, 1997). Basal traction sands are interpreted as one or more extremely high-magnitude floods (Leclerc and Hickin, 1997), while fine sands, silts, and clays above are deposited in lower-energy overbank deposition (Nanson and Croke, 1992). The anomalously coarse-grained upper meter of Core 7 is interpreted as a crevasse splay, since this core sits in a modern low near the modern channel. Dark-colored clay-rich horizons, gradational boundaries, and higher organic carbon and carbonate in the overbank sediments evince soil formation, including compound, composite, and cumulative soil profiles, suggestive of slow and/or episodic deposition.

No age constraints are available for this unit, except that the entire unit must be younger than 10.1 +/- 0.6 to 14.4 +/- 0.7 ka, the age range for sample S1 in Unit 3. However, sedimentation on the terrace surface has been observed during multiple flood events in 2006, indicating that slow, episodic deposition continues to today.

Summary of T1 Units

Data from the T1 landform, including 100 MHz GPR data and core sediment description and geochemistry, were collected and processed as described for the T2 data in Chapter 1. Two radiocarbon dates on charcoal recovered from Core 4 (ages provided under "T1-Unit 2 Description, Interpretation, and Age" below) were processed and dated by Beta Analytic. The T1 alluvial deposit is divided into two units based on lithology and bounding surfaces identified in the GPR data (Figure 2). Bedrock and contacts between bedrock units beneath the alluvium are also resolved by the GPR survey.

T1- Unit 1 Description, Interpretation, and Age

T1 Unit 1 (designated as such due to its deposition earliest in time for T1, not due to any relationship with T2's Unit 1) is comprised of coarse, angular, poorly sorted pebbles with matrix materials ranging from coarse sand to clay. Based on the bedrock channel elevation at around 4 m below the terrace surface, the B1 boundary at the base of Unit 1 is interpreted as the contact with bedrock. In GPR, the unit appears to average 1-3 m thick, pinching out onto bedrock highs and thickening in lows, building to the north through time. Geochemical data on this unit are derived from matrix sediments only, and show fluctuations of low concentrations of organic carbon and carbonate. The unit is capped by the B2 boundary, which shows no radar reflector truncation or core evidence of erosion.

Assuming that all T1 sediments were deposited later in time than the T2 sediments, the relative immaturity of the pebbles and matrix of T1 Unit 1 is surprising. One possible explanation is that coarse sediment slumping from an eroding edge of T2 were not transported a significant distance before they were buried, maintaining their immature character. A second and preferred explanation is that the larger, rounded cobbles that can be observed at the edge and base of the T1 in outcrop underlie the entire unit, but have been shattered into angular, pebble-sized fragments by the coring apparatus (an interpretation which could affect all coarser units at the study area). This unit is therefore interpreted as a channel gravel or point bar. Based on geochemistry and sediment description, no soil development is inferred.

No age dates are available for this unit. However, the radiocarbon ages obtained from Unit 2 (discussed below) provide a minimum age for Unit 1.

T1- Unit 2 Description, Interpretation, and Age

T1 Unit 2 averages 2-2.5m thick over the observed area, and thickens to the north and terminates against the B1 boundary, which rises in elevation to the south. Sediments consist of light to medium brown, coarse and medium sands interspersed with beds and mottles of fine sand and silt units. One iron-stained coarse sand unit at the base of the unit presents a bright red color. Organic carbon peaks within this unit correspond to multiple charcoal-bearing intervals, and do not coincide with other indicators of soil development. Carbonate values through the unit fluctuate, but are relatively low throughout. Charcoal samples obtained from a depth of 124 cm and 136 cm were dated to 210 +/- 40 ^{14}C years BP (Beta Analytic Sample 232849) and 270 +/- 40 ^{14}C years BP (Beta Analytic Sample 232850), respectively (Witte, personal communication- dates have not been published).

Overall, the coarse grain sizes of the unit are interpreted as traction and near-channel overbank sedimentation, punctuated by minimal periods of stability and extremely weak soil formation. Abundant mottling is interpreted as a consequence of bioturbation during periods of quiescence coupled with depositional rip-up clasts of other soils (pedoliths) transported from a point of origin upstream. Based on the two radiocarbon dates, a time-averaged deposition rate of 0.5-0.6 cm/yr is calculated, suggesting total deposition of Unit 2 during the past 416-500 years.

SIT T2 terrace- Parent material analysis

Alluvial materials have inherently distinct parent materials in the sense that different flood events deposit successive units. However, the sediment source and therefore composition of the material deposited may be roughly uniform through time, or may change in response to climate or environmental changes, intrinsic geomorphic thresholds, or other factors. Trace element ratios are commonly used to evaluate the parent material uniformity of a soil profile, since these elements are generally thought to be present in very resistant minerals not likely to be affected by leaching (Anda et al., 2009; Chapman & Horn, 1968; Evans & Adams, 1975; Marsan et al., 1988; Reheis, 1990; Xing et al., 2004). Data presented in Table 1 are derived from OSL samples S1-S4 described in Chapter 2.

Y_2O_3 : TiO_2 and ZrO_2 : TiO_2 are ratios commonly used to evaluate uniformity of parent material (Marsan et al., 1988; Reheis, 1990). However, some studies have suggested that a component of the Ti may be contained in less resistant minerals, and therefore be mobile during pedogenesis (Anda et al., 2009; Chapman & Horn, 1968; Evans & Adams, 1975). Therefore, Y : Zr (Anda et al., 2009) and Zr : Sr (Xing et al., 2004) ratios are also presented.

Based on sediment core descriptions, S3 and S4 are from the same bed, thus the same depositional event, and therefore should have identical parent material indicators. However, Zr is more abundant in S4 than S3, which may be due to rapid settling of heavier zircon grains during deposition.

Overall, $Y_2O_3 : TiO_2$ ratios for the four samples taken together have a coefficient of variability of 9.5%, indicating low variability and a high degree of similarity to one another. $ZrO_2 : TiO_2$ ratios show a higher coefficient of variability of 17%, indicating more dissimilarity between the samples. Offset between the ratios of S3 and S4 are explained almost entirely by the relative enrichment of Zr in S4. Higher values in samples S1 and S2 may be explained by some depletion of Ti during pedogenesis, since these two samples show other indications of leaching and addition of organic material and carbonate which also indicate soil development (see Chapter 2). Nonetheless, the higher ratio for S1 than S2 is unexpected, since S2 appears to have undergone significantly more weathering and soil development. This suggests extremely similar parent materials for the lower three samples, and a distinct parent material for the uppermost sample.

Y : Zr ratios have a coefficient of variability of 17%, similar to $ZrO_2 : TiO_2$. As with the ratios above, the difference between the values of S3 and S4 is due to higher Zr in S4, perhaps due to depositional sorting of grains. This ratio suggests nearly identical parent materials for samples S2 and S3, which are undeniably distinct depositional events separated by nearly three meters of sedimentation. The ratio for S1 is significantly lower than the ratios of S2 and S3, again indicating a separate parent material for this upper deposit.

Zr : Sr ratios show the widest range in values, with a coefficient of variability of 29%. Again, offset between the ratios of S3 and S4 are due to the relative enrichment of Zr in S4. Significantly higher values are present in sample S2, perhaps indicating a separate parent material for this sample compared to the lower two, contrary to the other three ratios. However, if some Sr has been depleted during pedogenesis, this may be explained in a manner similar to that for Ti above. Finally, the ratio for sample S1 is approximately twice that of the lower two samples, confirming a different parent material with a different initial chemical composition for this sample.

When coefficients of variability are calculated for samples S2-S4, values drop to ~10% for all ratios except Sr : Zr, which is ~16%. However, if Sr is concentrated in the soil, this higher variance can be explained by pedogenesis, rather than parent material (initial) composition. If correct, this analysis suggests that sediment composition and therefore presumably sediment source was constant below the unconformity, and changed immediately upon re-initiation of overbank deposition after the hiatus. The small number of available samples renders the preceding statistical analysis suspect, though, and a set of approximately 30 additional samples from all five SIT T2 depositional units have been prepared to confirm or reject the analysis when funds become available.

Alonso Depue House (ADH) OSL dating- Timing of eolian deposition

Sediments of core 1.2 at the ADH site (for location see Introduction, Figure 1) eolian landform consist of nearly 3 m of fine sand, very fine sand, and silt with modern roots down to 30 cm depth. Boundaries are extremely gradational throughout, and mottling is apparent, suggesting some pedogenic modification of the entire deposit. OSL samples were collected at depths of 65 cm (A1) and 177 cm (A2). Both samples showed decreased overdispersion values relative to the SIT samples, suggesting they are less likely to have been affected by bioturbation or partial bleaching. The 175-212 μm size fraction of each sample was used, and protocols for OSL dating were as described for the SIT samples in Chapter 2, without additional high-resolution gamma counting.

Eleven aliquots of sample A1 were treated with a 220 °C preheat and a 160 °C cutheat, resulting in a De of 21.857 +/- 0.066 Gy, giving the sample an age of 12.77 +/- 0.66 ka BP. Fewer aliquots of sample A2 were measured and with less consistent results; however, preliminary data give this sample a De of 8.957 +/- 0.237 Gy and an age of 4.99 +/- 0.29 ka BP. While more work is necessary to further characterize these deposits and firmly constrain their age, these OSL ages suggest that eolian landforms were reactivated during the mid-Holocene in the upper Delaware River valley.

Dingman's Ferry (DF) site T2 - Mid-Holocene channel reorganization

Figure 3 shows the logs for Core 10 from the DF site (for location see Intro Fig 1), located on the T2 landform as suggested by its roughly equivalent elevation to other T2 landforms in the valley (see Introduction). This core is comprised primarily of traction sands and pebbles below 462.5 cm, and finer overbank sediments with multiple organic carbon and carbonate peaks suggesting discrete episodes of stability and soil formation above. Four radiocarbon dates from charcoal samples from the overbank sediments yielded ages of 560 +/- 30 ^{14}C years BP (72.5 cm depth), 2650 +/- 35 ^{14}C BP (124.5 cm depth), 4950 +/- 35 ^{14}C BP (362 cm depth), and 5040 +/- 30 ^{14}C BP (371.5 cm depth). Based on these ages, deposition rates for the T2 landform at the DF site were relatively rapid at 0.106 cm/yr from ~5040 to 4950 ^{14}C BP and 0.103 from ~4950 to 2650 ^{14}C BP, slowed to 0.0249 between ~2650 and 560 ^{14}C BP, and then reached their highest rate of 0.129 cm/yr from ~560 ^{14}C BP to present. Assuming overbank sediments between 371.5

and 462.5 cm were deposited at the highest calculated deposition rate, the shift from channel to overbank deposition would have occurred around 5745 ^{14}C years BP, or around 6531 calendar years BP (Fairbanks et al., 2005).

Discussion: Fluvial processes and landscape formation history

The set of OSL ages considered most reliable (see Chapter 2) places the deposition of T2 Unit 1 and Unit 1a, incision of these units, and deposition of basal sheet sands of Unit 2 all prior to or around 16.2 +/-9 ka. However, significant warming, recolonization by vegetation, and isostatic rebound all occur later in time. Consequently, this time period is characterized by a notable paucity of forcing factors to drive the shifts in regime from deposition of Unit 1 and Unit 1a to incision of those two units and back to deposition of Unit 2, or the dramatic decrease in depositional grain size in comparing Units 1 and 1a to Unit 2. Therefore, the procedurally "most reliable" set of OSL ages must be rejected in favor of the younger set of ages calculated based on ICP measurements alone. These ages will be used to guide the following inferences regarding forcing of fluvial processes in the upper Delaware River Valley.

Geomorphic and sedimentary events represented at the SIT study site, their approximate timing, and interpreted forcing factors are summarized in Table 2. A timeline showing the correlation between regional/global climatic and environmental events and events at the SIT study site is shown in Figure 4. Beginning around 21.3 ka (based on the glacial moraine age a few km north of the study site reported by Ridge, 2003- see Introduction, Figure 1), postglacial sedimentation at the SIT study site began to deposit T2 Unit 1 and Unit 1a. Due to their similarity in timing and sedimentary character, these two units are interpreted as coincident with the T3 terrace elsewhere in the valley (described by Witte, 2001). Although the elevation of the T2 Unit 1 and 1a are much lower than the T3 height, these materials likely aggraded to different elevations at different locations due to localized geographic constraints such as the placement of a stalled ice margin or isolated blocks of glacial ice. Driven by abundant glacially-derived sediment, frost shattering and minimal vegetative stabilization of hillslopes, flashy meltwater discharge, and an isostatically-depressed gradient, these sediments were aggraded by a braided stream with a network of alluvial channels over a period of several thousand years as the climate slowly began to warm.

At some time prior to 14.8+/- 0.8 ka, incision of Unit 1 and 1a began (Table 2, Fig. 4), prior to the initiation of isostatic rebound (around 14 ka) and before most of the significant warming and increase in moisture associated with the Bølling event (around 15 ka). This sequence of events suggests that incision of the braidplain sediments was driven primarily by two factors: removal of glacial meltwater and establishment of early vegetation. A recessional moraine just north of the tip of the Delaware drainage basin in New York state shows that the receding ice sheet no longer provided meltwater to the basin as of 18.2 ka (Ridge, 2003). Instead, flashy meltwater discharge from the ablating ice sheet north of the Delaware watershed would have traveled down the Hudson and Susquehanna valleys after this time. In the absence of meltwater and abundant precipitation, water inputs to the Delaware at this time would likely have been dominated by less-flashy groundwater input. Simultaneously, pollen records show that tundra-boreal (taiga) vegetation was likely established (Peteet, 2000), decreasing sediment flux to the channel. Together, these two factors would have decreased and stabilized sediment inputs, allowing incision to begin and converting the braidplain sediments to a fill terrace.

The absence of multiple channels or a wide swath incised into Unit 1 and Unit 1a suggests that the river shifted its channel form from braided to meandering at the time when incision began. In contrast, the neighboring Susquehanna River to the west is believed to have established a meandering morphology around the early Holocene (Thieme, 2003), consistent with the timing of this shift in other northern-hemisphere valleys from the mighty Mississippi (Saucier, 1994) to small catchments in Germany (Andres et al., 2001).

This discrepancy may be interpreted to call into question even the youngest set of OSL dates or suggest that the upper Delaware is somehow anomalous for having switched channel forms so early in time. However, the period of incision would be difficult to constrain, since geochronological methods depend on materials deposited or surfaces exposed, and no such remnants can be clearly associated with the incision process. Therefore, if the single channel form were established during incision (as is posited here), this time could not be established by the available age control.

Furthermore, the chronologies referenced above, outside of this present study, are based primarily on radiocarbon ages. In the Delaware valley, radiocarbon dates from the base of the T2 landform elsewhere in the valley place the deposition of the basal overbank sediments at 11.5 ka (Witte, 2001). Since OSL dating can be used on sediments themselves and does not require organic material, it can be used to directly constrain the initiation of sedimentation, prior to the widespread deposition charcoal or microfossils.

Future use of OSL and other direct sediment dating methods may show that the shift to single channel morphology occurred earlier in other river valleys as well.

The initiation of incision left the B1/B1a surface exposed for an extended period of time, perhaps as long as three thousand years. Over this interval, seasonally-stratified lakes or ponds occupied paleotopographic lows (such as described in Leemann & Niessen, 1994), depositing the alternating layers of oxidized and reduced clays observed at the base of Unit 2 (Table 2, Fig. 4). Occasional thin, coarse and very coarse sand layers interrupt the clay facies, showing that high-magnitude flood events were rare but did occur during this interval.

Significant climatic amelioration and temperate vegetation occur with Bølling event at 15 ka and continued at 14 ka (Broecker & Denton, 1989; Ellis et al., 2004; Li et al., 2006; Peteet, 2000; Taylor et al., 1993; Yu, 2007), placing these driving factors squarely within the 14.8 +/- 0.8 OSL age of the sheet flood sands near the base of Unit 2 (Table 2). While environmental proxies do not indicate a significant increase in precipitation at this time, incision of the channel may not yet have been completed, leaving the channel not far beneath the elevation of the fill terrace. Therefore, a small change in precipitation in the form of one or more high-magnitude precipitation events may have been sufficient to allow the channel to overtop its banks and deposit these sands, while continued incision may have provided the necessary sediment to fuel the aggradation of Unit 2 (Table 2, Fig. 4).

Subsequent to the sheet sand units at 14.8 +/- 0.8, a more stable precipitation regime and continuing incision of the channel resulted in successive layers of overbank fines atop the fill terrace. A general fining-upward trend to the sediments and increasing soil formation toward the top of Unit 2 likely resulted primarily from increasing separation height between the channel and terrace surface. This increasing separation is a natural geomorphic effect of progressive floodplain deposition in many locations, even in the absence of channel incision. However, the T2 unit 2 is deposited as the effects of isostatic rebound begin to impact the area (Stanford et al., 2001; Stanford, 1993), perhaps causing renewed or accelerated channel incision at that time. This isostatically-driven incision process increase the pace at which the separation between channel and terrace tread progressed, contributing to the observed fining-upward trend and increasing soil development indicators up-section through Unit 2 (Table 2, Fig. 4).

Unit 2 culminated in the formation of the B2 paleosol (Table 2, Fig. 4), coincident with an apparent change in T2 parent material below versus above. The extended decrease in flood magnitude and frequency represented by the B2 paleosol may be associated with the decreasing moisture flux approaching the solar insolation maximum at 9 ka (Berger & Loutre, 1991). Independent records of low soil moisture values relative to modern (Webb et al., 1993) and low lake levels across the region (Dwyer et al., 1996; Newby et al., 2011) confirm arid conditions at this time. The change in parent material is hypothesized to represent a shift from dominantly glacially-derived sediment to colluvial materials at this time. The extended period of stability represented by the B2 boundary and the warming climate permitted greater in-situ hillslope weathering than during Unit 2 deposition, providing increased colluvial inputs with different geochemical characteristics for the deposition of Unit 3 above.

Burial of the B2 surface is believed to have occurred sometime between 10.1 +/- 0.6 and 7.8 +/- 0.5 ka, based on the two OSL dates above and below the boundary, respectively (which are reversed, and are both somewhat affected by pedogenesis; see discussion in Chapter 2). While it arrives fairly late within this time interval, the increase in summer precipitation subsequent to the final collapse of the ice sheet and its attendant cold, dry air mass around 8.2 ka (Shuman & Donnelly, 2006) most likely explains the re-initiation of deposition on the terrace surface that resulted in the Unit 3 levee landform (Table 2, Fig. 4).

Other researchers studying this section of the Delaware Valley have posited a channel reorganization event during the warm Hypsithermal around 6-5 ka (Stinchcomb et al., 2012). Although indicators of soil moisture suggest near normal values during this interval (Webb et al., 1993), and regional lake records vary from wet (Dwyer et al., 1996) to dry (Li et al., 2006), the observed dune reactivation at the ADH site around 5 ka suggests sufficient aridity to decrease stabilizing vegetative cover in the northern Delaware River Valley. Radiocarbon dates at the DF site T2 landform indicating that the channel in this area stabilized by 6531 ka, and while the discrepancy between the two dating methods is disconcerting, these OSL dates are still preliminary. Taken together, these two pieces of evidence firmly support the interpretation of landscape destabilization and channel reorganization during the Hypsithermal.

At the SIT site, the coarse sheet sands blanketing the entire T2 terrace surface at the base of Unit 4 may represent increased flood magnitude and sediment supply associated with the Hypsithermal at the study location (Table 2, Fig. 4). Sedimentation within the lower half of Unit 4 resulted in the most significant infilling of topographic lows since the deposition of Unit 1. As climate began to cool between 6-4 ka (Ellis et al., 2004; Kirby et al., 2002; Mullins, 1998; Zhao et al., 2010) and the channel re-stabilized, flood magnitude and frequency again decreased, resulting in the deposition of finer-grained sediments and increased soil formation in the upper part of the SIT site T2 Unit 1.

Beginning around 0.9 ka, the warm and dry Medieval Climate Anomaly began to influence the region (Cronin et al., 2010; Cronin et al., 2005; Li et al., 2006; Mullins, 1998; Pederson et al., 2005), and agriculture and land use by Native Americans intensified (Stinchcomb et al., 2011). These factors resulted in destabilization of the landscape and increased sediment flux to the channel, documented north of the study site by other researchers (Stinchcomb et al., 2011). I hypothesize that this interval resulted in a second, localized channel reorganization event from 0.9-0.5 ka, during which time the banks of T2 were eroded in some locations and the gravels of T1 Unit 1 were deposited in the channel (Table 2). Further landscape destabilization by European timber harvesting and increased runoff during the cool, wet Little Ice Age (Cronin et al., 2010; Pederson et al., 2005) then led to a dramatic increase in sediment flux to the channel, causing the rapid deposition of T1 Unit 2 at low-energy channel margins between 0.5 ka and today (Table 2). The five-fold increase in deposition rates at the DF site T2 during the past 560 ^{14}C (558 calendar) years support these interpretations.

Finally, comparison between the OSL ages of the SIT site T2 landform to the radiocarbon dates from the DF site T2 landform indicates that the two examples of the terraces reached similar heights over different time periods, though the two sites are only approximately 7 km apart. This complex history for the T2 landform at different locations throughout the valley has been noted in studies examining the archaeological record for some time. However, the factors determining differential formation histories have not been systematically examined, and this direction for future research has the potential to contribute to the growing body of theory on alluvial terrace formation.

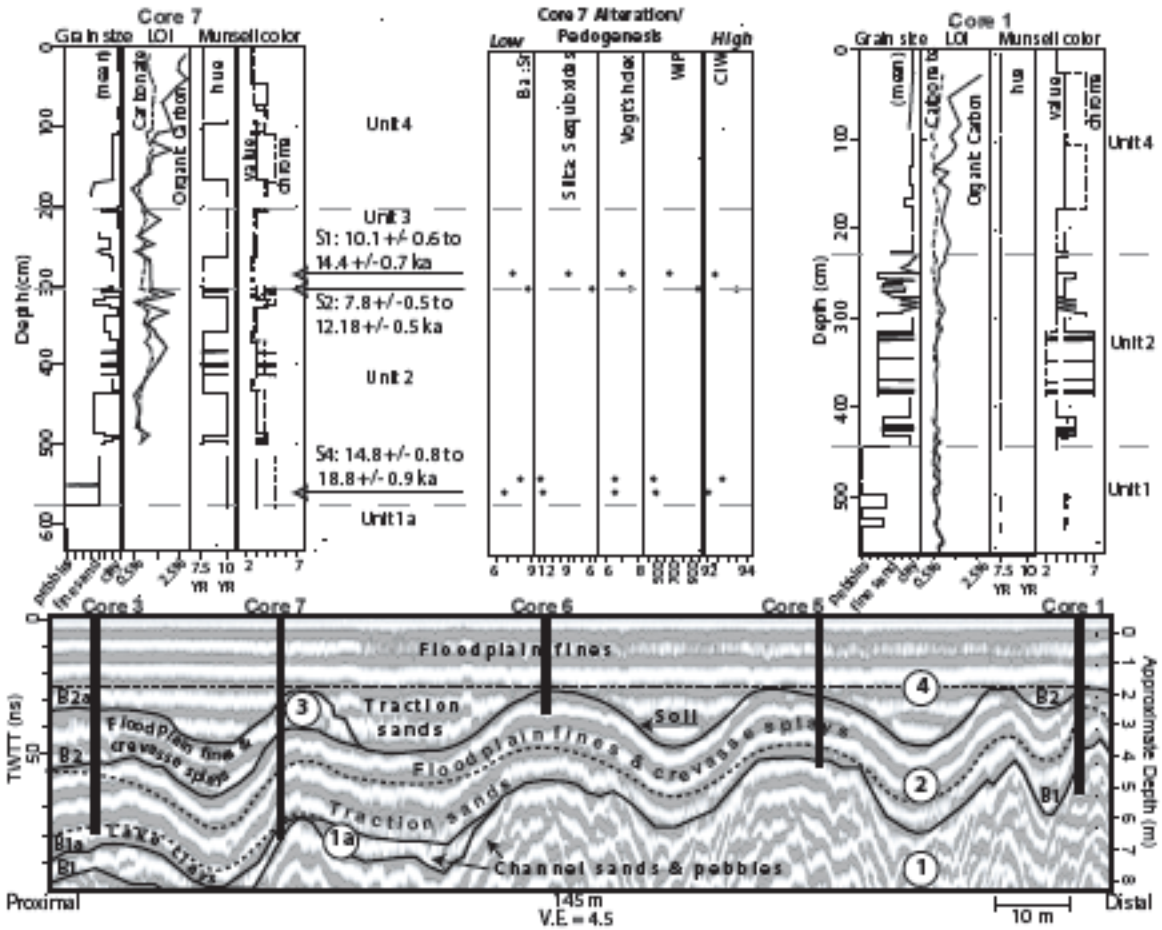

Figure 1: Logs of cores 1 and 7 plus OSL ages and chemical weathering based on samples in core 7 (upper) from among several cores arranged along GPR line 4 (lower; map location shown on Chapter 1, Figure 2). These analyses and interpretations provide a history of the evolution of the T2 landform described in the text.

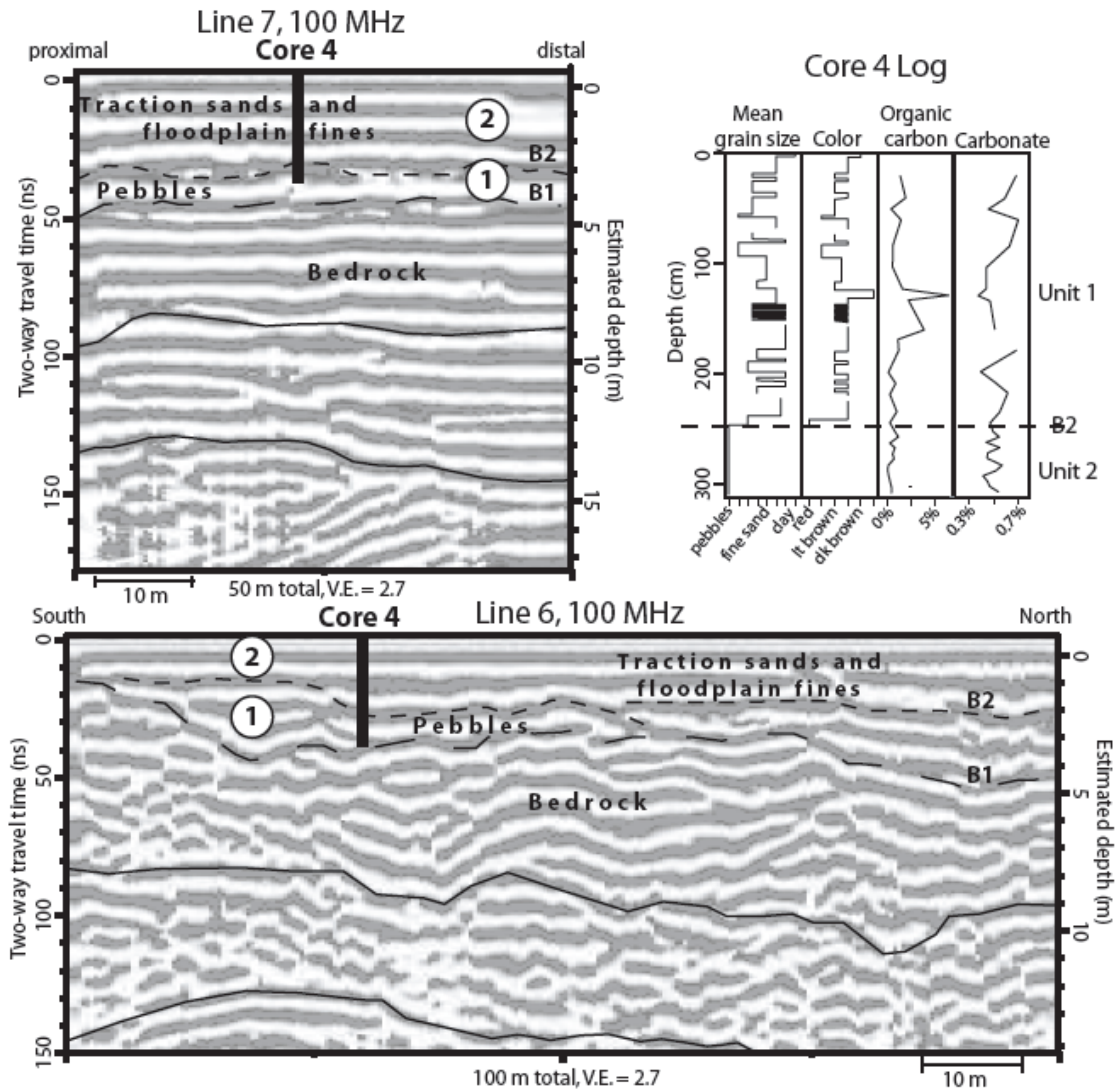

Figure 2: Two GPR lines and Core 4 (map of locations in Chapter 1, Figure 2) document the composition and internal structure of the T1 landform. For the sandier sediments of T1, a radar velocity of 10 cm/ns is used to estimate depth, slightly faster than the 9 cm/ns for the T2. The upper bounding surface, marked with the small-dash line, denotes the bounding surface for the top of the gravel units. The modern channel, which rests on bedrock, is approximately 4 m lower in elevation, suggesting that the second bounding surface, outlined with a larger-dash line, may be the bedrock surface, with deeper boundaries representing contacts between bedrock units. The two GPR lines cross within 5 m of the core, marked with the bold black line.

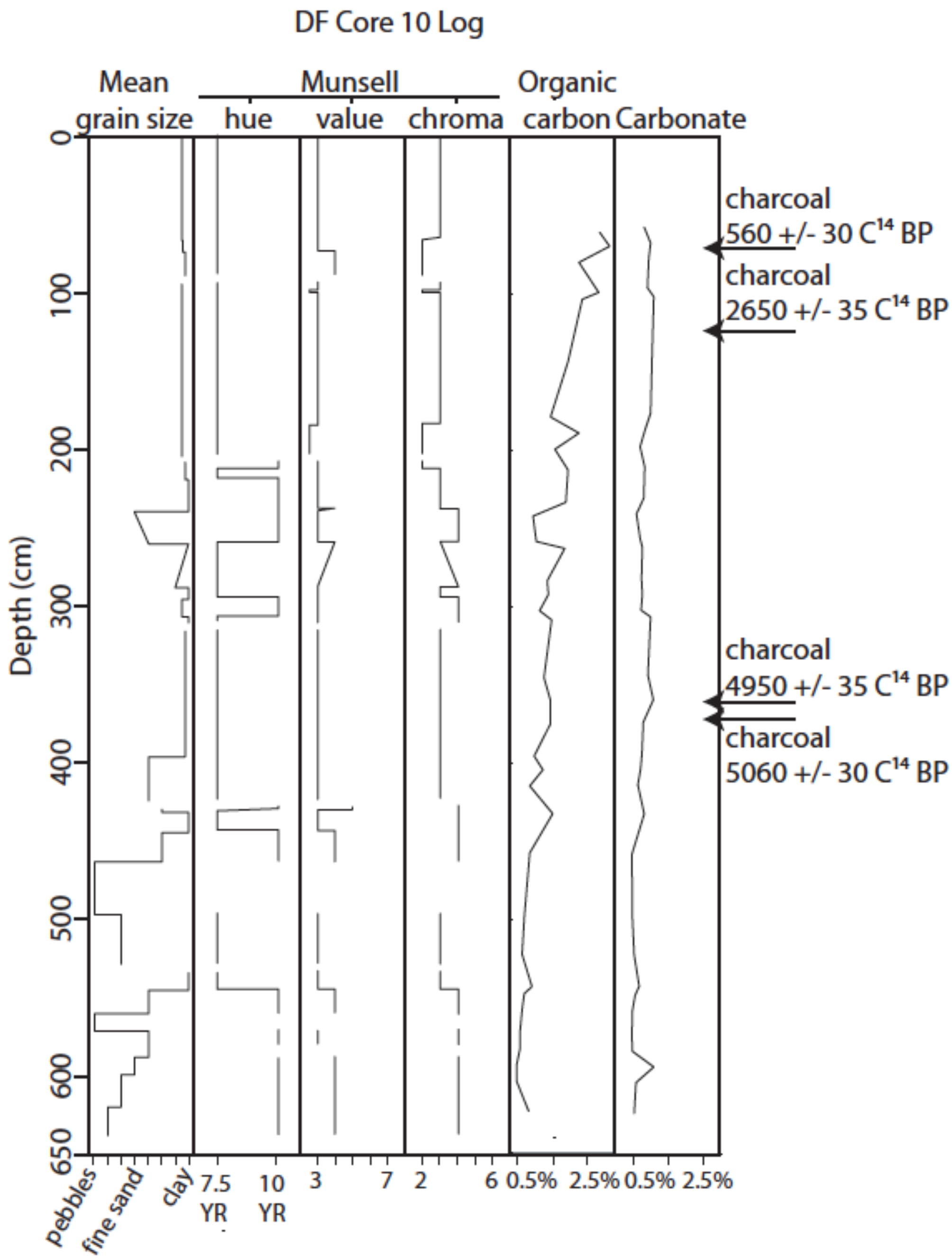

Figure 3: Mean grain size, Munsell color data, % organic carbon, and % carbonate logs for core 10 from the DF site (location shown in Introduction, Figure 1). Four radiocarbon dates are provided by Beta Analytic on charcoal samples.

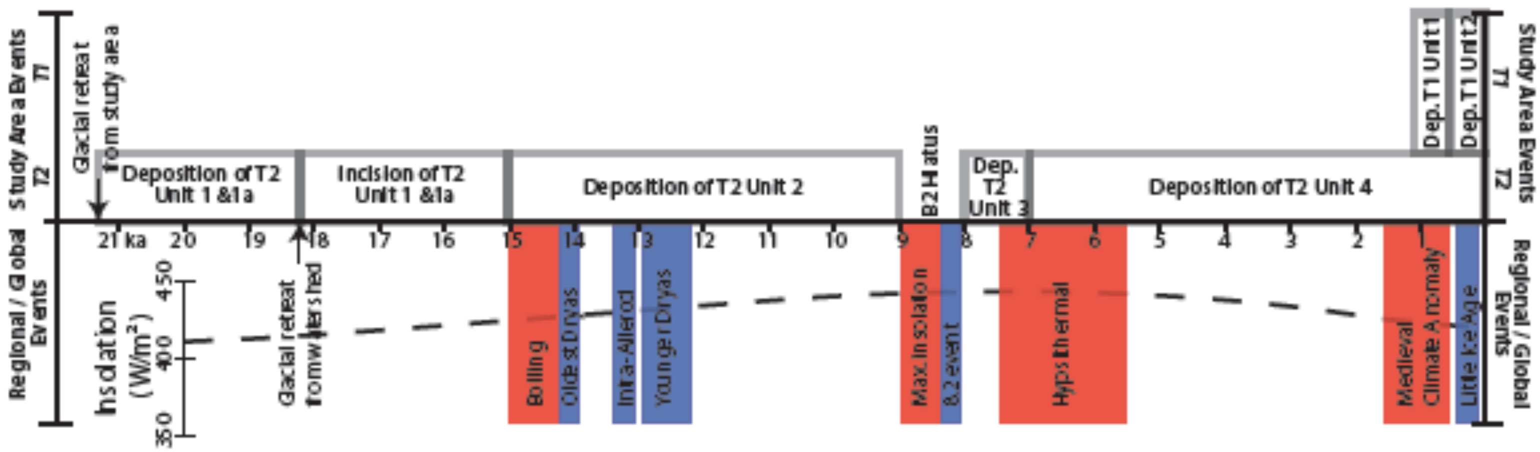

Figure 4: Timeline of events at the study site (above) and regional to global forcing factors (below), with summer (June, July, and August) solar insolation curve for 60°N (study site is 41°N latitude). Glacial retreat ages are based on Ridge, 2003 compilation of moraine ages. Bølling warming event was the first significant step toward increased temperatures at around 15 ka (Ellis et al., 2004; Li et al., 2006; Peteet, 2000; Yu, 2007). Early warming was punctuated by multiple cold-dry reversals, including the Intra-Allerød cooling event around 13.5-13.2 ka (Donnelly et al., 2005; Ellis et al., 2004; Yu, 2007) and the Younger Dryas at approximately 13-11.6 ka (Peteet, 2000; Maenza-Gmelch, 1996; Ellis et al., 2004; Yu, 2007; Zhao et al., 2010). The Holocene peak in Northern Hemisphere summer solar insolation occurred around 9000 BP (Berger & Loutre, 1991), followed by the 8.2 ka abrupt cool and dry event (Newby et al., 2011; Shuman et al., 2006). The warm Holocene Hypsithermal period's influence peaks in the region between 7 and 6 ka (Carbotte et al., 2004; Mullins, 1998; Stinchcomb et al., 2012). Later cooling is interrupted by the warm, locally dry Medieval Climate Anomaly around 1.4-0.7 ka (Cronin et al., 2010; Cronin et al., 2005; Li et al., 2006; Pederson et al., 2005), followed by the cool, wet Little Ice Age around 0.35-0.2 ka (Cronin et al., 2010; Pederson et al., 2005). Insolation curve from http://courses.washington.edu/holocene/IntroGHR.pdf, after calculations made by Berger & Loutre, 1991.

	S1	S2	S3	S4	CV (%)	CV (S2, S3, S4) (%)	CV (S1 and S2) (%)	CV (S3 and S4) (%)
Y : Zr	0.054	0.084	0.083	0.067	17	10	22	9
Sr : Zr	14.54	10.20	6.95	8.25	29	16	18	11
Y : Sr	0.786	0.854	0.579	0.55	19	21	41	3
Y: Ba	0.105	0.098	0.080	0.081	12	9	35	7

Table 1: Four elemental ratios are used to evaluate parent material uniformity according to the statistical coefficient of variability (CV). Y : Zr and Y : Ba are considered more reliable than ratios using Sr, which may be soluble. Higher values of CV indicate greater internal variability of the sample population. Since CV values decrease when calculated for samples S2-S4 compared to CV values including S1 (for all ratios except Y : Sr), samples S2-S4 (deposited prior to the B2 unconformity) likely share a common source, while sample S1 (deposited above the B2 surface in the levee unit, Unit 3) has a distinct source. High CV values for S1 and S2 suggest that these two samples have two different parent materials, suggesting the change in parent material occurred with the unconformity that separates these two samples. Low CV values for samples S3 and S4 suggest these two samples share an almost identical source.

Event	Timing	Interpreted Forcing
Deposition of T1 Unit 2 traction sands and overbank fines	~0.5 ka to modern	Abundant sediment input derived from additional destabilization of landscape by European deforestation and Little Ice Age increased runoff
Deposition of T1 Unit 1 gravels and localized channel reorganization/ erosion of T2 banks	~0.9-0.5 ka	Medieval Warm Period dry conditions and Anthropogenic landscape disturbance
Deposition of T2 Unit 4 overbank fines and soil development	~5ka to present	Decreasing flood frequency and magnitude during cooling in the late Holocene
Deposition of T2 Unit 4 sheet sands	~6-5 ka	High-magnitude summer precipitation events driving channel reorganization
Deposition of T2 Unit 3 levee and soil formation	After ~8.2-8 ka	Increased summer precipitation causing occasional localized flooding of tread
Paleosol and B2 unconformity	~9 ka	Dry conditions at the solar insolation maximum
Deposition of T2 Unit 2 overbank fines and soil development	14.8 +/- 0.8 ka to ~9 ka	Decreasing flood frequency and magnitude due to isostatic rebound increasing channel incision and increasing elevation of terrace tread
Deposition of T2 Unit 2 sheet sands	14.8 +/- 0.8 ka	Flooding during relatively high-magnitude events associate with Bølling and 14 ka warming
Incision of T2 Unit 1 and 1a to create fill terrace, deposition of T2 Unit 2 oxidized-reduced lake clays	18.2 (or soon after)-14.8 +/ -0.8	Decreased sediment input due to retreat of glacier from drainage basin and establishment of tundra/boreal vegetation
Deposition of T2 Unit 1 and Unit 1a	20.3-18.2 ka (or soon after)	Abundant glacial and periglacial sediment input, depressed gradient, minimal vegetation to stabilize slopes

Table 2: Summary of landscape and terrace formation events at the SIT study site for both terraces, including approximate timing and the factors interpreted as having forced or influenced these events.

STUDY CONCLUSIONS

Answers to Study Questions and Methodological Contributions

In the introduction to this dissertation, three basic questions and a number of methodological objectives were posited. Here, the questions are directly answered and the accomplishments toward the methodological objectives are summarized using Chapters 1, 2, and 3 and the information presented therein.

Question 1: What is the detailed depositional history of the T2 and T1 landforms at the SIT site?

This question includes the following sub-questions: 1a. What stream morphologies and 1b. alluvial processes are responsible for the construction of this terrace? Chapters 1 and 3 answer Question 1 and the associated two sub-questions.

Chapter 1 characterized the alluvial architecture of the T2 terrace at the SIT study site using GPR survey, core sediment description, and geochemistry. Drawing from these multiple sources of evidence, this chapter demonstrated that the T2 landform at the SIT site is comprised of five units of varying sedimentary composition, radar facies, and degree of soil formation. These five alluvial units are separated by four bounding surfaces that are identified by radar terminations, changes in grain size, or the presence of buried soils. Based on this evidence, Chapter 1 posited that a braided morphology stream is responsible for the construction of T2 Unit 1 and 1a, and that the modern, single-channel morphology is associated with Units 2, 3, and 4 (Question 1a). Further, core sediment analyses showed that Unit 1 and 1a were comprised of traction deposits within a channel setting, basal sands of Unit 2 and possibly Unit 4 were deposited as traction sheet sands, and the remaining sediments were deposited across the floodplain as suspended load (Question 1b). Chapter 3 examined the T1 landform, and showed that the modern single-channel river deposited units 1 and 2 identificd with GPR and lithostratigraphy (Question 1a). The basal unit was comprised of traction channel deposits while the upper unit accreted through both traction and suspended-load deposition during flood events (Question 1b).

Question 2: What is the temporal framework associated with this depositional history?

This question includes the following sub-questions: 2a. Over what time periods were individual sedimentary units deposited, and 2b. when did significant shifts in depositional character occur? Chapters 2 and 3 come together to answer Question 2 and its sub-questions.

Chapter 2 documented the application of OSL dating methods to four sediment samples from the T2 landform at the SIT site, which provided a set of age ranges for three of the four samples (corresponding to three of the five sedimentary units that comprise the landform). Chapter 3 reported two radiocarbon ages constraining the timing of deposition of the upper unit of the T1 landform, reported four radiocarbon ages from the T2 landform at the DF site (7 km north of the SIT site) to corroborate interpretations of the T2 geochronology at the study site. Drawing from the conclusions of Chapters 1 and 2 and this additional data, Chapter 3 then used the climatic and environmental record to infer the timing of all five T2 units (Question 2a), both T1 units (Question 2a), and the relevant bounding surfaces (Question 2b).

The T2 Units 1 and 1a were deposited between approximately 21.3-18.2 ka. Incision of these two units began around 18.2 ka, and by that time the river had established a single-channel morphology. Deposition of T2 Unit 2 began during incision, as seasonally-stratified lakes left behind oxidized and reduced clays on the fill terrace. Abundant, relatively high-energy sheet sand sedimentation of T2 Unit 2 began around 14.8 +- 0.8 ka, followed by fining-upward floodplain sediments. The B2 unconformity and paleosol at the top of Unit 2 occurs around 9 ka. T2 levee Unit 3 was deposited starting around 8.2 ka, while widespread flooding and increased sediment flux at the base of T2 Unit 4 are inferred to occur around 6-5 ka. The remaining T2 floodplain fines of Unit 4 were deposited thereafter. Formation of the T1 occurred entirely within the past 1 ka or less.

Question 3: What is the impact of postglacial climate, environment, isostatic rebound, and humans on the development of these landforms?

Within this main question, the following sub-questions were identified: 3a. How have water budget, deposition rate, and sediment source changed through time? 3b. How does the documented sedimentary record correspond to the timing of climatic and environmental changes, isostatic uplift, and human landscape alterations documented to have affected the region in the scientific literature? Chapter 3 draws from the previous two chapters and additional datasets to answer Question 3 and its associated sub-questions.

The T2 Units 1 and 1a represent the remnants of an aggradational braidplain deposited between approximately 21.3-18.2 ka, and are interpreted as coincident with the deposition of the T3 landform elsewhere in the valley. Incision of these two basal units began around 18.2 ka as a result of stabilized discharge due to the diversion of meltwater from the basin and decreased sediment input to the channel resulting from the re-establishment of tundra-boreal vegetation. By the time of incision, the river had established a single-channel morphology, as evidenced by a lack of evidence of multi-channel or wide-swath erosion into T2 Unit 1 and Unit 1a in the GPR data. During incision, seasonally-stratified lakes occupied low areas on the fill terrace, leaving behind alternating layers of oxidized and reduced clays interrupted by infrequent high-energy flood events. Abundant, relatively high-energy sheet sand sedimentation of T2 Unit 2 began around 14.8 +- 0.8 ka, at a time of rapid climate change in the region and the Northern Hemisphere as a whole. Fining-upward floodplain sediments above in Unit 2 are affected by increasing pedogenesis up-section due to the increasing elevation of the terrace tread relative to the channel, likely due to both geomorphic (progressive deposition) and isostatic (uplift-driven incision) factors. The B2 unconformity and paleosol at the top of Unit 2 occurs with decreased flooding at the 9 ka solar insolation maximum, and a change in parent material for sediments across this boundary is believed to reflect hillslope stability during the time when the B2 surface was forming. Increasing summer precipitation after the final collapse of the ice sheet and its cold air mass at 8.2 ka led to localized deposition of the T2 levee Unit 3. Widespread flooding and increased sediment flux interpreted from the sheet sands at the base of T2 Unit 4 are thought to coincide with a channel reorganization event around 6-5 ka, and landscape destabilization at this time is supported by reactivation of an eolian dune at the ADH site around the same time. The remaining T2 floodplain fines of Unit 4, with increasing markers of soil alteration, were deposited during late-Holocene cooling.

Formation of the T1 and its two units are hypothesized in Chapter 3 to have occurred entirely within the past 1 ka or less. Channel gravels of T1 Unit 1 resulted from increased sediment flux to the channel, destabilization of the T2 banks, and a second period of localized channel reorganization due to the Medieval Warm Period and increasing Native American land use between 0.9-0.5 ka. Further increases in sediment delivery to the channel associated with European deforestation and increased runoff during the Little Ice Age resulted in rapid deposition of T1 Unit 2 since 0.5 ka. These inferences are further supported by radiocarbon dates at the T2 terrace at the DF site, which show a five-fold increase in sedimentation rates during the past ~600 years.

While these paleoclimatological connections are not inherently demanded by the data, the similarities between shifts at the study site and those observed elsewhere in association with these climatic events, as well as the age dates available for the study site, support these interpretations.

Methodological objective 1: To utilize GPR stratigraphic analyses to guide coring and excavation, identify relevant subsurface horizons such as paleosols, and target horizons for OSL dating.

Chapter 1 contributed to a growing body of literature establishing the value of 100 MHz GPR surveying to characterize alluvial architecture and provide insight into the thickness, distribution, and geometry of stratal units that would be difficult to decipher based on cores and outcrops alone. However, distinguishing T2 channel and overbank sediments proved to be difficult using the 100 MHz antenna, and smaller-scale deposits such as crevasse splays and lake clays observed in cores could not be resolved at all. Nonetheless, given the clear representation of depositional architecture, GPR profiles were an excellent guide in selecting core locations and extrapolating information derived from the cores to the larger context of landform evolution. Chapter 2 builds on the GPR identification of units described in Chapter 1 to guide additional coring efforts and sample collection for OSL dating of the T2 sediments at the SIT site.

Methodological objective 2: To identify obstacles to accurate OSL dating in terrestrial depositional settings characterized by unconformities and paleosols, and move toward developing procedures for optimizing results in these situations.

As documented in Chapter 2, OSL dating efforts are complicated in this instance by soil formation processes, which result in leaching and other complications beyond the consideration of many OSL studies. This chapter fully elucidates these potential complications for future OSL workers, both in the Delaware valley and in other terrestrial environments affected by soil formation. In addition, this chapter established that samples from northern Delaware Valley alluvial deposits require higher preheat samples than typical for sedimentary deposits of this age, and are locally affected by Uranium series radiometric disequilibrium at intervals coincident with buried soils. Finally, based on complications associated with small-diameter (5-cm) core samples taken with the Geoprobe device, homogenization of 10-cm-thick samples prior to any OSL treatment or measurement, or collection of multiple closely-spaced cores and aggregation of multiple samples at the same depth, is recommended where core diameters are comparable to those used in this study.

Methodological objective 3: To seek methods that will provide an alternate, and less time- and labor-intensive, means for OSL studies to identify disequilibrium in radioactive decay series using established methods for analysis of chemical weathering and pedogenic (soil) development.

By examining a number of chemical weathering ratios in the soils literature used to infer alteration, Chapter 2 suggests that the Chemical Index of Weathering or Plagioclase Index of Alteration, two previously-established chemical weathering ratios, may be especially useful for researchers seeking preliminary indicators of disequilibrium. However, more work is needed to confirm the value of these ratios in other locations and to identify quantitative threshold values at which concerns are raised, if such values exist.

Study Relevance

Current studies examining the impacts of "global warming" have shown that temperature and precipitation patterns are responding to anthropogenic impacts very differently in different regions, resulting in the shift to discussion of "climate change" rather than warming. Thus, each region must find local archives documenting past conditions as they seek to infer the range of possible future conditions and the ways that natural systems are likely to respond.

Traditionally, persistent archives such as lake sediments have been referenced in the northeast to understand late Pleistocene to Holocene climatic conditions, since they often contain fairly complete records in terms of time. However, naturally-transient landforms such as floodplains and river terraces make up a significant portion of the areas utilized for agriculture, settlement, and commerce. Thus, the impacts of fluctuating climate on these microenvironments have wide-ranging implications for our society.

The northeastern region is one of the most densely-populated portions of the United States, which increases the possible consequences of drastic climate change in this area. Nonetheless, the prevailing temperate climate in this area means that vegetation often blankets landscapes, resulting in sparse outcrops for subsurface examination. Demand for waterfront real estate further inhibits access due to structures and pavements, while dams built to control flooding in other locations submerge these landforms entirely. Thus, few areas remain where in-depth study of stream terraces and floodplains is possible. In areas where terraces and floodplains remain accessible, rapid decay of organic material leaves little for radiocarbon methods to use to construct a detailed chronology of events, and tephrachronology is inapplicable in the tectonically-stable eastern half of the U.S.

The detailed depositional history and general OSL chronology of the SIT site provided by this dissertation is therefore a critical contribution to our understanding of the impact of past and future climate and environmental change on fluvial landforms in the Northeastern U.S. As suggested by the literature (Cronin et al., 2010; Pederson et al., 2005), climate change appears to be the dominant driving force behind terracing, river morphology, and alluvial sedimentation in the upper Delaware. Observed latest Pleistocene to Hoocene shifts connected to these forcing factors include aggradation vs.

incision, changes in channel form, alterations in deposition rates and pedogenesis, and even changes in parent material.

Further insights for the archaeological record can be gleaned from the T2 landform at both the SIT and DF study locations. The B2 unconformity and paleosol, believed to date to between ~9 to 8.2 ka, represents an archaeological condensed section that would allow for the simultaneous accumulation of artifacts and evidence of habitation over a 1000 year period. Additionally, this surface may represent the first time for Native American populations when landscape stability allowed for long-term occupation of the terrace tread without the constant threat of flooding Finally, this hiatus occurred during the Archaic period, the least-well-represented interval in the valley's archaeological records. Targeted excavation of this surface can be easily guided by GPR, but should not be undertaken without that guidance, since the difference in the SIT and DF sites show it will not be present at all localities.

This high-resolution examination also provides valuable insight into the range of responses of the channel to Holocene events that may mimic or predict future events. For example, warming at the time of the solar insolation maximum at 9 ka, especially under continued suppression of summer precipitation due to winds off the dwindling ice sheet, was sufficient to reduce flooding dramatically for an extended period of time by human standards (perhaps nearly 1000 years). Further warming at the time of the Holocene Hypsithermal and Medieval Warm Period resulted in channel destabilization that, if replicated today, would result in dramatic loss of cultural resources and modern property. Preliminary evidence from the eolian landform at the ADH site suggests that

Hypsithermal warming may have been accompanied by a significant decrease in vegetative cover with potential significance for farming yields in a similar future event.

Ultimately, the dramatic increase in sediment yield and channel destabilization evinced by the upper ~70 cm of the DF site T2 and the formation of the T1 at the SIT site serve as a dire warning regarding soil loss in the modern era regardless of anthropogenic influences. Soil loss similar to what occurred in the Medieval Warm Period-Little Ice Age interval could be much more severe in coming years due to increased population density, continued deforestation and poor land use. If left unchecked, this trend could wreak havoc on human settlements along the river and disrupt the natural agricultural floodplain soils upon which many depend.

<u>Remaining Questions and Future Work</u>

Results of this dissertation point to a number of additional questions and hypotheses to be tested in future work in the valley. First, Chapter 3 uses the early age of the T2 Unit 1 and 1a and their similarity in sediment character and formation process (coarse-grained, braided stream channel traction deposition) to hypothesize that these two units are coincident in time with the T3 elsewhere in the valley and that the deposits of this type would have built to varying heights at different locations throughout the previously-glaciated reach of the valley. No age constraints have been available for the bulk of the T3 terrace thus far since no radiocarbon-datable materials have been recovered below the top 1-2 m. While OSL dating within this study was challenging, this method has the potential to provide age control on sand units within the T3 landform and test the hypothesis that it is coincident with T2 Unit 1 and 1a. GPR surveying at a number of T2 locations throughout the valley could then establish whether units of similar character are widespread beneath the T2 landform, and to what degree their elevation varies.

Chapter 3 also notes that the localized depositional histories of T2 landforms varies between the SIT and DF sites, and that this variability is noted throughout the archaeological literature. Between the two sites examined in this study, I hypothesize that the DF T2 begins with the 6-5 ka channel reorganization due to its location at a sharp curve in the river. This bend would have created additional turbulence that eroded the edge of the previous bank, creating accommodation space for the new T2 to form when the channel stabilized. The T2 at the DF site accreted to approximately the same elevation as the T2 and the SIT site over half as much time: Again I attribute this to the sharp bend in the river at DF, which created a hydrologic impediment and caused more rapid slackwater deposition there. A broader survey of T2 characteristics and timing relative to localized channel character would support or reject these ideas.

Additional geochemical data on the T2 landform at the study site will allow firm statistical analysis to confirm or reject the assertion in Chapter 3 that parent material for the alluvial sediments was different before versus after the B2 boundary. If this change were confirmed, chemical analyses of T3 glacial materials and local upland soils should then be undertaken to test whether these two materials are consistent with those parent material characteristics.

The geographic distribution of the B2 boundary, both within the entire Delaware River watershed from upstate New York to the Delaware Bay, and in neighboring watersheds, should be established to clarify the spatial extent of the drought it represents. I hypothesize that the conditions related to the B2 boundary unconformity and soil formation would have impacted at least proximal portions of the Susquehanna and Hudson River Valleys, but may not have extended downstream to the lower portions of the Delaware or Susquehanna, or upstream to the upper Susquehanna or Hudson.

Finally, OSL dating in the neighboring Susquehanna and Hudson River Valleys has the potential to isolate the shift from glacial meltwater to groundwater discharge as the dominant factor driving the establishment of a single-channel morphology during the postglacial period. All three valleys have similar climates and vegetation at present, tundra-boreal vegetation was likely reestablished at similar times as the glacier retreated. However, since the Hudson and Susquehanna drainage basins extend much further north, they transported flashy meltwater discharge for much longer than the Delaware. If OSL dating of the oldest sediments associated with a single-channel morphology in these two valleys confirms previous radiocarbon dating and places this shift at the early Holocene, the Delaware's earlier change in morphology can only be explained by the removal of meltwater from the basin.

APPENDIX

List of Supplementary Files

Surficial map of Milford Quadrangle (north of the study area)- Adobe PDF

SIT Site Core Descriptions- Microsoft Word

SIT Site Core Photographs- Compressed folder of JPEG Files

SIT Site Loss-on-Ignition Measurements- Microsoft Excel

SIT Site Uninterpreted GPR Lines- Adobe PDF

Data from DF Site- Compressed folder of .kdx, .txt, and .DZT and .SU files

- Table of GPR core latitude and longitude
- Radar data files
- Text file of GPR line latitude and longitude

Data from ADH Site

- Core Description for 1.2
- Radar data file
- Text file of GPR line locations

References

Adamiec, G., & Aitken, M. (1998). Dose-rate conversion factors: Update. *Ancient TL, 16*(2), 14-37.

Alley, R. B., & Agustsdottir, A. M. (2005). The 8k event: Cause and consequences of a major Holocene abrupt climate change. *Quaternary Science Reviews, 24*(10-11), 1123-1149. doi: 10.1016/j.quascirev.2004.12.004

Anda, M., Chittleborough, D. J., & Fitzpatrick, R. W. (2009). Assessing parent material uniformity of a red and black soil complex in the landscapes. *Catena, 78*(2), 142-153. doi: 10.1016/j.catena.2009.03.011

Andres, M. S., Bernasconi, S. M., McKenzie, J. A., & Rohl, U. (2003). Southern ocean deglacial record supports global Younger Dryas. *Earth and Planetary Science Letters, 216*(4), 515-524. doi: 10.1016/s0012-821x(03)00556-9

Andres, W., Bos, J. A. A., Houben, P., Kalis, A. J., Nolte, S., Rittweger, H., & Wunderlich, J. (2001). Environmental change and fluvial activity during the Younger Dryas in central Germany. *Quaternary International, 79*, 89-100. doi: 10.1016/S1040-6182(00)00125-7

Bailey, R. M., Smith, B. W., & Rhodes, E. J. (1997). Partial bleaching and the decay form characteristics of quartz OSL. *Radiation Measurements, 27*, 123-136. doi: 10.1016/S1350-4487(96)00157-6

Baker, V. R., & Ritter, D. F. (1975). Competence of rivers to transport coarse bedload material. *Geological Society of America Bulletin, 86*, 975-978.

Bateman, M. D., Boulter, C. H., Carr, A. S., Frederick, C. D., Peter, D., & Wilder, M. (2007a). Detecting post-depositional sediment disturbance in sandy deposits using optical luminescence. *Quaternary Geochronology, 2*(1-4), 57-64. doi: 10.1016/j.quageo.2006.05.004

Bateman, M. D., Boulter, C. H., Carr, A. S., Frederick, C. D., Peter, D., & Wilder, M. (2007b). Preserving the palaeoenvironmental record in drylands: Bioturbation and its significance for luminescence-derived chronologies. *Sedimentary Geology, 195*(1-2), 5-19. doi: 10.1016/j.sedgeo.2006.07.003

Berger, A., & Loutre, M. F. (1991). Insolation values for the climate of the last 10 million years. *Quaternary Science Reviews, 10*(4), 297-317. doi: 10.1016/0277-3791(91)90033-Q

Berger, G. W. (1990). Effectiveness of natural zeroing of the thermoluminescence in sediments. *Journal of Geophysical Research, 95*(B8), 12375-12397. doi: 10.1029/JB095iB08p12375

Berger, G. W., & Luternauer, J. J. (1987). Preliminary fieldwork for thermoluminescence dating studies at the fraser river delta, british columbia. *Geological Survey of Canada Paper 87-1A* (pp. 901-904) Geological Survey of Canada.

Birkeland, P. W. (1999). *Soils and Geomorphology: Third edition*. New York: Oxford University Press.

Blum, M. D. (1993). Genesis and architecture of incised valley fill sequences; a late quaternary example from the Colorado River, gulf coastal plain of Texas. In P.

Weimer, & H. W. Posamentier (Eds.), *Siliciclastic Sequence Stratigraphy; Recent Developments and Applications* (AAPG Memoir 58 ed., pp. 259-283) AAPG.

Blum, M. D., & Tornqvist, T. E. (2000). Fluvial responses to climate and sea-level change: A review and look forward. *Sedimentology, 47*, 2-48.

Blum, M. D., & Valastro, S. (1994). Late quaternary sedimentation, lower Colorado River, gulf coastal-plain of Texas. *Geological Society of America Bulletin, 106*(8), 1002-1016. doi: 10.1130/0016-7606(1994)106<1002:lqslcr>2.3.co;2

Bøtter-Jensen, L., Andersen, C. E., Duller, G. A. T., & Murray, A. S. (2003). Developments in radiation, stimulation and observation facilities in luminescence measurements. *Radiation Measurements, 37*(4-5), 535-541. doi: 10.1016/S1350-4487(03)00020-9

Bridgland, D., & Westaway, R. (2008). Climatically controlled river terrace staircases: A worldwide quaternary phenomenon. *Geomorphology, 98*(3-4), 285-315. doi: 10.1016/j.geomorph.2006.12.032

Bridgland, D. R., Philip, G., Westaway, R., & White, M. (2003). A long quaternary terrace sequence in the Orontes River valley, Syria: A record of uplift and of human occupation. *Current Science, 84*(8), 1080-1089.

Broecker, W. S., & Denton, G. H. (1989). The role of ocean-atmosphere reorganizations in glacial cycles. *Geochimica Et Cosmochimica Acta, 53*(10), 2465-2501. doi: 10.1016/0016-7037(89)90123-3

Brown, A. G., Basell, L. S., Toms, P. S., Bennett, J. A., Hosfield, R. T., & Scrivener, R. C. (2010). Later Pleistocene evolution of the Exe Valley: A chronostratigraphic model of terrace formation and its implications for palaeolithic archaeology. *Quaternary Science Reviews, 29*, 897-912. doi: 0.1016/j.quascirev.20 09.12.007

Bull, W. B. (1991). *Geomorphic Responses to Climate Change*. Oxford: Oxford University Press.

Bull, W. B., & Kneupfer, P. L. K. (1987). Adjustments by the Charwell River, New Zealand, to uplift and climatic changes. *Geomorphology, 1* (1), 15-32. doi: 10.1016/0169-555X(87)90004-3

Bull, W. B. (1979). Threshold of critical power in streams. *Geological Society of America Bulletin, 90*, 453-464.

Burns, D., Vitvar, T., McDonnell, J., Hassett, J., Duncan, J., & Kendall, C. (2005). Effects of suburban development on runoff generation in the Croton River basin, New York, USA. *Journal of Hydrology, 311*(1-4), 266-281. doi: 10.1016/j.jhydrol.2005.01.022

Bush, D. A., & Feathers, J. K. (2003). Application of OSL single-aliquot and single-grain dating to quartz from anthropogenic soil profiles in the SE United States. *Quaternary Science Reviews, 22*(10-13), 1153-1159. doi: 10.1016/S0277-3791(03)00058-1

Carbotte, S. M., Bell, R. E., Ryan, W. B. F., McHugh, C., Slagle, A., Nitsche, F., & Rubenstone, J. (2004). Environmental change and oyster colonization within the Hudson River estuary linked to Holocene climate. *Geo-Marine Letters, 24*(4), 212-224. doi: 10.1007/s00367-004-0179-9

Casana, J. (2008). Mediterranean valleys revisited: Linking soil erosion, land use and climate variability in the northern Levant. *Geomorphology, 101*(3), 429-442. doi: 10.1016/j.geomorph.2007.04.031

Chapman, S. L., & Horn, M. E. (1968). Parent material uniformity and origin of silty soils in northwest Arkansas based on zirconium-titanium contents. *Soil Science Society of America Journal, 32*, 265-271.

Chin, A. (2006). Urban transformation of river landscapes in a global context. *Geomorphology, 79*(3-4), 460-487. doi: 10.1016/j.geomorph.2006.06.033

Chittleborough, D. J. (1991). Indexes of weathering for soils and paleosols formed on silicate rocks. *Australian Journal of Earth Sciences, 38*(1), 115-120.

Connally, G. G., Krinsley, D. H., & Sirkin, L. A. (1972). Late Pleistocene erg in the upper Hudson Valley, New York. *Geological Society of America Bulletin, 83*, 1537-1542.

Costantini, E. A. C., Priori, S., Urban, B., Hilgers, A., Sauer, D., Protano, G., . . . Nannoni, F. (2009). Multidisciplinary characterization of the middle Holocene eolian deposits of the Elsa River basin (central Italy). *Quaternary International, 209*, 107-130. doi: 10.1016/j.quaint.2009.02.025

Coulthard, T. J., Lewin, J., & Macklin, M. G. (2005). Modelling differential catchment response to environmental change. *Geomorphology, 69* (1-4), 222-241. doi: 10.1016/j.geomorph.2005.01.008

Cronin, T. M., Dwyer, T. R., Kamiya, T., Schwede, S., & Willard, D. A. (2005). Medieval warm period, little ice age and 20th century temperature variability from Chesapeake Bay. *Global and Planetary Change, 36* (1-2), 17-29. doi: 10.1016/S0921-8181(02)00161-3

Cronin, T. M., Hayo, K., Thunell, R. C., Dwyer, G. S., Saenger, C., & Willard, D. A. (2010). The medieval climate anomaly and little ice age in Chesapeake Bay and the North Atlantic Ocean. *Palaeogeography, Palaeoclimatology, Palaeoecology, 297*, 299-310. doi: 10.1016/j.palaeo.2010.08.009

Crutzen, P.J. & Stoermer,E.F. (2000). "The 'Anthropocene.'" *Global Change Newsletter, 41*, 17-18.

Dale, F. T. (1996). *Delaware diary: Episodes in the life of a river*. New Brunswick, NJ: Rutgers University Press.

Deither, D. P. (2001). Pleistocene incision rates in the western United States calibrated using Lava Creek B Tephra. *Geology, 29*(9), 783-786. doi: 10.1130/0091-7613(2001)029<0783:PIRITW>2.0.CO;2

DeWitt, R. (2011), Associate Professor, Department of Physics, Oklahoma State University. Personal communication (email).

Donahue, J. J. (1977). Late Wisconsinan eolian activity near Albany, New York. *Geological Society of America Bulletin, 88* (12), 1756-1762. doi: 10.1130/0016-7606(1977)88<1756:LWEANA>2.0.CO;2

Donnelly, J. P., Driscoll, N. W., Uchupi, E., Keigwin, L. D., Schwab, W. C., Thieler, E. R., & Swift, S. A. (2005). Catastrophic meltwater discharge down the Hudson Valley: A potential trigger for the Intra-Allerod cold period. *Geology, 33* (2), 89-92.

Dotterweich, M. (2008). The history of soil erosion and fluvial deposits in small catchments of central Europe: Deciphering the long-term interaction between humans and the environment - A review. *Geomorphology, 101* (1-2), 192-208. doi: 10.1016/j.geomorph.2008.05.023

Dutta, S., Suresh, N., & Kumar, R. (2012). Climatically controlled late quaternary terrace staircase development in the fold- and thrust- belt of the sub-Himalaya. *Palaeogeography, Palaeoclimatology, Palaeoecology, 356-357*, 16-26. doi: 10.1016/j.palaeo.2011.05.006

Dwyer, T. R., Mullins, H. T., & Good, S. C. (1996). Paleoclimatic implications of Holocene lake-level fluctuations, Owasco Lake, New York. *Geology, 24*(6), 519-522. doi: 10.1130/0091-7613(1996)024<0519:PIOHLL>2.3.CO;2

Earley R. (2007). Personal communication (email).

Ellis, K. G., Mullins, H. T., & Patterson, W. P. (2004). Deglacial to middle Holocene (16,600 to 6000 calendar years BP) climate change in the northeastern United States inferred from multi-proxy stable isotope data, Seneca Lake, New York. *Journal of Paleolimnology, 31*(3), 343-361.

Evans, L. J., & Adams, W. A. (1975). Quantitative pedological studies on soils derived from Silurian mudstones: IV. Uniformity of the parent material and evaluation of internal standards. *European Journal of Soil Science, 26* (3), 319-326. doi: 10.1111/j.1365-2389.1975.tb01956.x

Fairbanks, R. G., Mortlock, R. A., Chiu, T., Cao, L., Kaplan, A., Guilderson, T. P., . . . Bloom, A. L. (2005). Marine radiocarbon calibration curve spanning 0 to 50,000 years B.P. based on Paired ^{230}Th, ^{234}U, ^{238}U and ^{14}C dates on pristine corals. *Quaternary Science Reviews, 24*, 1781-1796.

Fedo, C. M., Nesbitt, H. W., & Young, G. M. (1995). Unraveling the effects of potassium metasomatism in sedimentary-rocks and paleosols, with implications for paleoweathering conditions and provenance. *Geology, 23* (10), 921-924. doi: 10.1130/0091-7613(1995)023<0921:UTEOPM>2.3.CO;2

Formento-Trigilio, M. L., Burbank, D. W., Nicol, A., Schulmeister, J., & Rieser, U. (2002). River response to an active fold-and-thrust belt in a convergent margin setting, North Island, New Zealand. *Geomorphology, 49* (1-2), 125-152. doi: 10.1016/S0169-555X(02)00167-8

Forrest, B., Rink, W. J., Bicho, N., & Ferring, C. R. (2003). OSL ages and possible bioturbation signals at the upper paleolithic site of Lagoa do Bordoal, Algarve, Portugal. *Quaternary Science Reviews, 22* (10-13), 1279-1285. doi: 10.1016/s0277-3791(03)00028-3

Galbraith, R. F. (1990). The radial plot: Graphical assessment of spread in ages. *Nuclear Tracks and Radiation Measurements, 17*, 207-214. doi: 10.1016/1359-0189(90)90036-W

Galbraith, R. F., Roberts, R. G., Laslett, G. M., Yoshida, H., & Olley, J. M. (1999). Optical dating of single and multiple grains of quartz from Jinmium Rock Shelter, northern Australia. part I: Experimental design and statistical models. *Archaeometry, 41*, 339-364.

Galbraith, R. F., Roberts, R. G., & Yoshida, H. (2005). Error variation in OSL palaeodose estimates from single aliquots of quartz: A factorial experiment. *Radiation Measurements, 39* (3), 289-307. doi: 10.1016/j.radmeas.2004.03.023

Godfrey-Smith, D. I., Huntley, D. J., & Chen, W. H. (1988). Optical dating studies of quartz and feldspar sediment extracts. *Quaternary Science Reviews, 7*, 373-380. doi: 10.1016/0277-3791(88)90032-7

Goman, M., & Leigh, D. S. (2004). Wet early to middle Holocene conditions on the upper coastal plain of North Carolina, USA. *Quaternary Research, 61* (3), 256-264. doi: 10.1016/j.yqres.2004.02.007

Goudie, A. S. (2006). Global warming and fluvial geomorphology. *Geomorphology, 79* (3-4), 384-394. doi: 10.1016/j.geomorph.2006.06.023

Guibert, P., Lahaye, C., & Bechtel, F. (2009). The importance of U-series disequilibrium of sediments in luminescence dating: A case study at the Roc de Marsal Cave (Dordogne, France). *Radiation Measurements, 44* (3), 223-231. doi: 10.1016/j.radmeas.2009.03.024

Hancock, G. S., & Anderson, R. S. (2002). Numerical modeling of fluvial strath-terrace formation in response to oscillating climate. *Geological Society of America Bulletin, 114* (9), 1131-1142. doi: 10.1130/0016-7606(2002)114<1131:NMOFST>2.0.CO;2

Harnois, L. (1988). The CIW index- A new chemical index of weathering. *Sedimentary Geology, 55* (3-4), 319-322. doi: 10.1016/0037-0738(88)90137-6

Harrison, S. P., Kutzbach, J. E., Liu, Z., Bartlein, P. J., Otto-Bliesner, B., Muhs, D., . . . Thompson, R. S. (2003). Mid-holocene climates of the Americas: A dynamical response to changed seasonality. *Climate Dynamics, 20*, 663-688. doi: 10.1007/s00382-002-0300-6

Huntley, D. J., Godfrey-Smith, D. I., & Thewalt, M. L. W. (1985). Optical dating of sediments. *Nature, 313*, 105-107. doi: 10.1038/313105a0

http://delawarewatergap.org/TOCKS_ISLAND_DAM_PROJECT.html

http://courses.washington.edu/holocene/IntroGHR.pdf

Inman, D. L., & Jenkins, S. A. (1999). Climate change and the episodicity of sediment flux of small California rivers. *Journal of Geology, 107* (3), 251-270. doi: 10.1086/314346

Ivanovich, M., & Harmon, R. S. (1992). *Uranium-series disequilibrium: Applications to earth, marine and environmental sciences*. Oxford: Clarendon Press.

Jennings, D., & Jarnagin, T. S. (2002). Changes in anthropogenic impervious surfaces, precipitation and daily streamflow discharge: A historical perspective in a mid-atlantic subwatershed. *Landscape Ecology, 17*, 471-489. doi: 10.1023/A:1021211114125

Jenny, H. (1941). *Factors of soil formation*. New York: McGraw-Hill.

Kirby, M. E., Mullins, H. T., Patterson, W. P., & Burnett, A. W. (2002). Late glacial-Holocene atmospheric circulation and precipitation in the northeast United States inferred from modern calibrated stable oxygen and carbon isotopes. *GSA Bulletin, 114* (10), 1326-1340.

Kneller, M., & Peteet, D. (1993). Late-quaternary climate in the ridge and valley of Virginia, USA: Changes in vegetation and depositional environment. *Quaternary Science Reviews, 12* (8), 613-628. doi: 10.1016/0277-3791(93)90003-5

Kneller, M., & Peteet, D. (1999). Late-glacial to early holocene climate changes from a central appalachian pollen and macrofossil record. *Quaternary Research, 51*(2), 133-147. doi: 10.1006/qres.1998.2026

Knox, J. C. (1975). Concept of the graded stream. In W. N. Melhorn, & R. C. Flemal (Eds.), *Theories of landform development: Proceedings of the 6th annual binghamton symposium, publications in geomorphology* (pp. 169-198). Binghamton, NY: State University of New York.

Knox, J. C. (1993). Large increases in flood magnitude in response to modest changes in climate. *Nature, 361* (6411), 430-432. doi: 10.1038/361430a0

Knox, J. C. (2000). Sensitivity of modern and Holocene floods to climate change. *Quaternary Science Reviews, 19* (1-5), 439-457. doi: 10.1016/S0277-3791(99)00074-8

Knox, J. C. (2006). Floodplain sedimentation in the upper Mississippi Valley: Natural versus human accelerated. *Geomorphology, 79*(3-4), 286-310. doi: 10.1016/j.geomorph.2006.06.031

Koteff, C., Robinson, G. R., Goldsmith, R., & Thompson, W. B. (1993). Delayed postglacial uplift and synglacial sea levels in coastal central New England. *Quaternary Research, 40*, 46-54.

Kraus, M. J. (1999). Paleosols in clastic sedimentary rocks: Their geologic applications. *Earth-Science Reviews, 47*, 41-70.

Krbetschek, M. R., Rieser, U., Zöller, L., & Heinicke, J. (1994). Radioactive disequilibria in palaeodosimetric dating of sediments. *Radiation Measurements, 23*(2-3), 485-489. doi: 10.1016/1350-4487(94)90083-3

Leeman, A., & Niessen, F. (1994). Varve formation and the climatic record in an Alpine proglacial lake: calibrating annually- laminated sediments against hydrological and meteorological data. *The Holocene, 4* (1), 1-8.

Leigh, D. S., & Feeney, T. P. (1995). Paleochannels indicating wet climate and lack of response to lower sea level, southeast Georgia. *Geology, 23* (8), 687-690. doi: 10.1130/0091-7613(1995)023<0687:PIWCAL>2.3.CO;2

Lewin, J., & Gibbard, P. L. (2010). Quaternary river terraces in England: Forms, sediments and processes. *Geomorphology, 120*, 293-311. doi: 10.1016/j.geomorph.2010.04.002

Li, Y., Yu, Z., Kodama, K. P., & Moeller, R. E. (2006). A 14,000-year environmental change history revealed by mineral magnetic data from White Lake, New Jersey, USA. *Earth and Planetary Science Letters, 246* (1-2), 27-40. doi: 10.1016/j.epsl.2006.03.052

Litchfield, N., & Berryman, K. (2006). Relations between postglacial fluvial incision rates and uplift rates in the North Island, New Zealand. *Journal of Geophysical Research-Earth Surface, 111* (F2) doi: F02007 10.1029/2005jf000374

Loget, N., & Van Den Driessche, J. (2009). Wave train model for knickpoint migration. *Geomorphology, 106* (3-4), 376-382. doi: 10.1016/j.geomorph.2008.10.017

Macklin, M. G., & Lewin, J. (2003). River sediments, great floods and centennial-scale Holocene climate change. *Journal of Quaternary Science, 18* (2), 101-105. doi: 10.1002/jqs.751

Maddy, D. (1997). Uplift-driven valley incision and river terrace formation in southern England. *Journal of Quaternary Science, 12* (6), 539-545. doi: 10.1002/(SICI)1099-1417(199711/12)12:6<539::AID-JQS350>3.3.CO;2-K

Maddy, D., Bridgland, D., & Westaway, R. (2001). Uplift-driven valley incision and climate-controlled river terrace development in the Thames Valley, UK. *Quaternary International, 79*, 23-36. doi: 10.1016/S1040-6182(00)00120-8

Maddy, D., & Bridgland, D. R. (2000). Accelerated uplift resulting from Anglian glacioisostatic rebound in the middle Thames Valley, UK?: Evidence from the river terrace record. *Quaternary Science Reviews, 19* (16), 1581-1588. doi: 10.1016/S0277-3791(99)00105-5

Maenza-Gmelch, T. E. (1996). Vegetation, climate, and fire during the late-glacial--Holocene transition at Spruce Pond, Hudson Highlands, southeastern New York, USA. *Journal of Quaternary Science, 12* (1), 15-24. doi: 10.1002/(SICI)1099-1417(199701/02)12:1<15::AID-JQS283>3.0.CO;2-T

Markewich, H. W., Litwin, R. J., Pavich, M. J., & Brook, G. A. (2009). Late Pleistocene eolian features in southeastern Maryland and Chesapeake Bay region indicate strong WNW-NW winds accompanied growth of the Laurentide Ice Sheet. *Quaternary Research, 71* (3), 409-425. doi: 10.1016/j.yqres.2009.02.001

Marsan, F. A., Bain, D. C., & Duthie, D. M. L. (1988). Parent material uniformity and degree of weathering in a soil chronosequence, northwestern Italy. *Catena, 15*, 507-517. doi: 10.1016/0341-8162(88)90002-1

McNett, C. W., Jr., McMillan, B. A., & Marshall, S. B. (1977). The Shawnee-Minisink Site. *Annals of the New York Academy of Sciences, 288: Amerinds and their Paleoenvironments in Northeastern North America.*

Meyers, P. A. (2002). Evidence of mid-Holocene climate instability from variations in carbon burial in Seneca Lake, New York. *Journal of Paleolimnology, 28* (2), 237-244. doi: 10.1023/A:1021662222452

Milly, P. C. D., Wetherald, R. T., Dunne, K. A., & Delworth, T. L. (2002). Increasing risk of great floods in a changing climate. *Nature, 415* (6871), 514-517.

Montgomery, D. R. (2004). Observations on the role of lithology in strath terrace formation and bedrock channel width. *American Journal of Science, 304*, 454-476.

Mullins, H. T. (1998). Holocene lake level and climate change inferred from marl stratigraphy of the Cayuga Lake basin, New York. *Journal of Sedimentary Research, 68*(4), 569-578.

Mullins, H. T., & Halfman, J. D. (2001). High-resolution seismic reflection evidence for middle Holocene environmental change, Owasco Lake, New York. *Quaternary Research, 55* (3), 322-331. doi: 10.1006/qres.2001.2232

Murray, A. S., & Roberts, R. G. (1998). Measurement of the equivalent dose in quartz using a regenerative-dose single-aliquot protocol. *Radiation Measurements, 29*, 503-515. doi: 10.1016/S1350-4487(98)00044-4

Murray, A. S., & Wintle, A. G. (1998). Factors controlling the shape of the OSL decay curve in quartz. *Radiation Measurements, 29* (1), 65-79. doi: DOI:10.1016/S1350-4487(97)00207-2

Murray, A. S., & Wintle, A. G. (2000). Luminescence dating of quartz using an improved single-aliquot regenerative-dose protocol. *Radiation Measurements, 32* (1), 57-73. doi: 10.1016/S1350-4487(99)00253- X

Murray, A. S., & Wintle, A. G. (2003). The single aliquot regenerative dose protocol: Potential for improvements in reliability. *Radiation Measurements, 37* (4-5), 377-381. doi: 10.1016/S1350-4487(03)00053-2

Nanson, G. C., & Croke, J. C. (1992). A genetic classification of floodplains. *Geomorphology, 4* (6), 459-486. doi: 10.1016/0169-555X(92)90039-Q

Nesbitt, H. W., & Young, G. M. (1989). Formation and diagenesis of weathering profiles. *Journal of Geology, 97*, 19-129. doi: 10.1086/629290

Nesci, O., & Savelli, D. (2003). Diverging drainage in the Marche Apennines (central Italy). *Quaternary International, 101-102*, 203-209. doi: 10.1016/S1040-6182(02)00102-7

Newby, P. E., Shuman, B. N., Donnelly, J. P., & MacDonald, D. (2011). Repeated century-scale droughts over the past 13,000 yr near the Hudson River watershed, USA. *Quaternary Research, 75* (3), 523-530. doi: 10.1016/j.yqres.2011.01.006

Notebaert, B., Verstraeten, G., Ward, P., Renssen, H., & Van Rompaey, A. (2011). Modeling the sensitivity of sediment and water runoff dynamics to Holocene climate and land use changes at the catchment scale. *Geomorphology, 126* (1-2), 18-31. doi: 10.1016/j.geomorph.2010.08.016

Oakley, B. A., & Boothroyd, J. C. (2012). Reconstructed topography of southern New England prior to isostatic rebound with implications of total isostatic depression and relative sea level. *Quaternary Research, 78* (1), 110-118. doi: 10.1016/j.yqres.2012.03.002

Olley, J. M., Murray, A., & Roberts, R. G. (1996). The effects of disequilibria in the uranium and thorium decay chains on burial dose rates in fluvial sediments. *Quaternary Science Reviews, 15* (7), 751-760. doi: 10.1016/0277-3791(96)00026-1

Olszak, J. (2011). Evolution of fluvial terraces in response to climate change and tectonic uplift during the Pleistocene: Evidence from Kamienica and Ochotnica River valleys (Polish Outer Carpathians). *Geomorphology, 129*, 71-78. doi: 10.1016/j.geomorph.2011.01.014

Orr, D., & Campana, D. (Eds.) (1991). *The People of Minisink*. Philadelphia: National Park Service.

Parker, A. (1970). An index of weathering for silicate rocks. *Geological Magazine, 107*, 4-401. doi: 10.1017/S0016756800058581

Patton, P. C., & Schumm, S. A. (1975). Gully erosion, northwestern Colorado; A threshold phenomenon. *Geology, 3* (2), 88-89. doi: 10.1130/0091-7613(1975) 3<88:GENCAT>2.0.CO;2

Pazzaglia, F. J. (in press). 9.23 Fluvial Terraces. In E. Wohl (Ed.), *Treatise on geomorphology*. Elsevier.

Pazzaglia, F. J., & Brandon, M. T. (2001). A fluvial record of long-term steady-state uplift and erosion across the Cascadia forearc high, western Washington state. *American Journal of Science, 301* (4-5), 385-431. doi: 10.2475/ajs.301.4-5.385

Pazzaglia, F. J., & Gardner, T. W. (1993). Fluvial terraces of the lower Susquehanna River. *Geomorphology, 8* (2-3), 83-113. doi: 10.1016/0169-555X(93)90031-V

Pederson, D. C., Peteet, D. M., Kurdyla, D., & Guilderson, T. (2005). Medieval warming, little ice age, and European impact on the environment during the last millennium in the lower Hudson Valley, New York, USA. *Quaternary Research, 63* (3), 238-249. doi: 10.1016/j.yqres.2005.01.001

Peteet, D. (1995). Global Younger-Dryas. *Quaternary International, 28*, 93-104.

Peteet, D. (2000). Sensitivity and rapidity of vegetational response to abrupt climate change. *Proceedings of the National Academy of Sciences of the United States of America, 97* (4), 1359-1361. doi: 10.1073/pnas.97.4.1359

Peteet, D. M., Daniels, R., Heusser, L. E., Vogel, J. S., Southon, J. R., & Nelson, D. E. (1994). Wisconsinan late-glacial environmental change in southern New England: A regional synthesis. *Journal of Quaternary Science, 9* (2), 151-154. doi: 10.1002/jqs.3390090209

Peteet, D. M., Daniels, R. A., Heusser, L. E., Vogel, J. S., Southon, J. R., & Nelson, D. E. (1993). Late-glacial pollen, macrofossils and fish remains in northeastern USA--the Younger Dryas oscillation. *Quaternary Science Reviews, 12* (8), 597-612. doi: 10.1016/0277-3791(93)90002-4

Peteet, D. M., Vogel, J. S., Nelson, D. E., Southon, J. R., Nickmann, R. J., & Heusser, L. E. (1990). Younger Dryas climatic reversal in northeastern USA? AMS ages for an old problem. *Quaternary Research, 33* (2), 219-230. doi: 10.1016/0033-5894(90)90020-L

Prescott, J. R., & Hutton, J. T. (1994). Cosmic ray contributions to dose rates for luminescence and ESR dating - large depths and long-term time variations. *Radiation Measurements, 23* (2-3), 497-500. doi: 10.1016/1350-4487(94)90086-8

Prescott, J. R., & Hutton, J. T. (1995). Environmental dose rates and radioactive disequilibrium from some Australian luminescence dating sites. *Quaternary Science Reviews, 14* (4), 439-448. doi: 10.1016/0277-3791(95)00037-2

Price, J. R., & Velbel, M. A. (2003). Chemical weathering indices applied to weathering profiles developed on heterogeneous felsic metamorphic parent rocks. *Chemical Geology, 202* (3-4), 397-416. doi: 10.1016/j.chemgeo.2002.11.001

Rawling, J. E., Hanson, P. R., Young, A. R., & Attig, J. W. (2008). Late Pleistocene dune construction in the central sand plain of Wisconsin, USA. *Geomorphology, 100* (3-4), 494-505. doi: 10.1016/j.geomorph.2008.01.017

Reheis, M. C. (1990). Influence of climate and eolian dust on the major-element chemistry and clay mineralogy of soils in the northern Bighorn Basin, USA. *Catena, 17*(3), 219-248. doi: 10.1016/0341-8162(90)90018-9

Retallack, G. J. (1990). *Soils of the Past: An Introduction to Paleopedology*. Boston: Unwin Hyman, Inc.

Ridge, J. C. (2003). The last deglaciation of the northeastern United States: A combined varve, paleomagnetic, and calibrated ^{14}C chronology. In D. L. Cremeens, & J. P.

Hart (Eds.), *Geoarchaeology of landscapes in the glaciated northeast* (pp. 15-45; 3). Albany, NY: The New York State Education Department.

Ridge, J. C., Evenson, E. B., & Sevon, W. D. (1992). A model of late Quaternary landscape development in the Delaware Valley, New Jersey and Pennsylvania. *Geomorphology, 4* (5), 319-345. doi: 10.1016/0169-555X(92)90027-L

Ritter, D. F., Kochel, C. R., & Miller, J. R. (2002). *Process Geomorphology, 4th ed.* Long Grove, IL: Waveland Press, Inc.

Ritter, J. B., Miller, J. R., Enzel, Y., Howes, S. D., Nadon, G., Grubb, M. D., . . . Wells, S. G. (1993). Quaternary evolution of Cedar Creek alluvial fan, Montana. *Geomorphology, 8* (4), 287-304. doi: 10.1016/0169-555X(93)90025-W

Ritter, J. B., Miller, J. R., & Husek-Wulforst, J. (2000). Environmental controls on the evolution of alluvial fans in Buena Vista Valley, north central Nevada, during late Quaternary time. *Geomorphology, 36* (1-2), 63-87. doi: 10.1016/S0169-555X(00)00048-9

Rodnight, H., Duller, G. A. T., Wintle, A. G., & Tooth, S. (2006). Assessing the reproducibility and accuracy of optical dating of fluvial deposits. *Quaternary Geochronology, 1* (2), 109-120. doi: 10.1016/j.quageo.2006.05.017

Roe, G. H., Montgomery, D. R., & Hallet, B. (2002). Effects of orographic precipitation variations on the concavity of steady-state river profiles. *Geology, 30*, 143-146. doi: 10.1130/0091-7613(2002)030<0143:EOOPVO>2.0.CO;2

Rose, S., & Peters, N. E. (2001). Effects of urbanization on streamflow in the Atlanta area (Georgia, USA): A comparative hydrological approach. *Hydrological Processes, 15* (8), 1441-1457. doi: 10.1002/hyp.218

Rosholt, J. N., Doe, B. R., & Tatsumoto, M. (1966). Evolution of the isotopic composition of uranium and thorium in soil profiles. *Geological Society of America Bulletin, 77*, 17-987. doi: 10.1130/0016-7606(1966)77[987:EOTICO]2.0.CO;2

Russell, E.W.B., Davis, R.B., Anderson, R.S., Rhodes, T.E., & Anderson, D.S. (1993). Recent centuries of vegetational change in the glaciated north-eastern United States. *Journal of Ecology, 81*, 647-664.

Russell, E. W. B., & Stanford, S. D. (2000). Late-glacial environmental changes south of the Wisconsinan terminal moraine in the eastern United States. *Quaternary Research, 53* (1), 105-113. doi: 10.1006/qres.1999.2103

Ruxton, B. P. (1968). Measures of the degree of chemical weathering of rocks. *Journal of Geology, 76*, 10-518. doi: 10.1086/627357

Saucier, R. T. (1994). *Geomorphology and quaternary geologic history of the lower mississippi valley.* Vicksburg: Mississippi River Commission.

Schaetzl, R. J., & Loope, W. L. (2008). Evidence for an eolian origin for the silt-enriched soil mantles on the glaciated uplands of eastern upper Michigan, USA. *Geomorphology, 100* (3-4), 285-295. doi: 10.1016/j.geomorph.2008.01.002

Schrabish, M. (1915). *NJGS bulletin 13; Indian habitations in Sussex County New Jersey*. Dispatch Printing Company, Union Hill, NJ.

Schumm, S. A. (1993a). River response to baselevel change: Implications for sequence stratigraphy. *Journal of Geology, 101* (2), 279-294. doi: 10.1086/648221

Shulkov, A. L., Usova, M. G., Shakhovets, S. A., & Voskovskaya, L. T. (1997). New techniques of absolute dating of Quaternary sediments. Message posted to http://www.aha.ru/~shlukov/discus.htm

Shuman, B., Bravo, J., Kaye, J., Lynch, J. A., Newby, P., & Webb, T. (2001). Late Quaternary water-level variations and vegetation history at Crooked Pond, southeastern Massachusetts. *Quaternary Research, 56* (3), 401-410. doi: 10.1006/qres.2001.2273

Shuman, B., & Donnelly, J. P. (2006). The influence of seasonal precipitation and temperature regimes on lake levels in the northeastern United States during the Holocene. *Quaternary Research, 65* (1), 44-56. doi: 10.1016/j.yqres.2005.09.001

Shuman, B., Huang, Y., Newby, P., & Wang, Y. (2006). Compound-specific isotopic analyses track changes in seasonal precipitation regimes in the northeastern United States at ca 8200 cal yr BP. *Quaternary Science Reviews, 25* (21-22), 2992-3002. doi: 10.1016/j.quascirev.2006.02.021

Singarayer, J. S., & Bailey, R. M. (2003). Component-resolved bleaching spectra of quartz optically stimulated luminescence: Preliminary results and implications for dating. *Radiation Measurements, 38* (1), 111-118. doi: 10.1016/S1350-4487(03)00250-6

Singarayer, J. S., Bailey, R. M., Ward, S., & Stokes, S. (2005). Assessing the completeness of optical resetting of quartz OSL in the natural environment. *Radiation Measurements, 40* (1), 13-25. doi: 10.1016/j.radmeas.2005.02.005

Sinha, S. K., & Parker, G. (1996). Causes of concavity in longitudinal profiles of rivers. *Water Resources Research, 32*, 1417-1428.

Sklar, L., & Dietrich, W. E. (1998). River longitudinal profiles and bedrock incision models: Stream power and the influence of sediment supply. In K. J. Tinkler (Ed.), *Rivers over rock: Fluvial processes in bedrock channels.* (pp. 237-260) American Geophysical Union.

Spencer, J. Q. G., & Robinson, R. A. J. (2008). Dating intramontane alluvial deposits from NW Argentina using luminescence techniques: Problems and potential. *Geomorphology, 93* (1-2), 144-155. doi: 10.1016/j.geomorph.2006.12.021

Spencer, J.Q.G. (2011), Assistant Professor, Department of Geology, Kansas State University. Personal communication (email).

Stanford, S. D. (2003). Late Miocene to Holocene geology of the New Jersey coastal plain. *Periglacial Features of Southern New Jersey, Geological Association of New Jersey Annual Meeting Field Guide and Proceedings,* 21-50.

Stanford, S. D., Ashley, G. M., & Brenner, G. J. (2001). Late Cenozoic fluvial stratigraphy of the New Jersey piedmont: A record of glacioeustasy, planation, and incision on a low-relief passive margin. *Journal of Geology, 109* (2), 265-276. doi: 10.1086/319242

Stanford, S. D. (1993). Late Cenozoic surficial deposits and valley evolution of unglaciated northern New Jersey. *Geomorphology, 7* (4), 267-288. doi: 10.1016/0169-555X(93)90058-A

Starkel, L. (2003). Climatically controlled terraces in uplifting mountain areas. *Quaternary Science Reviews, 22* (20), 2189-2198.

Stewart, M. (1991). Archaeology and environment in the upper Delaware Valley. In D. &. C. Orr D. (Ed.), *The People of Minisink*. Philadelphia: National Park Service.

Stewart, R. M. (2005). A summary of archaeological explorations of Hendrick Island. *Bulletin of the Archaeological Society of New Jersey, 60*, 13-19.

Stinchcomb, G. E., Messner, T. C., Driese, S. G., Nordt, L. C., & Stewart, R. M. (2011). Pre-colonial (A.D. 1100-1600) sedimentation related to prehistoric maize agriculture and climate change in eastern North America. *Geology, 39* (4), 363-366. doi: 10.1130/g31596.1

Stinchcomb, G. E., Driese, S. G., Nordt, L. C., & Allen, P. M. (2012). A mid to late Holocene history of floodplain and terrace reworking along the middle Delaware River Valley, USA. *Geomorphology, 169-170*, 123-141. doi: 10.1016/j.geomorph.2012.04.018

Taylor, K. C., Lamorey, G. W., Doyle, G. A., Alley, R. B., Grootes, P. M., Mayewski, P. A., . . . Barlow, L. K. (1993). The 'flickering switch' of late Pleistocene climate change. *Nature, 361*, 432-436.

Thieme, D. M. (2003). *A stratigraphic and chronometric investigation of the alluvial deposits of the north branch of the Susquehanna River.* University of Georgia, *Ph.D.*, 616.

Thorson, R. M., & Schile, C. A. (1995). Deglacial eolian regimes in New England. *GSA Bulletin, 107* (7), 751-761.

Turowski, J. M., Lague, D., Crave, A., & Hovius, N. (2006). Experimental channel response to tectonic uplift. *Journal of Geophysical Research-Earth Surface, 111* (F3) doi: 10.1029/2005JF000306

van den Berg, M. W. (2006). *Fluvial sequences of the Maas: A 10 ma record of neotectonics and climatic change at various time-scales.* (Ph.D., Landbouwuniversiteit te Wageningen).

van den Berg, M. W., & van Hoof, T. (2001). The Maas terrace sequence at Maastricht, SE Netherlands; evidence for 200 m of late Neogene and Quaternary surface uplift. In D. Maddy, M. G. Macklin & J. C. Woodward (Eds.), *River basin sediment systems: Archives of environmental change* (pp. 45-86). Netherlands: A.A. Balkema Publishers.

Vandenberghe, J. (2003). Climate forcing of fluvial system development: An evolution of ideas. *Quaternary Science Reviews, 22*, 2053-2060.

Vandenberghe, J. (2008). The fluvial cycle at cold-warm-cold transitions in lowland regions: A refinement of theory. *Geomorphology, 98* (3-4), 275-284. doi: 10.1016/j.geomorph.2006.12.030

Webb, R. S., Anderson, K. H., & Webb, T. (1993). Pollen-response surface estimates of late-Quaternary changes in moisture balance of the northeastern United States. *Quaternary Research, 40* (2), 213-227. doi: 10.1006/qres.1993.1073

Wegmann, K., & Pazzaglia, F. J. (2009). Late Quaternary fluvial terraces of the Romagna and Marche Apennines, Italy: Climatic, lithologic, and tectonic controls on terrace genesis in an active orogen. *Quaternary Science Reviews, 28*, 137-165. doi: 10.1016/j.quascirev.20 08.10.0 06

Westaway, R., Bridgland, D. R., Sinha, R., & Demir, T. (2009). Fluvial sequences as evidence for landscape and climatic evolution in the late Cenozoic: A synthesis of data from IGCP 518. *Global and Planetary Change, 68* (4), 237-253. doi: 10.1016/j.gloplacha.2009.02.009

Wintle, A. G. (1997). Luminescence dating: Laboratory procedures and protocols. *Radiation Measurements, 27* (5-6), 769-817. doi: 10.1016/S1350-4487(97)00220-5

Wintle, A. G., & Murray, A. S. (1999). Luminescence sensitivity changes in quartz. *Radiation Measurements, 30*, 107-118. doi: 10.1016/S1350-4487(98)00096-1

Wintle, A. G., & Murray, A. S. (2000). Quartz OSL: Effects of thermal treatment and their relevance to laboratory dating procedures. *Radiation Measurements, 32*, 387-400. doi: 10.1016/S1350-4487(00)00057-3

Wintle, A. G., & Murray, A. S. (2006). A review of quartz optically stimulated luminescence characteristics and their relevance in single-aliquot regeneration dating protocols. *Radiation Measurements, 41* (4), 369-391. doi: 10.1016/j.radmeas.2005.11.001

Witte, R. W. (2001). Late Wisconsinan deglaciation and postglacial history of Minisink Valley: Delaware Water Gap to Port Jervis, New York. *A Delaware River Odyssey, Guidebook, 66th Annual Field Conference of Pennsylvania Geologists, Shawnee on Delaware.* 99-118.

Witte, R.W. (2006, 2007, 2008, 2009, 2010, 2011), Research Scientist 2, New Jersey Geologic Survey. Personal communication (emails).

Xing, B. S., Liu, X. B., Zhang, Z. Y., Wang, K. J., & Li, K. (2004). Evaluation of parent material uniformity of white clay soils in Heilongjiang Province, China. *Communications in Soil Science and Plant Analysis, 35*(13-14), 1839-1850. doi: 10.1081/lcss-200026803

Yu, Z. (2000). Ecosystem response to lateglacial and early Holocene climate oscillations in the Great Lakes region of North America. *Quaternary Science Reviews, 19* (17-18), 1723-1747. doi: 10.1016/S0277-3791(00)00080-9

Yu, Z. (2007). Rapid response of forested vegetation to multiple climatic oscillations during the last deglaciation in the northeastern United States. *Quaternary Research, 67* (2), 297-303. doi: 10.1016/j.yqres.2006.08.006

Zaprowski, B. J., Pazzaglia, F. J., & Evenson, E. B. (2005). Climatic influences on profile concavity and river incision. *Journal of Geophysical Research-Earth Surface, 110* (F3) doi: F03004 10.1029/2004jf000138

Zhao, C., Yu, Z., Ito, E., & Zhao, Y. (2010). Holocene climate trend, variability, and shift documented by lacustrine stable-isotope record in the northeastern United States. *Quaternary Science Reviews, 29* (15-16), 1831-1843. doi: 10.1016/j.quascirev.2010.03.018

Zhou, L. P., & Wintle, A. G. (1994). Sensitivity change of thermoluminescence signals after laboratory optical bleaching: Experiments with loess fine grains. *Quaternary Geochronology, 13* (5-7), 457-463. doi: 10.1016/0277-3791(94)90058-2